

Energy

On the Performance Improvement of an Inverted Brayton Cycle using a Regenerative Heat and Mass Exchanger

--Manuscript Draft--

Manuscript Number:	EGY-D-21-07651R4
Article Type:	Full length article
Keywords:	Inverted Brayton cycle; Indirect evaporative cooler; Waste heat utilisation; Power Generation
Corresponding Author:	Kyaw Thu, Ph.D. Kyushu University Fukuoka, JAPAN
First Author:	Kohei Matsui
Order of Authors:	Kohei Matsui
	Jie Lin
	Kyaw Thu, Ph.D.
	Takahiko Miyazaki
Abstract:	<p>Recovery of the low-temperature waste heat for electricity generation has been gaining a significant interest. An Inverted Brayton Cycle (IBC) is often employed to convert the low-temperature waste-heat to electricity while the thermal efficiency and specific work output are poor. In this paper, a new energy recovery scheme is introduced incorporating the IBC with a Regenerative Heat and Mass Exchanger (RHME). The RHME is a heat and mass exchanger that consolidates a recuperator (for thermal efficiency improvement) and an Indirect Evaporative Cooler (for enhanced specific work). Numerical models for RHME and the IBC were judiciously developed where possible condensation in the product air channel was accounted for. The model was validated with the experimental data and the cycle was investigated for various waste-heat sources (50 – 150 °C). When compared to a conventional air-cooling IBC system, incorporating the current energy recovery scheme increases the thermal efficiency from 8.13% to 14.36% and specific work output from 10.38 to 12.46 kJ/kg equivalent to 76.63% and 20.1% improvements, respectively. The unprecedented performance improvement is realised from the exploitation of the regenerative and air-saturation (cooling) mechanisms for both energy recovery and cooling of the working fluid.</p>

Conflict of Interest Statement

We wish to confirm that there are no known conflicts of interest associated with this publication and there has been no significant financial support for this work that could have influenced its outcome.

We confirm that the manuscript has been read and approved by all named authors and that there are no other persons who satisfied the criteria for authorship but are not listed. We further confirm that the order of authors listed in the manuscript has been approved by all of us. We confirm that we have given due consideration to the protection of intellectual property associated with this work and that there are no impediments to publication, including the timing of publication, with respect to intellectual property. In so doing we confirm that we have followed the regulations of our institutions concerning intellectual property.

We understand that the Corresponding Author is the sole contact for the Editorial process (including Editorial Manager and direct communications with the office). He/she is responsible for communicating with the other authors about progress, submissions of revisions and final approval of proofs.

We confirm that we have provided a current, correct email address which is accessible by the Corresponding Author and which has been configured to accept email from kyaw.thu.813@m.kyushu-u.ac.jp.

Kyaw Thu, Ph.D.

Associate Professor

Department of Advanced Environmental Science and Engineering

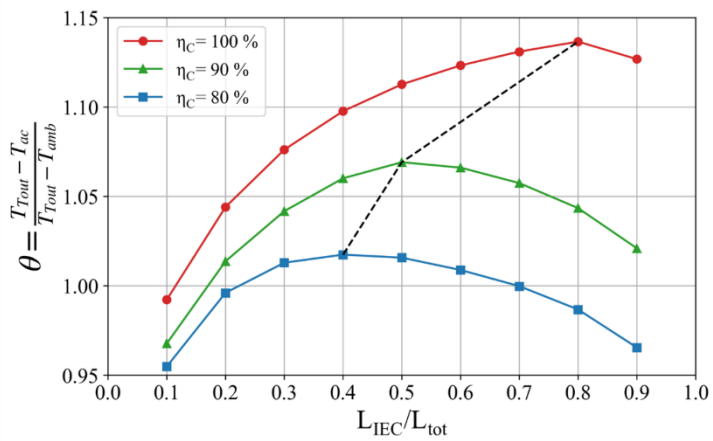
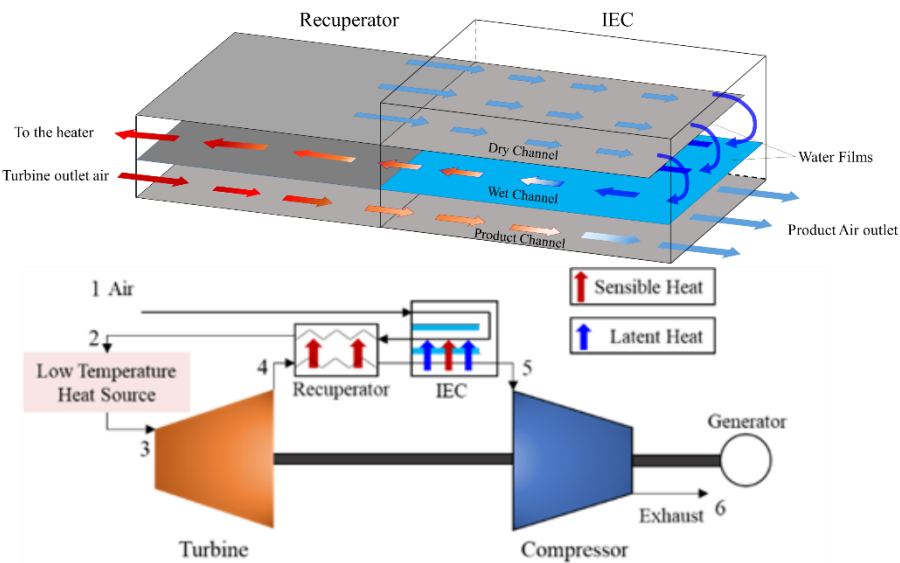
Faculty of Engineering Sciences

Kyushu University,

Kasuga-koen 6-1, Kasuga-shi, Fukuoka 816-8580, Japan

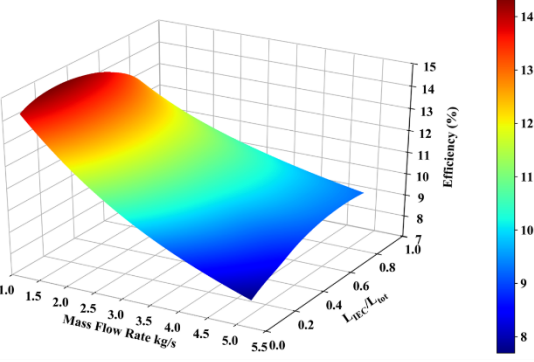
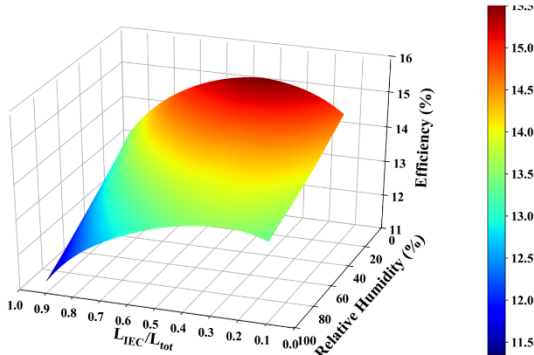
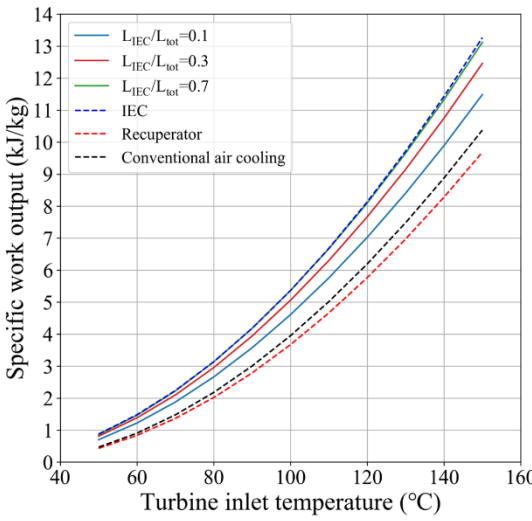
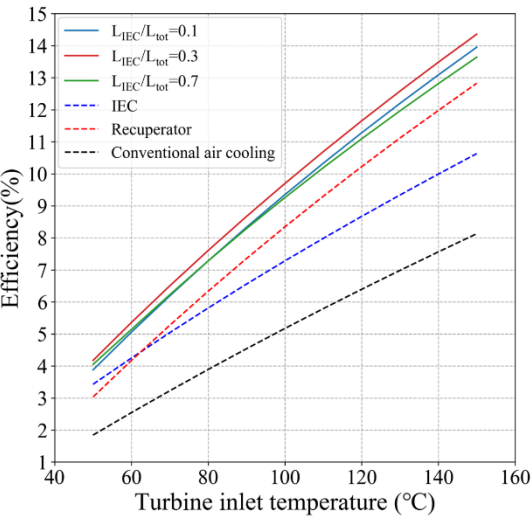
Tel:+81-92-583-7831, Fax:+81-92-583-7833, Email: kyaw.thu.813@m-kyushu-u.ac.jp

Inverted Brayton Cycle with a regenerative M-power cycle



Efficiency improvement : 77 %

Specific work output improvement : 20%



Highlights

- Proposed a recuperation and air saturation device for improved IBC performance
- Compared RHME-IBC system with the recuperative and conventional IEC-IBC systems
- Evaluated optimized L_{IEC} / L_{tot} for thermal efficiency and specific work output
- The cycle delivers improved thermal efficiency from 8.13% to 14.36%

Credit Author Statement

Kohei Matsui: Conceptualization, Methodology, Software, Writing – original draft, Visualization.

Jie Lin: Writing – review, revision & editing.

Kyaw Thu: Conceptualization, Supervision, Visualization, Writing – original draft, review, revision & editing

Takahiko Miyazaki: Conceptualization, Supervision & Review

On the Performance Improvement of an Inverted Brayton Cycle using a Regenerative Heat and Mass Exchanger

Kohei Matsui¹, Jie Lin², Kyaw Thu^{1,3,*}, Takahiko Miyazaki^{1,3,*}

¹ Department of Advanced Environmental Science and Engineering, Faculty of Engineering
Sciences, Kyushu University

Kasuga-koen 6-1, Kasuga-city, Fukuoka 816-8580, Japan

² Department of Engineering Science, University of Oxford
Parks Road, Oxford OX1 3PJ, United Kingdom

³ Thermal Science and Engineering Division, International Institute of Carbon-Neutral
Energy Research (I2CNER), Kyushu University
744 Motoooka, Nishi-ku, Fukuoka 819-0395, Japan

Corresponding authors' email: kyaw.thu.813@m.kyushu-u.ac.jp (K. Thu)
miyazaki.takahiko.735@m.kyushu-u.ac.jp (T. Miyazaki)

Abstract

Recovery of the low-temperature waste heat for electricity generation has been gaining a significant interest. An Inverted Brayton Cycle (IBC) is often employed to convert the low-temperature waste-heat to electricity while the thermal efficiency and specific work output are poor. In this paper, a new energy recovery scheme is introduced incorporating the IBC with a Regenerative Heat and Mass Exchanger (RHME). The RHME is a heat and mass exchanger that consolidates a recuperator (for thermal efficiency improvement) and an Indirect Evaporative Cooler (for enhanced specific work). Numerical models for RHME and the IBC were judiciously developed where possible condensation in the product air channel was accounted for. The model was validated with the experimental data and the cycle was investigated for various waste-heat sources (50 – 150 °C). When compared to a conventional air-cooling IBC system, incorporating the current energy recovery scheme increases the thermal efficiency from 8.13% to 14.36% and specific work output from 10.38 to 12.46 kJ/kg

equivalent to 76.63% and 20.1% improvements, respectively. The unprecedented performance improvement is realised from the exploitation of the regenerative and air-saturation (cooling) mechanisms for both energy recovery and cooling of the working fluid.

Keywords: Inverted Brayton cycle; Indirect evaporative cooler; Waste heat utilisation; Power generation

Nomenclature

c_p	specific heat capacity	kJ/kg/K
d	channel height	m
D	mass diffusivity	m ² /s
D_h	hydraulic diameter	m
Gz	Graetz number	–
h	convective heat transfer coefficient, specific enthalpy	W/m ² /K, kJ/kg
h_m	convective mass transfer coefficient	m/s
k	thermal conductivity	W/m/K
l	length	m
Nu	Nusselt number	–
P	pressure	Pa
Pr	Prandtl number	–
q	specific thermal energy	kJ/kg
RH	relative humidity	%
Re	Reynolds number	–
Sc	Schmidt number	–
Sh	Sherwood number	–
St	Stanton number	–
St_m	mass transfer Stanton number	–
T	temperature	K
t	thickness	m
v	velocity	m/s
w	specific work	kJ/kg
x	humidity ratio	g/kg [DA]
z	distance	m

Greek symbols

ε	convergence criteria	—
η	efficiency	—
κ	specific heat ratio	—
λ	friction coefficient	—
μ	viscosity	Pa s
π	pressure ratio	—
ρ	density	kg/m ³
ϕ	thermal resistance ratio	—

Subscripts

d	dry channel
en	entry region
H	heater
IEC	indirect evaporative cooler
net	net
opt	optimum
p	product channel
rec	recuperator
s	surface
th	thermal
tot	total
w	wet channel
wd	w adjacent to d
wp	w adjacent to p

1 Introduction

Electricity, considered as the most flexible and convenient form of energy, plays an important role in multi-energy system (MES) and integrated energy systems [1,2]. Hence, demand and generation of electricity are increasing with the latest demand in the electrification of transport sector [3–6] while, transitions to renewable power generation have been actively pursued [7,8]. On the other hand, recovery and utilisation of waste heat from multiple processes can be effective means for securing power since waste heat accounts for 23 – 53% of the world's energy input [9]. Tchanche [10] and Ammar et al. [11] reported the temperature range and capacities of waste heat from various sources, such as transportation and industrial sectors.

Waste heat is often converted into cooling/heating [12–14] (absorption [15–17] and adsorption [18–20] heat pumps) and/or potable water [21–23]. However, these commodities are not exchangeable to other forms or

among them without the additional energy input. On the other hand, electricity can be utilised to obtain any of the aforesaid commodities using systems such as mechanical vapour compression [24], capacitive deionization [25] and reversed osmosis [26,27] at reasonable efficiencies. Thus, the direct conversion of waste heat to electricity has been gaining significant attention. Electricity generating cycles using low-temperature waste heat include Organic Rankine Cycle (ORC) [28–30], Organic Flash Cycles (OFC) [31–33], Trilateral Flash Cycle (TFC) [34–36], Kalina cycle [37,38] and Brayton-type cycles (conventional and inverted type) [39–42]. Detailed reviews on the thermodynamic cycles for electricity generation from low-temperature heat sources can be found in the works of Galanis et al. [43] and Garcia et al. [44].

An Inverted Brayton Cycle (IBC) which is the interest of the present article, operates at atmosphere to sub-atmospheric pressures. The advantages of an IBC over other cycles (e.g. ORC and Kalina cycle) lie in its simplicity and availability of the required turbomachinery components [42,45]. A typical IBC exerts a back pressure below the atmospheric pressure on the working air, and the cycle does not raise the pressure significantly above the atmosphere which is ideal for co-generative applications [46–48]. An influential study by Bianchi and De Pascale [49] compared three bottoming cycles (ORC, Stirling and IBC) for various heat source temperatures. The specific energy output of the IBC was reported to be in the range of 10 – 70 kJ/kg depending on the temperature and amount of condensable water at the inter-cooler outlet. The authors concluded that IBC systems were innovative and promising solutions yet with lower performance than the ORC technology, especially, for low temperatures (200 – 400 °C).

Interest in IBC has been growing. IBCs were adopted in many applications over the last few years. For example, Chen et al. proposed an IBC system for heat recovery from the exhaust gas of a gasoline turbocharged engine and reported 3.15% reduction in the fuel consumption at the optimal turbine pressure ratio [45]. Experimental and numerical works on IBC systems for waste-heat recovery from the internal combustion (IC) engine with the exhaust gas condensation were reported by Kennedy et al. [47,50]. The authors concluded that the turbine inlet temperature, turbine expansion ratio, heat exchanger pressure drop and coolant temperature were the most significant parameters that influenced the performance. Recently, Battista et al. reported that utilisation of an IBC for the waste-heat recovery of a reciprocating IC engine lead to an average power recovery of approximately 2% of the engine brake power [51].

The temperature of the compressor suction air significantly influences the performance of the IBC. According to Kakaras et al., the high-temperature intake of the compressor resulted in up to 20% power loss [52]. Fujii et al. utilized a multi-stage cooling and multi-stage compression cycle configuration and identified the inlet coolant temperature as one of the most significant parameters for the performance [53]. Various cooling schemes have been attempted for the performance improvement of the IBC [54,55]. These works considered the direct vaporisation technique where the wet-bulb temperature of the air was often the limit. On the other hand, an indirect evaporative cooler (IEC) can cool the air to temperatures close to the dew point [56,57]. Another significant benefit of using an IEC in the gas turbine cycle is the increased moisture content of the working fluid. For instance, Zhu et al. highlighted a higher system efficiency when using the humidified gas turbine cycle [58]. Thus, Brayton Cycles were often hybridized with IECs for improved performance [59–

61]. Our previous work [62] investigated the performance of the IEC-IBC system and compared with a conventional air cooling cycle and a recuperative cycle. The improved specific work output was realised by the IEC-IBC system. However, the thermal efficiency of the IEC-IBC could be higher than that of a recuperative cycle only for intake air with low humidity (20 – 40 %). This is because heat recuperation improves the thermal efficiency of a power cycle. In IEC-IBC systems, most of the thermal energy from the turbine outlet air is utilized by the IEC for moisture saturation and cooling of the air, resulting in lower thermal efficiency when compared to a recuperative cycle. Most of the sensible heat recovered in an IEC-IBC system is used up for the vaporisation of water, which subsequently increases the amount of heat input to the system.

To further advance the IBC system for effective waste-heat recovery, it is necessary to develop recovery scheme for both improved thermal efficiency and specific work output; yet, very few or no previous research work is reported in this regard. Filling the knowledge gap, thus the objective of the present work is to introduce an innovative concept, i.e., a regenerative heat and mass exchanger (RHME) which significantly improves both thermal efficiency and specific work output. The proposed RHME apportions the recovered energy for the sensible heat recuperation and evaporative cooling. The RHME consolidates the recuperative and IEC components in one unit. The performance of the RHME-IBC cycle was evaluated for various turbine inlet temperatures, mass flow rates and relative humidity values of the outdoor air. One crucial parameter that significantly influences the performance of the RHME-IBC system is the apportionment of the energy for the heat recuperation and vaporisation, i.e., the ratio of the length of the intercooler (IEC part) to the total length i.e., L_{IEC} / L_{tot} . The system was studied for various L_{IEC} / L_{tot} values. The performance of the proposed RHME-IBC system was compared with those of the recuperative and conventional IEC-IBC systems.

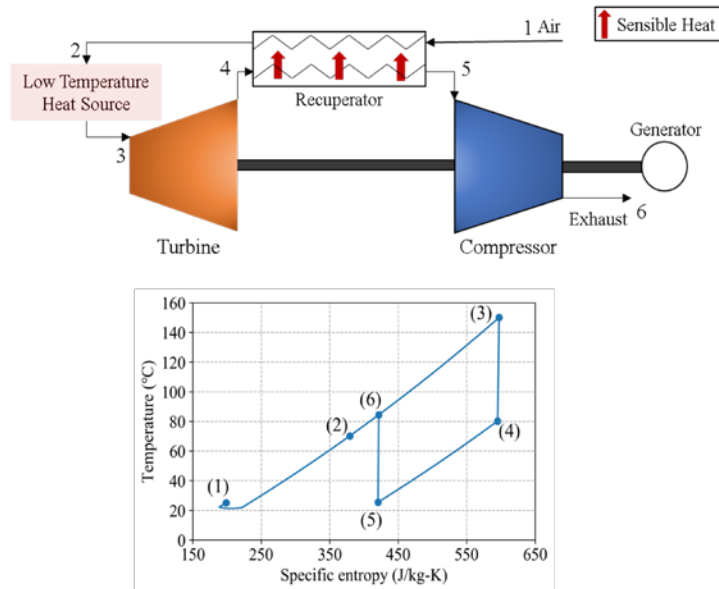
2 Description of the cycles

The objective of the present work is to develop an energy recovery scheme for an IBC for improved thermal efficiency and specific work output with the effective conversion of the waste heat to electricity. In an IBC, the heated air first flows through the turbine while rejecting the heat before being exhausted by the compressor. The power produced by the turbine exceeds that to the compressor, and thus the cycle produces a net power output. However, the thermal efficiency of a typical IBC is known to be low when operated using low-temperature heat source. For the performance improvement of the IBC in terms of thermal efficiency and the specific work output, an innovative cycle is introduced by hybridising the IBC with a regenerative heat and mass exchanger (RHME).

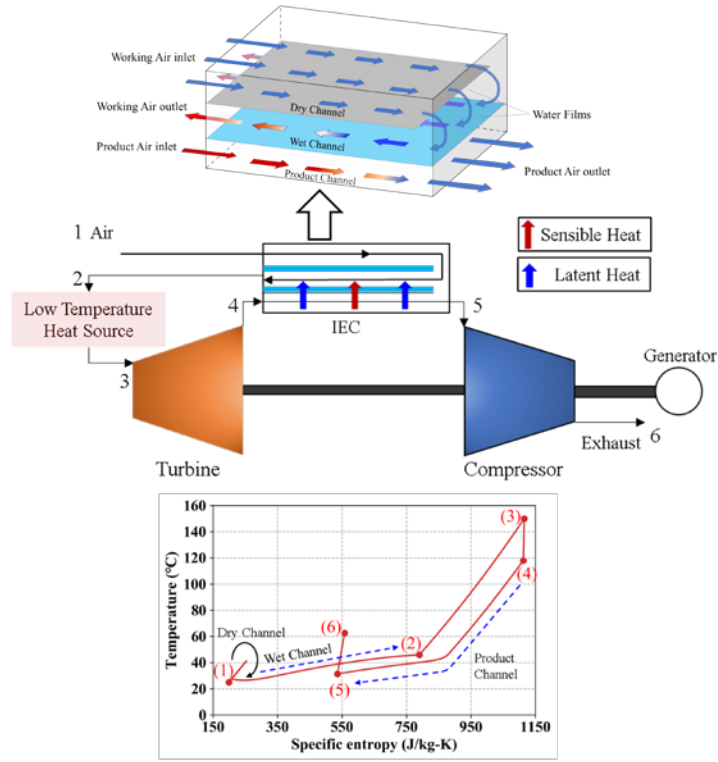
Figure 1 shows three configurations of IBC systems with different heat recovery or cooling schemes and their thermodynamic states on the temperature-entropy diagrams. Figure 1(a) shows the cycle with the sensible heat recovery only using a recuperator for the intermediate cooling. In this configuration, the outdoor air is utilised to cool down the turbine outlet temperature using a recuperator for the sensible heat exchange. Thus, the temperature and entropy of the outdoor air increase (state points 1 – 2 on the T-s diagram) and the reverse is true for the turbine outlet air (4 – 1 on the T-s diagram of Fig. 1(a)). Heat addition occurs in the process 2 to

3.

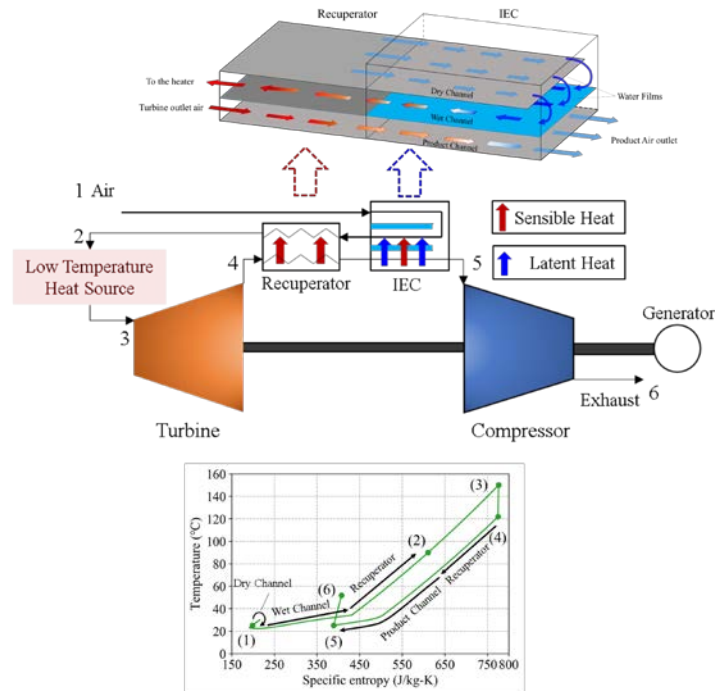
Figure 1(b) shows the hybrid IBC-IEC system that applies an indirect evaporative cooler to introduce the air cooling and saturation of the working fluid (see our previous work [62] for more details.). In this configuration, 100% of the thermal energy from the turbine outlet air is utilized in the indirect evaporative cooler (IEC) for cooling while the air temperature at state point 2 is lower when compared to that of the air at the same point in the configuration shown in Fig. 1(a). Thus, the energy input to the system in this configuration increases. Figure 1(c) shows the IBC system that incorporates the proposed regenerative heat and mass exchanger (RHME) for the recuperation, cooling and saturation of the working fluid. The RHME is a heat and mass exchanger device consolidating a recuperator (for sensible heat recovery) and an IEC (for air saturation and cooling). The objective here is to recover the sensible heat from the turbine outlet air for humidification of the intake air while cooling it down. Besides, the IEC is an essential component for reducing the compressor power. In the RHME device, the turbine outlet air is first utilized to heat up the air coming out from the wet channel of the IEC before being further cooled by the IEC. Thus, air saturation (humidification) of the outdoor air is achieved in the wet channel of the IEC which is part of the RHME while the sensible heat recovery in the recuperator. The process is illustrated on the T-s diagram in Fig. 1(c) where two slopes can be observed for the process 1 to 2 due to the air saturation in the IEC and sensible heating in the recuperator. It is expected that incorporating the RHME device will provide a significant performance improvement both in terms of thermal efficiency and the specific work output. This is because the increase in the inlet air temperature (sensible heat recovery) reduces the required heat input to the cycle. On the other hand, higher moisture content in the intake air is desirable as the specific heat of the working air increases at high humidity.



(a)



(b)



(c)

Fig. 1: Schematic diagrams and T-s plots of the inverted Brayton cycles with (a) Recuperator, (b) Indirect Evaporative Cooler, and (c) Regenerative Heat and Mass Exchanger (the proposed system)

3 Mathematical models

3.1 Regenerative heat and mass exchanger

The mathematical model of a counterflow-type regenerative heat and mass exchanger (RHME) was established by considering the energy and material balances in each channel. A steady-state, one-dimensional model was developed accounting for the distributions of the temperature and humidity along each channel. The following assumptions were adopted in the present model:

- (1) Adiabatic boundary between the system and the surrounding i.e., no heat loss from the RHME, the recuperator and the IBC.
- (2) The wet channel is covered with a very thin saturated water film, which is stationary [63].
- (3) The advection term is dominant, with a negligible diffusion term.
- (4) Fluid properties are assumed to be constant with uniform properties within each control volume.

Figure 2 shows the schematic diagrams of the proposed regenerative heat and mass exchanger (RHME) highlighting the air channels and the differential control volumes in an Eulerian system emphasising the inlet and outlet temperatures, and the humidity ratio in the IEC section, Fig. 2(b), and the recuperator section Fig. 2(c). Applying the assumption of stationary and dominant advection terms in the IEC dry channel, the temperature distribution is written as [62],

$$\left(\rho c_p v d \frac{\partial T}{\partial z} \right)_d = h_d (T_{ds} - T_d) \quad (1)$$

Here, ρ is the density of air, v is the velocity, c_p is the specific heat and h is the heat transfer coefficient of the air in the dry channel. Applying the assumptions mentioned above, the heat and mass transfer in the wet channel are modelled as [62],

$$\left(\rho c_p v d \frac{\partial T}{\partial z} \right)_w = h_w (T_{wsd} + T_{wsp} - 2T_w) \quad (2)$$

$$\left(v d \frac{\partial x}{\partial z} \right)_w = h_{mw} (x_{wsd} + x_{wsp} - 2x_w) \quad (3)$$

where x is the humidity of the wet channel air and h_{mw} is the convective mass transfer coefficient while the subscript, w , stands for the wet channel. Similarly, within the product channel, temperature and humidity changes are expressed as,

$$\left(\rho c_p v d \frac{\partial T}{\partial z} \right)_p = h_p (T_{ps} - T_p) \quad (4)$$

$$\left(\nu d \frac{\partial x}{\partial z} \right)_p = h_m (x_{ps} - x_p) \quad (5)$$

The surface temperatures of the plate separating the dry channel and the wet channel (dry channel side; T_{ds} , wet channel side; T_{wsd}) derived from the energy balance are written as,

$$T_{ds} = (1 - \phi_d) T_d + \phi_d \left[T_w - \frac{St_m}{St_w} \frac{L_w}{c_{pw}} (x_{ws} - x_w) \right] \quad (6)$$

$$T_{wsd} = \phi_{wd} T_d + (1 - \phi_{wd}) \left[T_w - \frac{St_m}{St_w} \frac{L_w}{c_{pw}} (x_{ws} - x_w) \right] \quad (7)$$

The temperatures of the plate surface separating the wet channel and the product channel were derived in the similar fashion. Note that the condensation can occur in the product channel because of the possibility of the working air in the product channel with high humidity. In the present model, the amount of condensation is calculated from the gradient between the humidity of the working air in the product channel and the plate surface humidity. Therefore, the surface temperatures of the partition plate on the wet channel side and the product channel side T_{wsp} and T_{ps} are respectively expressed by the following equations.

$$T_{wsp} = \phi_{wp} T_p + (1 - \phi_{wp}) \left[T_w - \frac{St_{mw}}{St_w} \frac{L_w}{c_{pw}} (x_{wsp} - x_w) - \frac{St_{mp}}{St_p} \frac{L_{wp}}{c_{pp}} (x_{ps} - x_p) \right] \quad (8)$$

$$T_{ps} = (1 - \phi_p) T_p + \phi_p \left[T_w - \frac{St_{mw}}{St_w} \frac{L_w}{c_{pw}} (x_{wsp} - x_w) - \frac{St_{mp}}{St_p} \frac{L_{wp}}{c_{pp}} (x_{ps} - x_p) \right] \quad (9)$$

If the surface saturation humidity is higher than the humidity of the working air in the product channel, (i.e., condensation does not occur in the channel), the third term in the brackets of the above two equations is zero. Here, ϕ is a dimensionless number calculated from the ratio of the thermal resistance. The expressions of ϕ in the dry channel and the wet channel are described as,

$$\phi_d = \frac{1/h_d}{1/h_d + t_{pl}/k_{pl} + 1/h_w} \quad (10)$$

$$\phi_{wd} = \frac{1/h_w}{1/h_d + t_{pl}/k_{pl} + 1/h_w} \quad (11)$$

Figure 2(c) shows the control volume of the recuperator section of the RHME where the low-temperature side of the recuperator is connected to the wet channel of the IEC, and the high-temperature side (turbine outlet air-flow path) of the recuperator is connected to the product channel. Here, the subscripts w and p , as well as rec , are adopted. The energy balances of the air streams in the control volume of the recuperator part of RHME (Fig. 2(c)) are written as,

$$\left(\rho c_p v d \frac{\partial T}{\partial z} \right)_{w,rec} = h_{w,rec} (T_{ws,rec} - T_{w,rec}) \quad (12)$$

$$\left(\rho c_p v d \frac{\partial T}{\partial z} \right)_{p,rec} = h_{p,rec} (T_{ps,rec} - T_{p,rec}) \quad (13)$$

The humidity change in the high-temperature channel of the recuperator is expressed by equation (14). Again, the change in humidity is zero if the saturation humidity of air does not exceed the saturation humidity of the wall surface.

$$\left(v d \frac{\partial x}{\partial z} \right)_{p,rec} = h_{m,p,rec} (x_{ps,rec} - x_{p,rec}) \quad (14)$$

The wall temperature, $T_{ws,rec}$ and $T_{ps,rec}$, in the recuperator are expressed by the following equations. Similar to equations (8) and (9), if the saturation humidity of air does not exceed the saturation humidity of the wall surface, the second term in the brackets becomes zero.

$$T_{wsp,rec} = \phi_{wp,rec} T_{p,rec} + (1 - \phi_{wp,rec}) \left[T_{w,rec} - \frac{St_{mp,rec} L_{ps,rec}}{St_{p,rec} c_{pp,rec}} (x_{ps,rec} - x_{p,rec}) \right] \quad (15)$$

$$T_{ps,rec} = (1 - \phi_{p,rec}) T_{p,rec} + \phi_{p,rec} \left[T_{w,rec} - \frac{St_{mp,rec} L_{ps,rec}}{St_{p,rec} c_{pp,rec}} (x_{ps,rec} - x_{p,rec}) \right] \quad (16)$$

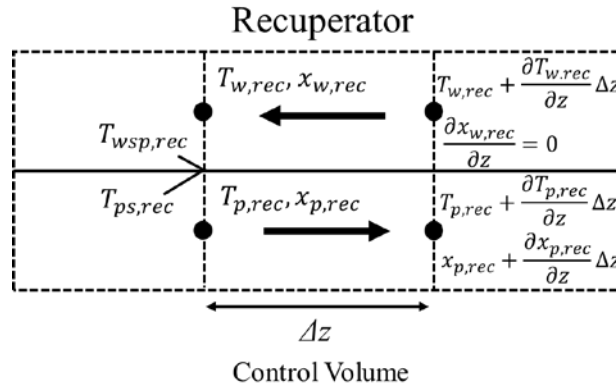
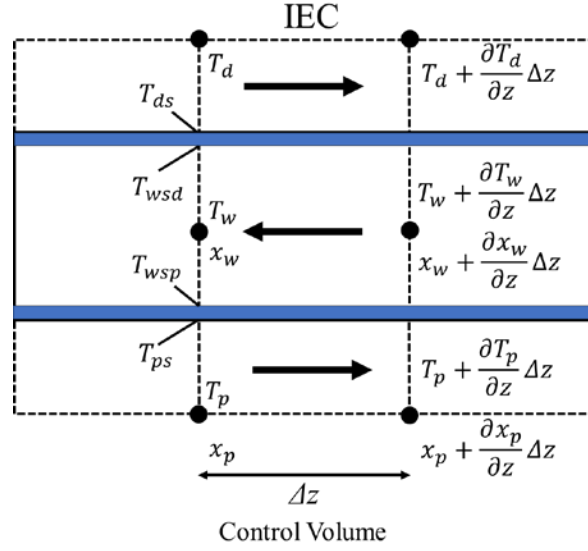
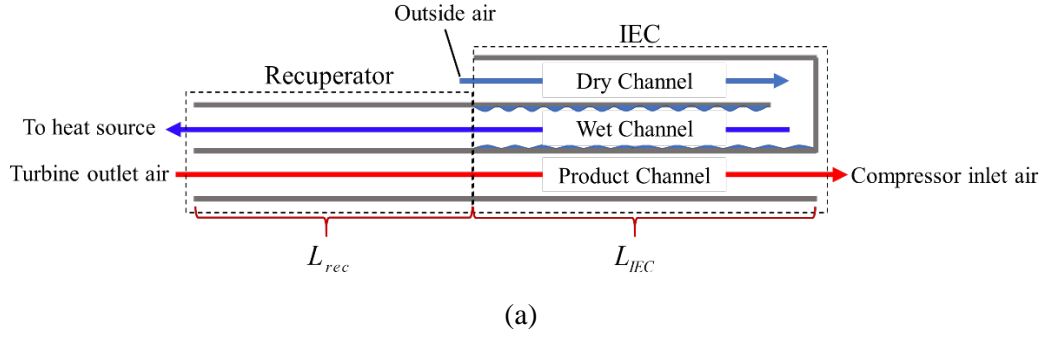


Fig. 2: Flow direction in the proposed cycle and control volumes describing the temperature and humidity for the model development, (a) flows in the channels of RHME, (b) control volume of the IEC section of the RHME and (c) control volume of the Recuperator section of RHME

The Nusselt number is used for estimating the heat transfer coefficient. As the surface temperature varies in a small range [63], the Nusselt number at constant temperature in laminar flow is employed to approximate the convective heat transfer between the channel surface and the air flow, except for the entry region [64,65];

and the following constant values are assumed except for the entry region [64] as,

$$Nu = 7.54 \quad (17)$$

The entry length l_{en} is calculated from Reynolds number Re , Prandtl number Pr and hydraulic diameter $D_h = 4A/P$ as [64],

$$l_{en} = 0.05 Re Pr D_h \quad (18)$$

Nusselt number in the entry region is calculated using Greatz number, $Gz = D_h Re Pr / z$ and Prandtl number, Pr , by the following equation [63] as

$$Nu = \frac{\frac{7.54}{\tanh\left(2.264 Gz^{\frac{1}{3}} + 1.7 Gz^{\frac{2}{3}}\right)} + 0.0499 Gz \tanh(Gz^{-1})}{\tanh\left(2.432 Pr^{\frac{1}{6}} Gz^{\frac{1}{6}}\right)} \quad (19)$$

The mass transfer coefficient is obtained from Sherwood number $Sh = h_m D_h / D$, applying the analogy of heat transfer and mass transfer, and is expressed in terms of Schmidt number $Sc = \mu / \rho D$, and Prandtl number Pr as,

$$Sh = Nu \left(\frac{Sc}{Pr} \right)^{\frac{1}{3}} \quad (20)$$

The mass diffusivity, D , used in Sherwood number is computed as [66],

$$D = 22.0 \times 10^{-6} \left(\frac{T}{273.15} \right)^{1.75} \left(\frac{101325}{p} \right) \quad (21)$$

Stanton number, St , and mass transfer Stanton number, St_m are given as,

$$St = \frac{h}{\rho c_p v} \quad (22)$$

$$St_m = \frac{h_m}{v} \quad (23)$$

The pressure loss in the channel is accounted for and calculated using the Darcy–Weisbach equation as [67][68],

$$\Delta p = \lambda \frac{\Delta z}{D_h} \frac{\rho v^2}{2} \quad (24)$$

Here, λ is the laminar friction coefficient, $\lambda=64/Re$. The temperature and humidity distributions of the working air in the recuperator and IEC shown above were solved using the fourth-order Runge-Kutta method [69], and the surface temperature of the partition was solved using the modified Powell method [70]. Figure 3 shows the simulation flow of the system. The area to be calculated was divided into multiple control volumes, and calculations were performed sequentially based on the initial conditions. First, equations for the working fluid were solved followed by computation of the temperatures of the partition plate surface from the temperature, humidity, velocity, and pressure. These calculations were repeated until the solution converged. Thermodynamic properties of moist air and water were adopted from HAPropsSI routines of CoolProp [71].

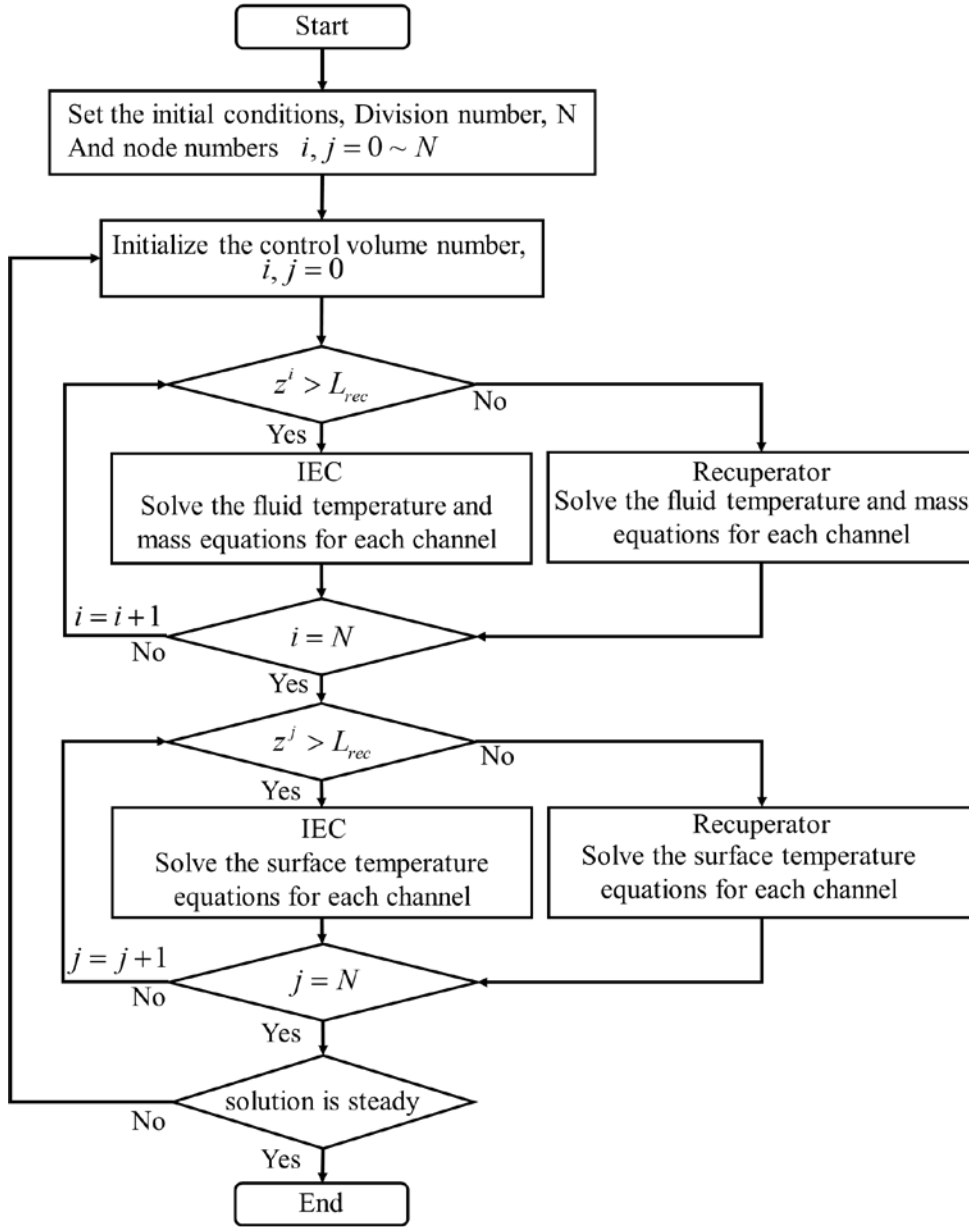


Fig. 3: The calculation flow of the indirect evaporative cooler

3.2 Validation of the numerical model

The numerical model was first validated using the experimental data of a counterflow IEC conducted by Riangvilaikul and Kumar [72]. Table 1 summarises the outlet air temperatures for various temperatures and humidity values of the inlet air comparing the experimental data. The maximum absolute average deviation (AAD) is observed to be 3.95% while the lowest AAD is 0.12% showing a good agreement between experimental data and predictions of the current model.

Table 1. The validation of the IEC model with the experimental results of Riangvilaikul and Kumar [72]

Humidity	Inlet	Air	Outlet Air Temperature (°C)	AAD (%)
----------	-------	-----	-----------------------------	---------

(g/kg [DA])	Temperature (°C)	<i>Experiment</i>	<i>Present model</i>	
6.9	25.01	15.51	15.05	2.94
	30.02	16.45	16.30	0.93
	35.03	17.32	17.30	0.12
	39.92	17.97	18.12	0.81
	45.02	18.62	18.81	1.02
11.2	24.84	19.35	18.58	3.95
	30.11	20.43	19.76	3.31
	35.03	21.09	20.64	2.10
	40.53	21.88	21.45	1.99
	45.02	22.68	21.99	3.06
20.0	30.02	26.23	25.82	1.58
	35.00	26.88	26.52	1.35
	40.04	27.68	27.10	2.10
	45.02	28.48	27.58	3.17
26.4	32.32	30.07	29.84	0.79
	35.43	30.51	30.18	1.07
	40.33	31.45	30.65	2.54
	44.99	32.10	31.03	3.35

3.3 Thermodynamic model of the inverted Brayton cycle (IBC)

Referring to the schematic diagram of the IBC (Fig. 1c), the thermodynamic model is summarised in Table 2. General assumptions invoked in the IBC models are: (1) constant specific heat and specific heat ratio across the turbine and compressor, (2) the same pressure ratios for the compressor and turbine with no pressure drop, and (3) ideal gas assumption for the working fluid. The optimum pressure ratio π_{opt} that maximises the cycle thermal efficiency can be obtained by differentiating w_{net} with respect to π and setting it to zero while the derivation can be found in [62]. The cycle calculation was carried out following the flow chart as shown in Fig. 4 until the convergence criteria was met. The thermophysical properties of the air (enthalpy, specific heat, etc.) in the turbine and compressor were computed at their inlets as functions of temperature, pressure and humidity ratio at specific points using the Humid Air Properties (HAPropsSI routines) of CoolProp.

Table 2. Summary of the mathematical equations for the cycle performance calculation of the IBC

No.	Component	Equation	Remarks
-----	-----------	----------	---------

			$h(T, p, x)$ values were adopted from HAPropsSI of CoolProp.
1	Net specific work, w_{net}	$w_{net} = (h_3 - h_4) - (h_6 - h_5)$	
2	Pressure ratio, π	$\pi = \frac{p_4}{p_3}$	
3	Turbine outlet temperature, T_4	$T_4 = T_3 \pi^{\frac{\kappa-1}{\kappa} \eta_r}$	$\kappa = 1.4$, constant $c_p(T, p, x)$ across the turbine and compressor.
4	Compressor outlet temperature, T_6	$T_6 = T_5 \pi^{\frac{\kappa-1}{\kappa} \frac{1}{\eta_c}}$	
5	Optimum pressure ratio, π_{opt}	$\pi_{opt} = \left(\frac{1}{\eta_T \eta_C} \frac{c_{p,5} T_5}{c_{p,3} T_3} \right)^{\frac{1}{\eta_r + \frac{1}{\eta_c}}}$	$c_p(T, p, x)$ values were adopted from HAPropsSI of CoolProp.
6	Specific heat input, q_H	$q_H = h_3 - h_2$	
7	Cycle thermal efficiency, η_{th}	$\eta_{th} = \frac{w_{net}}{q_H}$	

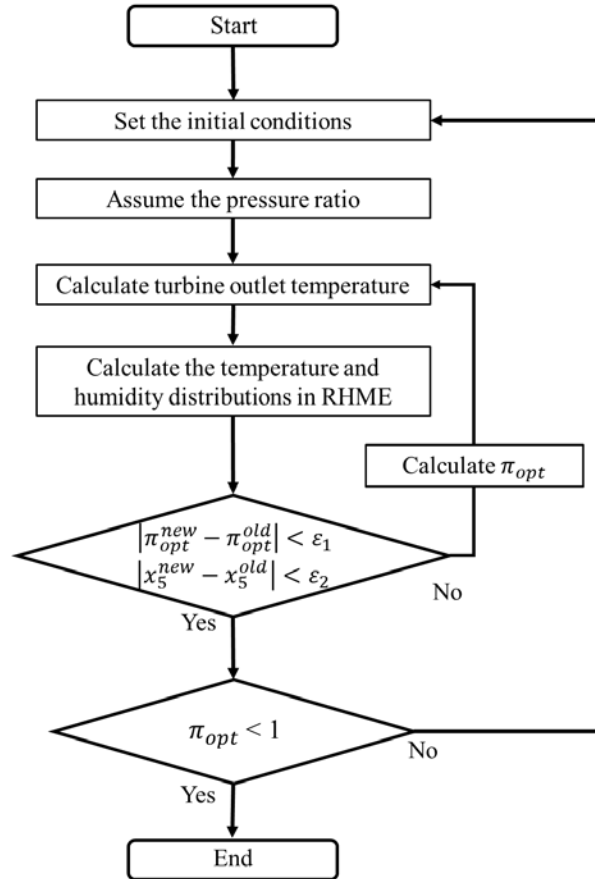


Fig. 4: Cycle calculation flow of the proposed RHME-IBC system

4 Results and Discussion

The performance of the proposed RHME-IBC system is investigated for various operating conditions and Table 3 lists the parameters used in the calculations. These conditions (compressor inlet temperatures, efficiencies of the compressor and turbine etc.) are adopted from many studies on IBC systems reported in the literature [41,45,49,58]. This section first describes the effect of the adiabatic efficiency of the compressor on the cycle performance. The temperature distribution and the humidity distribution in the recuperator and IEC in the cycle are confirmed, and detailed behaviour is scrutinised. Then, the effects of various parameters on cycle performance are evaluated and discussed. Finally, the performance of the present RHME-IBC is compared with other configurations, i.e., a conventional air-cooling system, a recuperative IBC system and an IEC-IBC system.

Table 3 List of parameters used in simulations

Parameter (Unit)	Value	Nominal values
Ambient temperature (°C)	25	25
Ambient pressure (Pa)	101325	101325
Ambient Relative humidity (%)	20 – 100	60
Turbine inlet temperature (°C)	50 – 150	150
Total length, L_{tot} (m)	2 – 10	5
Ratio of IEC length to total length, L_{IEC} / L_{tot} (–)	0.1 – 0.9	0.3
Channel height (mm)	10	10
Total inflow area (m ²)	1.0	1.0
Inlet mass flow rate (kg/s)	1.0 – 5.0	1.0
Compressor isentropic efficiency, η_C (%)	80 – 100	100
Turbine isentropic efficiency, η_T (%)	80 – 100	100
Other mechanical efficiency (%)	100	100

4.1 Cycle performance analysis with varying turbine and compressor efficiencies

The effect of turbine and compressor efficiencies on the cycle performance was first examined (Figure 5). The adiabatic efficiencies of both turbine and compressor were varied independently from 80% to 100%, while other parameters were set at their nominal values given in Table 3. In general, the thermal efficiency and specific work output improve at higher turbine and compressor efficiency. The maximum thermal efficiency

of the cycle was observed to be 10.63% at ideal turbine and compressor efficiency (i.e., 100%), corresponding to the specific work output of 13.43 kJ/kg. At the bottom left of the figure, where the turbine and compressor efficiency values approach 80%, the thermal efficiency and specific work output are gradually reduced.

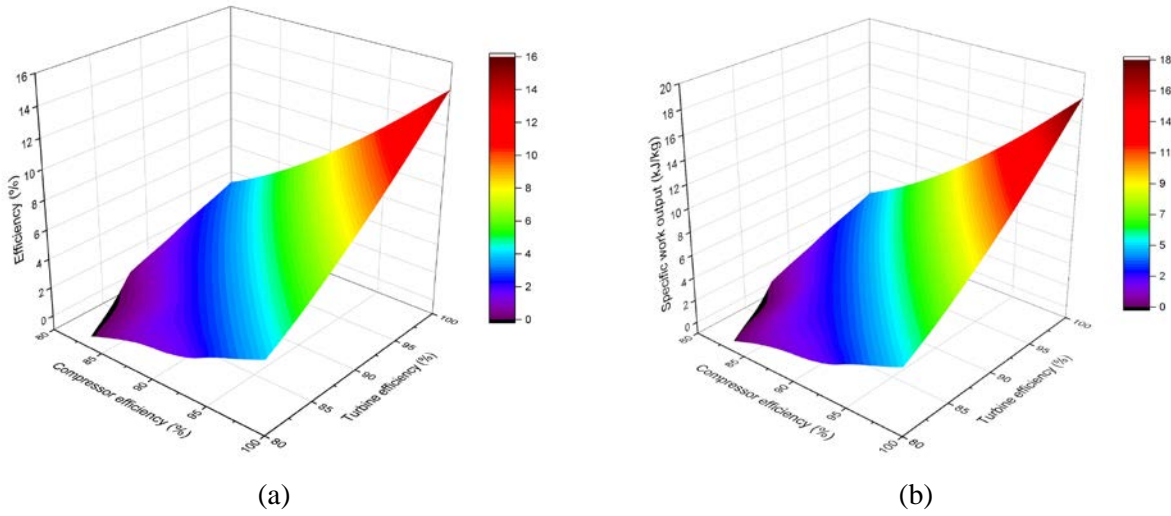
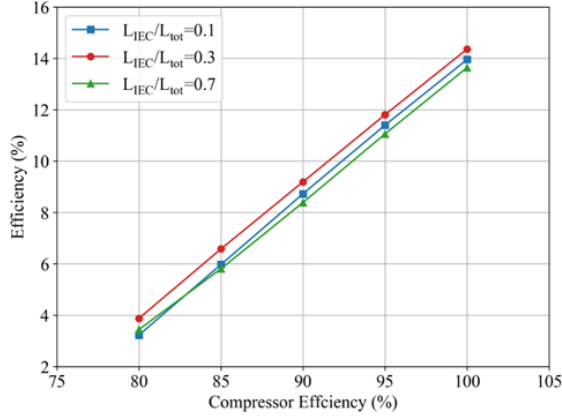
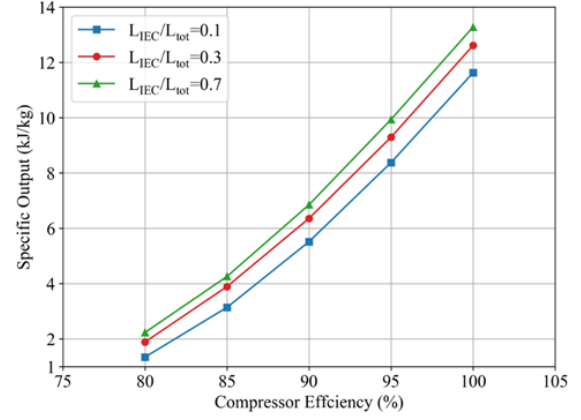


Fig.5: The performance of the cycle for various turbine and compressor efficiency (a) Thermal efficiency, and (b) Specific work output

The effects of varying apportionments of the recuperator and the IEC of the RHME, L_{IEC} / L_{tot} , were investigated. Figure 6 shows the effects of the compressor adiabatic efficiency on the cycle thermal efficiency, and the specific work output for L_{IEC} / L_{tot} values of 0.1, 0.3 and 0.7. The ratio, L_{IEC} / L_{tot} , is an important parameter in optimising the system performance. It is noted that higher values of L_{IEC} / L_{tot} prioritise the recovery for the latent heat and air saturation while the lower ratios favour the sensible heat recovery. From Fig. 6(a), it can be observed that the thermal efficiency linearly varies with the compressor efficiency as a general trend. The efficiency first increases with increasing value of L_{IEC} / L_{tot} , i.e., from 0.1 to 0.3. However, a further increase in L_{IEC} / L_{tot} value leads to a lower efficiency. This is because the amount of recuperative heat influences the heat input to the cycle and increasing L_{IEC} / L_{tot} results in the substantial heat input to the cycle. On the other hand, a higher specific work is realised when the IEC section is increased, i.e., the increased L_{IEC} / L_{tot} value (see Fig. 6(b)) irrespective of the compressor efficiency. The thermal efficiency results highlight the existence of the optimal ratio of the heat recuperation and air-saturation (cooling) by the IEC sections. Figure 7 shows the cycle thermal efficiency and the specific work output for varying L_{IEC} / L_{tot} value at constant turbine inlet temperature of 150 °C while keeping the compressor efficiency values 100% (Fig. 7(a)) and 80% (Fig. 7(b)). The maximum thermal efficiency is realised at the L_{IEC} / L_{tot} value of 0.3 for both cases. However, the rates of change in the thermal efficiency and specific work output are different. In Fig. 7(a), when L_{IEC} / L_{tot} exceeds 0.3, the decrease in the thermal efficiency is relatively steep. On the other hand, from Fig. 7(b), the efficiency decrement is rather gradual, highlighting the sensitivity of the performance to the compressor adiabatic efficiency.

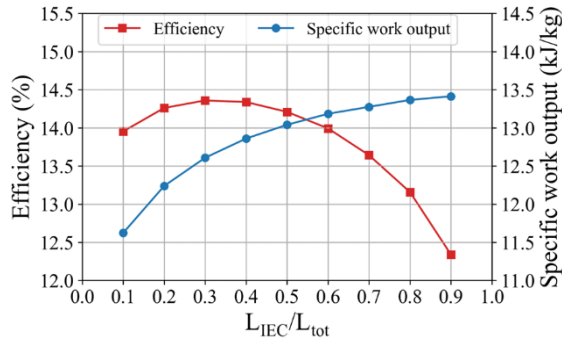


(a)

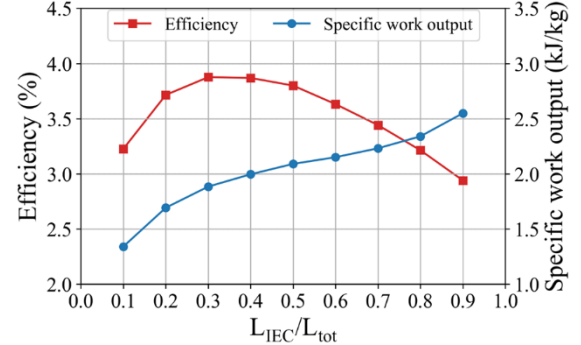


(b)

Fig.6: The effect of the compressor efficiency for three sets of L_{IEC} / L_{tot} values on (a) Efficiency, and (b) Specific output



(a)



(b)

Fig.7: Thermal efficiency and specific work output at various L_{IEC} / L_{tot} values at the constant turbine inlet temperature of 150 °C with (a) 100% compressor adiabatic efficiency, and (b) 80% compressor adiabatic efficiency

Figure 8 shows the temperature and humidity distributions in the channels of the regenerative heat and mass exchanger (RHME) highlighting the recuperator and IEC sections for the compressor efficiency of 100%. The left side of the dotted line in Fig. 8 is the recuperator section and the right side the IEC part. As shown in Fig. 1(c), the atmospheric air flows into the dry channel before flowing into the wet channel at the right end of the RHME device. The turbine outlet air enters the product channel from the left end while being cooled along the channel. From Fig. 8, it can be observed that the increase in the ratio of L_{IEC} / L_{tot} leads to the decrease in the product air temperature which correctly demonstrates the influence of the heat and mass exchanger (IEC). Note, however, that the temperature of the air at the wet channel outlet also decreases, consequently, leading to the increase in the heat input to the cycle for the isobaric heating process. The results highlight the trade-off between the heat recuperation and the intermediate cooling of the working air, which can be adjusted by

varying L_{IEC} / L_{tot} value. From the perspectives of thermal efficiency and specific work output, it is necessary to employ the optimal L_{IEC} / L_{tot} value.

As highlighted in the previous section, condensation may occur in the channels for some apportionments of the recuperator and IEC sections. Figure 9 shows the temperature and humidity distribution in the RHME when the compressor efficiency is set at 80%. It is noted that condensation occurs in the product channel for L_{IEC} / L_{tot} values greater than 0.1. Condensation in the product channel occurs due to the increase in the humidity of the working air, which can be seen from the humidity distribution plots. When the condensation occurs, the cooling of the working air in the product channel is limited by the release of latent heat. The cycle is further

analysed using the cooling efficiency, $\theta = \frac{T_{Tout} - T_{ac}}{T_{Tout} - T_{amb}}$, which is the ratio of the temperature difference of the air across the product channel to that between the RHME outlet and the ambient air. Figure 10 shows the relationship between the cooling efficiency, θ , and L_{IEC} / L_{tot} values for the compressor efficiency values of 80%, 90%, and 100%. As can be seen from Fig. 10, L_{IEC} / L_{tot} values for the maximum cooling efficiency decreases with decreasing compressor efficiency. This is because of the increase in the turbine outlet air temperature, which is attributable to the increase in the pressure ratio at low compressor efficiencies. The results further highlight that extending the IEC region of the RHME does not necessarily improve cooling efficiency.

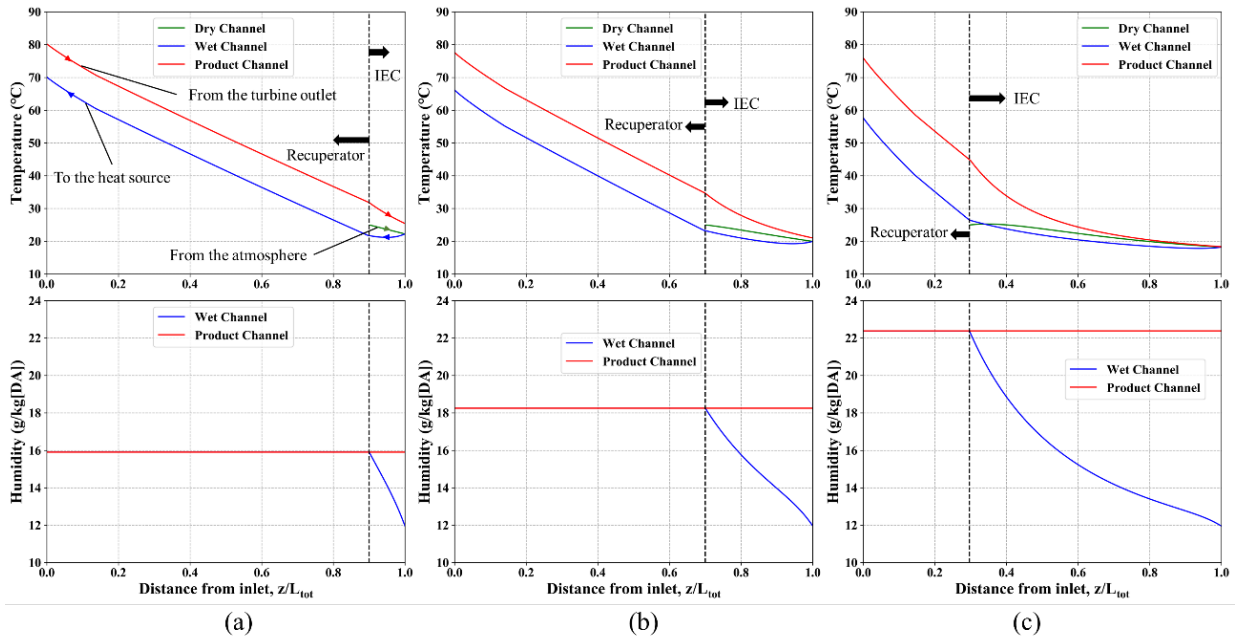


Fig.8: Temperature and humidity distribution along the channels at the compressor efficiency of 100 % with
(a) $L_{IEC} / L_{tot} = 0.1$, (b) $L_{IEC} / L_{tot} = 0.3$, and (c) $L_{IEC} / L_{tot} = 0.7$

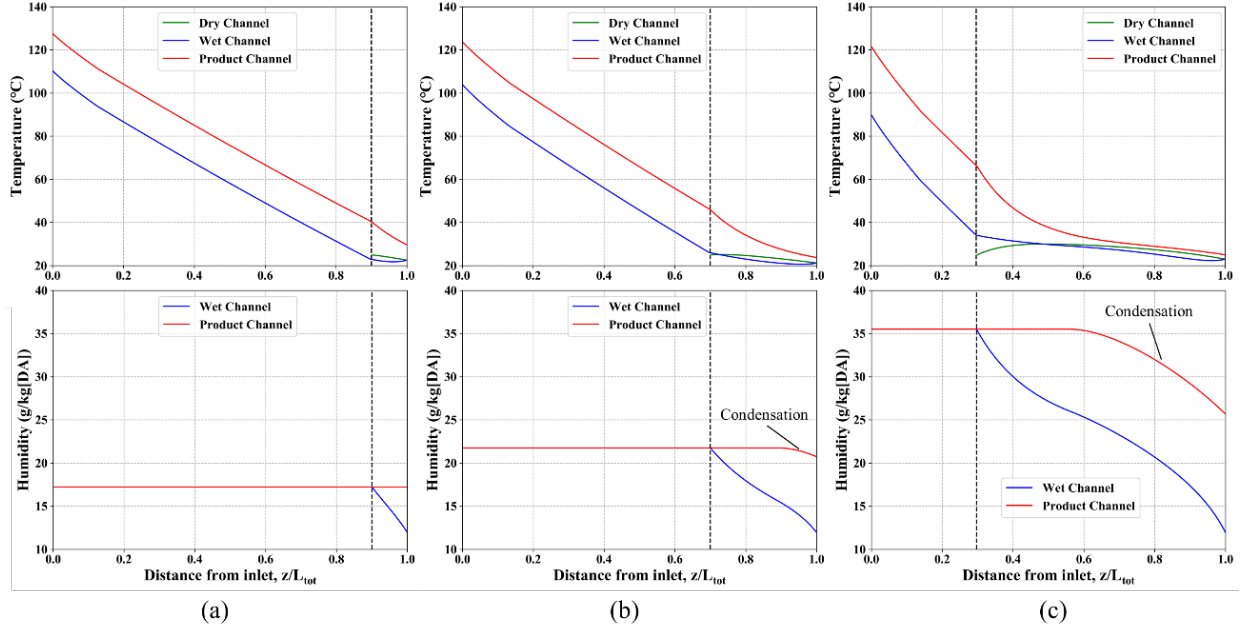


Fig.9: Temperature and humidity distribution along the channels at the compressor efficiency of 80 % with (a) $L_{IEC} / L_{tot} = 0.1$, (b) $L_{IEC} / L_{tot} = 0.3$, and (c) $L_{IEC} / L_{tot} = 0.7$ highlighting condensation

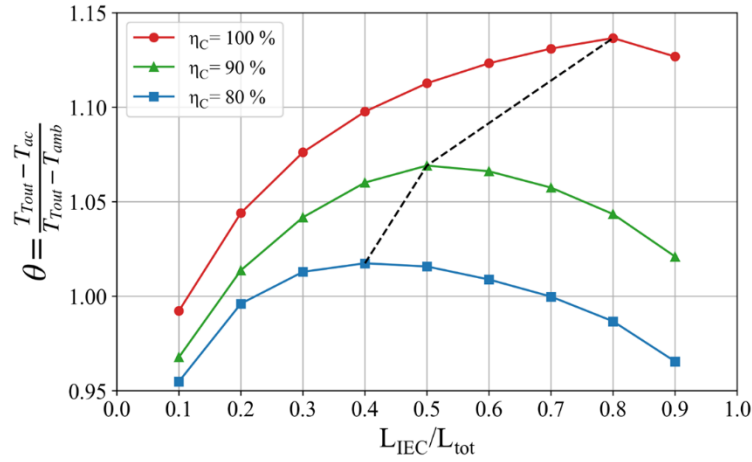


Fig. 10: The effect of varying L_{IEC} / L_{tot} value on the cooling efficiency, θ

4.2 Effect of the turbine inlet air temperature

The optimal recuperative to IEC ratio of the RHME is further confirmed by varying the turbine inlet temperature. Figure 11 shows the change in the cycle thermal efficiency and specific work output depending on the turbine inlet temperature where the highest cycle thermal efficiency is observed when L_{IEC} / L_{tot} equals 0.3 for all turbine inlet temperatures (Fig. 11(a)). It is noted that larger apportionment of the IEC in the RHME device provides higher thermal efficiency when the turbine inlet temperature is below 80 °C. However, a further increase in the turbine inlet temperature favours a smaller apportionment of the IEC. The lower the

turbine inlet temperature, the lower sensible heat regeneration by the recuperator, and the greater the specific work output. This is because the increase in the humidity of the air by the IEC contributes to a high cycle thermal efficiency. Nevertheless, the specific work output increases if the IEC portion of the RHME is increased for all turbine inlet temperatures.

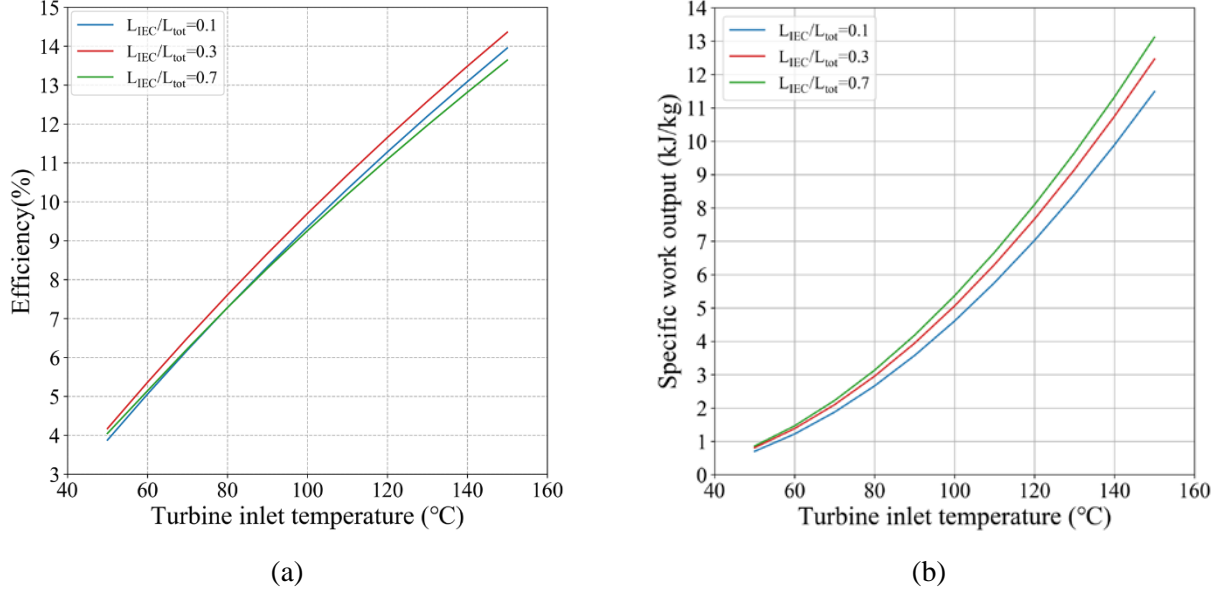


Fig. 11: The impact of the turbine inlet temperature on (a) Thermal efficiency, and (b) Specific work output for three sets of L_{IEC} / L_{tot} values

4.3 Effect of mass flow rate on the cycle performance

Changes in the intake mass flow lead to the variations in the fluid velocity inside the RHME device. As the intake mass flow increases, the fluid velocity in the cooler naturally increases while the cooling efficiency decreases due to the higher flow velocity. Figure 12 shows the cycle thermal efficiency and the specific work output with varying intake mass flow rates. It is noted that low flow rates of the intake air exhibit high efficiency and specific work output. As can be seen in Fig. 12(b), the specific work output increases with increasing L_{IEC} / L_{tot} value for all mass flow rates. However, the L_{IEC} / L_{tot} value for optimal thermal efficiency changes significantly highlighting that a shorter recuperative portion is desirable for low air velocities. For higher air flow rates, the temperature gradient along the channel decreases because of the higher velocity. The dependency of the thermal efficiency of the proposed cycle on the intake mass flow rate and L_{IEC} / L_{tot} value is depicted in Fig. 12 (c). The results further highlight that higher thermal efficiency values can be realised at low air intake flow and higher apportionment of the sensible heat recovery, i.e., low L_{IEC} / L_{tot} value.

Table 4 summarises the detailed cycle parameters for inlet mass flow rates of 1 kg/s and 5 kg/s with varying L_{IEC} / L_{tot} values. When the inlet air mass flow rate is 1 kg/s, the temperature difference of the product air, T_5 , between L_{IEC} / L_{tot} values of 0.1 and 0.9 is 6.9 °C. Therefore, the pressure ratio does not change significantly, and the effect of the recuperator on thermal efficiency becomes relatively large. On the other hand, when the

inlet mass flow rate is 5 kg/s, there is a large difference in the temperature after cooling, T_5 , i.e., 22.6 °C (51.7 °C for $L_{IEC} / L_{tot} = 0.1$ and 29.1 °C for $L_{IEC} / L_{tot} = 0.9$). The better intercooling performance due to the increase in the IEC ratio improves the pressure ratio and decreases the thermal efficiency since the rise in the inlet mass flow rate becomes insignificant.

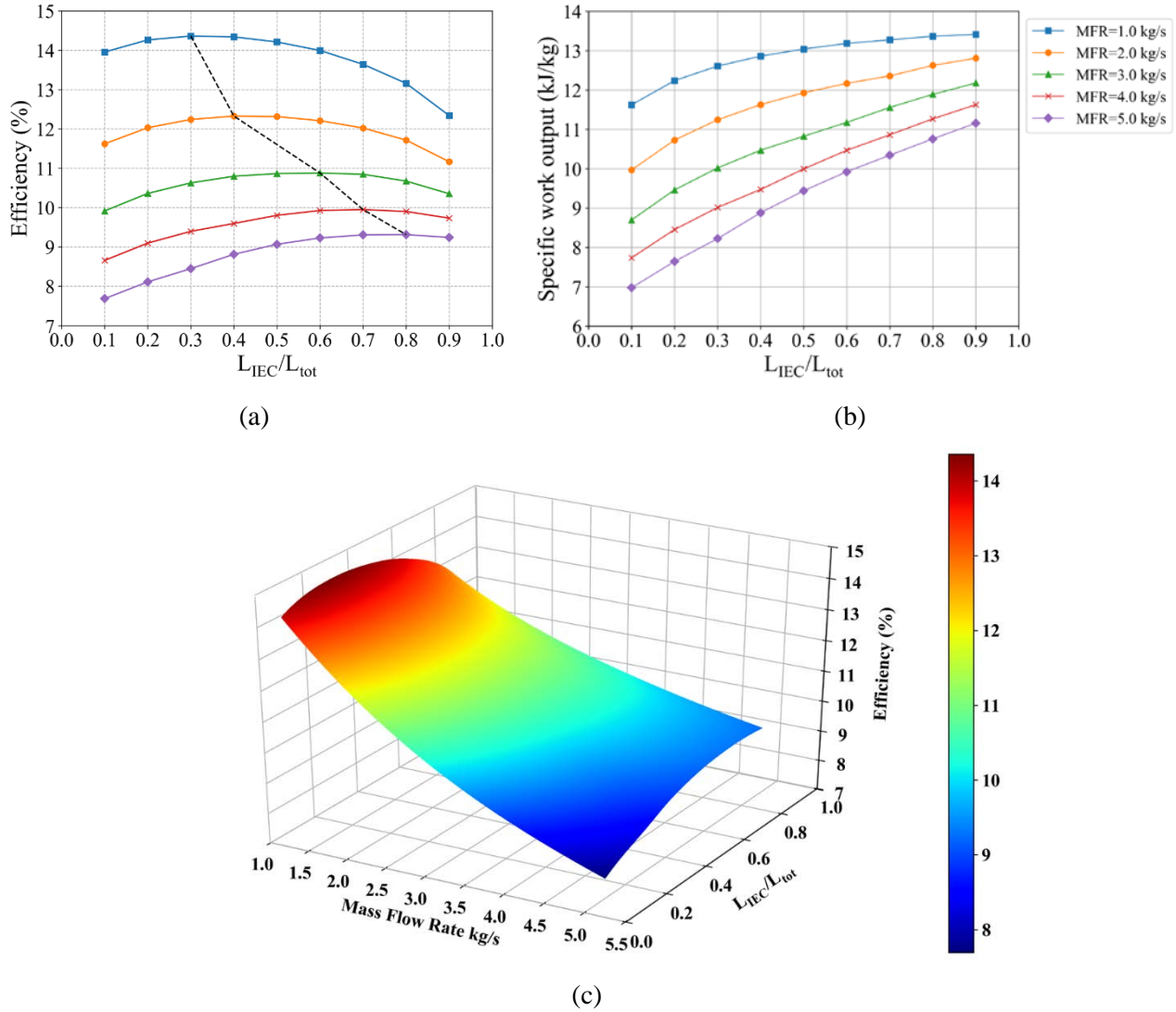


Fig. 12: The performance of the cycle for various L_{IEC} / L_{tot} values and mass flow rates (a) Thermal efficiency, (b) Specific work output and (c) Efficiency variation with mass flow rate and IEC ratio

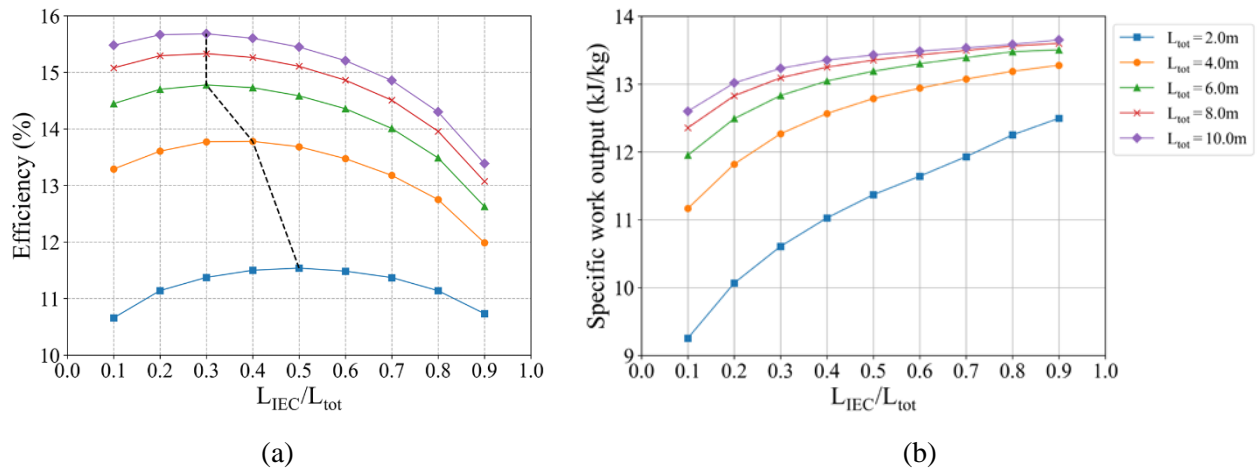
Table 4. Detailed on the cycle parameters for the inlet mass flow rates of 1 kg/s and 5 kg/s

Inlet mass flow rate (kg/s)	L_{IEC} / L_{tot}	Temperature before heating, T_2 (°C)	Input Heat, q_H (kJ/kg)	Pressure ratio, P_4/P_3	Temperature after cooling, T_5 (°C)
1.0	0.1	70.1	82.3	0.53	25.4
	0.3	66.1	86.8	0.52	21.0

		0.5	62.6	90.7	0.51	19.2
		0.7	57.7	96.2	0.51	18.3
		0.9	47.8	107.4	0.51	18.5
		0.1	62.7	89.7	0.62	51.7
		0.3	57.0	96.2	0.59	44.1
	5.0	0.5	51.2	102.9	0.57	37.4
		0.7	45.2	109.8	0.56	32.9
		0.9	37.0	119.3	0.54	29.1

4.4 Effect of the total length of RHME on the cycle performance

The performance of the RHME-IBC system is investigated for different lengths of the RHME device, as shown in Fig. 13. In general, increasing the length of the RHME device provides higher efficiency and specific work output. However, Fig. 13(b) depicts that improvement in the specific work output becomes insignificant when the length is more than 6.0 m. In Fig. 13(a), the thermal efficiency tends to decrease as the IEC ratio (L_{IEC} / L_{tot}) increases, so the total length and IEC ratio are always important factors to be considered. From these results (the effects of inlet mass flow rate and the total length), the ratio of IEC should be increased if the conditions are not favourable for the heat recuperation. Fig. 13(c) demonstrates the influence of the total length and L_{IEC} / L_{tot} value on the efficiency of the cycle depicting the improved thermal efficiency of the RHME-IBC system for low L_{IEC} / L_{tot} value and extended total length of the RHME unit. It is noted that air situation, i.e., the high L_{IEC} / L_{tot} value is beneficial for the RHME with shorter length in terms of thermal efficiency.



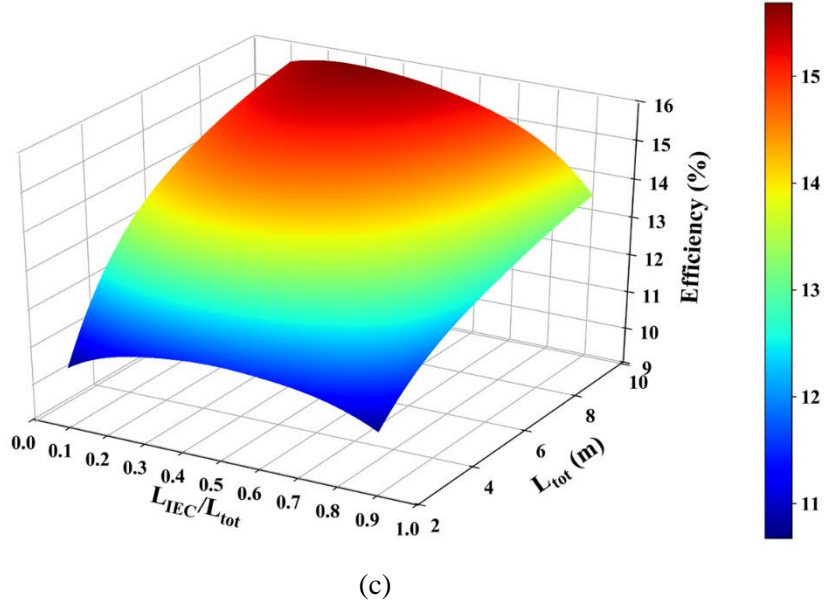
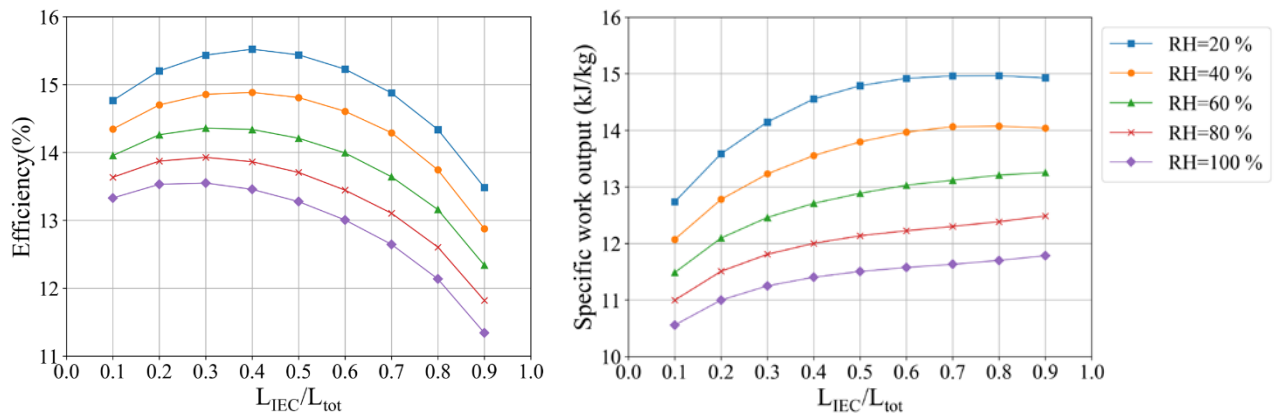


Fig. 13: The performance of the cycle for various L_{IEC} / L_{tot} values and the total length of RHME (a) Thermal efficiency, (b) Specific work output and (c) Efficiency variation with the total length and IEC ratio

4.5 Impact of relative humidity

The relative humidity of the working air is an important parameter for the performance of an IEC device. In general, the lower the atmospheric air humidity, the better the IEC cooling performance. Figure 14 shows the cycle performance with varying relative humidity of the surrounding air from 20% to 100%. From Fig. 14(a) and 14(b), it can be observed that the cycle performance improves for low relative humidity of the intake air. Thermal efficiency increases almost linearly with decreasing relative humidity. Figure 14(a) shows that the optimum L_{IEC} / L_{tot} value changes depending on the relative humidity of the intake air. Operating the system using the intake air with low relative humidity requires higher air situation ratio (higher L_{IEC} / L_{tot} value) to attain the optimal performance. This is because an extended section of the IEC is required for sufficient air situation in the wet channel. Fig. 14(c) shows the thermal efficiency with varying relative humidity and L_{IEC} / L_{tot} value highlighting the thermal efficiency at low RH and optimal L_{IEC} / L_{tot} value.



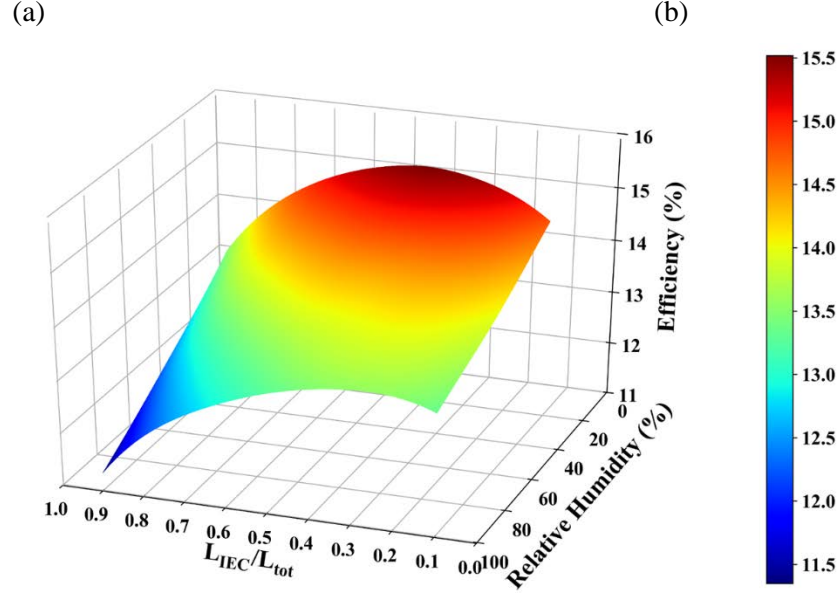


Fig. 14: The performance of the cycle for various L_{IEC} / L_{tot} values and the relative humidity of the intake air
 (a) Thermal efficiency, (b) Specific work output, (c) Efficiency variation with the humidity of the intake air and IEC ratio

4.6 Performance comparison with various IBC cycles

The performance improvement by the proposed RHME-IBC cycle is assessed against a conventional air-cooling system, a recuperative IBC system and an IEC-IBC system. Figure 15 shows the thermal efficiency and the specific work output of various IBC-based cycles for different turbine inlet temperatures. The proposed RHME-IBC cycle exhibits a significant improvement in thermal efficiency, for all L_{IEC} / L_{tot} values (0.1, 0.3 and 0.7). As reported in our previous work, the thermal efficiency of an IEC-IBC system is rather low since almost all sensible heat is used for the vaporisation of water. When comparing the present system having $L_{IEC} / L_{tot} = 0.3$ with the Recuperator IBC system, the thermal efficiency is improved to 4.12% from 3.0% at the turbine inlet temperature of 50 °C. The improvement in the thermal efficiency is more significant at higher turbine inlet temperatures. In terms of specific work output, the results highlight that higher L_{IEC} / L_{tot} ratios lead to the enhanced specific work at the expense of the thermal efficiency. Nevertheless, the proposed RHME-IBC cycle offers a comparable specific work output to that of an IEC-IBC system. It is observed that the apportionment of the recuperator and the IEC device in RHME (L_{IEC} / L_{tot}) at 0.3 provides the highest thermal efficiency with comparable specific work output with IEC-IBC system.

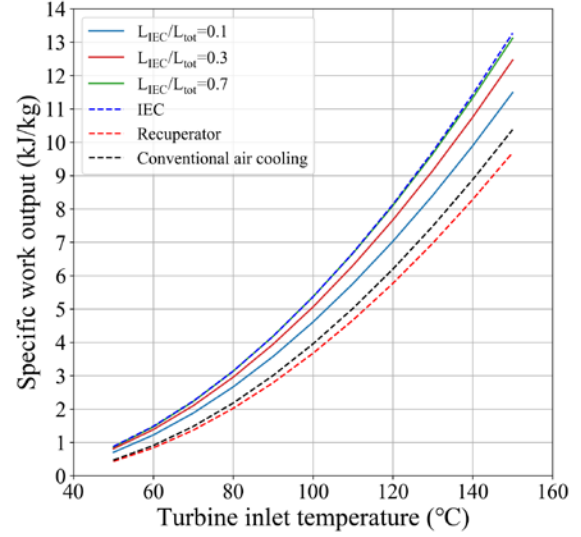
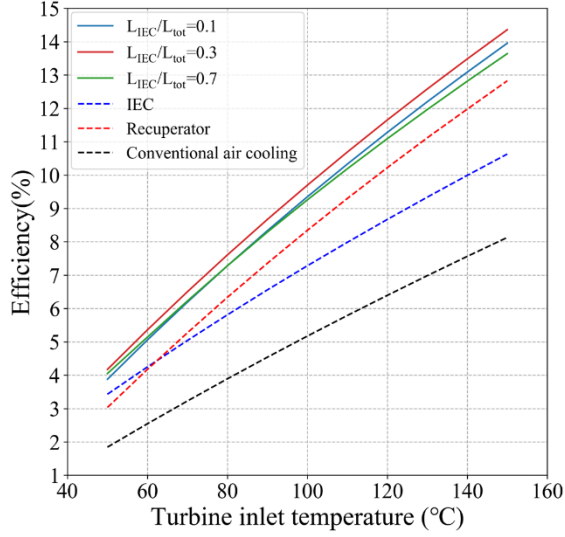


Fig. 15: Performance comparison of the RHME-IBC system with a conventional air-cooling cycle, a recuperative cycle and the hybrid IEC-IBC cycles (a) Thermal efficiency and (b) Specific work output

Table 5. The percentage improvement by the RHME-IBC system in terms of thermal efficiency and the specific work output

Parameter	Baseline	% improvement as compared to the baseline cycle (%)		
	Air-cooling	Recuperator	IEC-IBC	RHME-IBC ($L_{IEC} / L_{tot} = 0.3$)
η_{th} (%)	8.13	57.79	30.77	76.63
w_{net} (kJ/kg)	10.38	-6.66	27.86	20.08

Table 5 summarises the percentage improvement in the performance by the proposed regenerative heat and mass exchanger system incorporated with the IBC system keeping a conventional air-cooling cycle as a baseline. It is noted that the current cycle offers up to 76.63% improvement in thermal efficiency while exhibiting 20.08% increase in the specific work output. Such an unprecedentedly high performance (both thermal efficiency and specific work output) is realised due to exploitation of the regenerative and air-saturation (cooling) mechanisms for the energy recovery and cooling of the working fluid.

5 Conclusions

In this paper, an innovative energy recovery scheme for Inverted Brayton Cycles (IBCs) was introduced for improved thermal efficiency and specific work output realising the effective conversion of the waste heat to electricity. The proposed recovery scheme utilises a Regenerative Heat and Mass Exchanger (RHME) that consolidates the recuperator for the sensible heat recovery and an Indirect Evaporative Cooler (IEC) for the air situation. A numerical model for both RHME and the IBC has been judiciously developed accounting for the

possible condensation in the product air channel. The experimentally-verified IEC model was incorporated into the performance calculation of the cycle. The cycle was investigated for various low-temperature waste-heat (50 to 150 °C) sources. A comprehensive investigation was conducted to evaluate the influences of the adiabatic efficiencies of the compressor and the turbines, the air situation ratio (L_{IEC} / L_{tot} ratio), turbine inlet temperatures, intake air conditions (flow rates and relative humidity) and length of the recovery device comparing against the conventional IBC system. The key contributions and important observations of the present work are as follows:

- The proposed hybrid cycle achieves high cooling efficiency, thus high specific work output by using the latent heat of the water through an evaporative cooling technique.
- Different optimal values of situation ratio (L_{IEC} / L_{tot}) were observed; $L_{IEC} / L_{tot} = 0.3$ for the optimal thermal efficiency and $L_{IEC} / L_{tot} = 0.7$ for the specific work output.
- Both thermal efficiency and specific work output increase with lowering intake air flow rates while higher apportionment of sensible heat recovery (recuperator) in the RHME device is necessary for low air intake flows for optimal thermal efficiency ($L_{IEC} / L_{tot} = 0.3$ for air intake of 1.0 kg/s).
- For the RHME with a shorter total length, the increased air situation, i.e., the high L_{IEC} / L_{tot} value is beneficial for the thermal efficiency.
- The current cycle increases the thermal efficiency from 8.13% to 14.36% (76.63% improvement), while exhibiting 20.08% increase in the specific work output when comparing to a conventional air-cooling IBC cycle.

References

- [1] Kong X, Sun F, Huo X, Li X, Shen Y. Hierarchical optimal scheduling method of heat-electricity integrated energy system based on Power Internet of Things. *Energy* 2020;210:118590. doi:10.1016/J.ENERGY.2020.118590.
- [2] Dancker J, Klabunde C, Wolter M. Sensitivity factors in electricity-heating integrated energy systems. *Energy* 2021;229:120600. doi:10.1016/J.ENERGY.2021.120600.
- [3] Chen Y, Zhang L, Xu P, Di Gangi A. Electricity demand response schemes in China: Pilot study and future outlook. *Energy* 2021;224:120042. doi:10.1016/J.ENERGY.2021.120042.
- [4] Kan X, Reichenberg L, Hedenus F. The impacts of the electricity demand pattern on electricity system cost and the electricity supply mix: A comprehensive modeling analysis for Europe. *Energy* 2021;235:121329. doi:10.1016/J.ENERGY.2021.121329.
- [5] Eshraghi H, Rodrigo de Queiroz A, Sankarasubramanian A, DeCarolus JF. Quantification of climate-induced interannual variability in residential U.S. electricity demand. *Energy* 2021;236:121273. doi:10.1016/J.ENERGY.2021.121273.
- [6] Energy Information Administration U. International Energy Outlook 2019. 2019.
- [7] Nagatomo Y, Ozawa A, Kudoh Y, Hondo H. Impacts of employment in power generation on renewable-based energy systems in Japan— Analysis using an energy system model. *Energy* 2021;226:120350. doi:10.1016/J.ENERGY.2021.120350.
- [8] Lohrmann A, Child M, Breyer C. Assessment of the water footprint for the European power sector during the transition towards a 100% renewable energy system. *Energy* 2021;233:121098. doi:10.1016/J.ENERGY.2021.121098.
- [9] Firth A, Zhang B, Yang A. Quantification of global waste heat and its environmental effects. *Appl Energy* 2019;235:1314–34. doi:10.1016/J.APENERGY.2018.10.102.
- [10] F. Tchanche B, Pétrissans M, Papadakis G. Heat resources and organic Rankine cycle machines. *Renew Sustain Energy Rev* 2014;39:1185–99. doi:10.1016/J.RSER.2014.07.139.
- [11] Ammar Y, Joyce S, Norman R, Wang Y, Roskilly AP. Low grade thermal energy sources and uses from the process industry in the UK. *Appl Energy* 2012;89:3–20. doi:10.1016/J.APENERGY.2011.06.003.
- [12] Hiltunen P, Syri S. Low-temperature waste heat enabling abandoning coal in Espoo district heating system. *Energy* 2021;231:120916. doi:10.1016/J.ENERGY.2021.120916.
- [13] Wang S, Zhang L, Liu C, Liu Z, Lan S, Li Q, et al. Techno-economic-environmental evaluation of a combined cooling heating and power system for gas turbine waste heat recovery. *Energy* 2021;231:120956. doi:10.1016/J.ENERGY.2021.120956.
- [14] Xu J, Luo E, Hochgreb S. A thermoacoustic combined cooling, heating, and power (CCHP) system for waste heat and LNG cold energy recovery. *Energy* 2021;227:120341. doi:10.1016/J.ENERGY.2021.120341.

- [15] Aly WIA, Abdo M, Bedair G, Hassaneen AE. Thermal performance of a diffusion absorption refrigeration system driven by waste heat from diesel engine exhaust gases. *Appl Therm Eng* 2017;114:621–30. doi:10.1016/J.APPLTHERMALENG.2016.12.019.
- [16] Sun F, Li J, Fu L, Li Y, Wang R, Zhang S. New configurations of district heating and cooling system based on absorption and compression chillers driven by waste heat of flue gas from coke ovens. *Energy* 2020;193:116707. doi:10.1016/J.ENERGY.2019.116707.
- [17] Hu T, Shen Y, Kwan TH, Pei G. Absorption chiller waste heat utilization to the desiccant dehumidifier system for enhanced cooling – Energy and exergy analysis. *Energy* 2022;239:121847. doi:10.1016/J.ENERGY.2021.121847.
- [18] Chan CW, Ling-Chin J, Roskilly AP. A review of chemical heat pumps, thermodynamic cycles and thermal energy storage technologies for low grade heat utilisation. *Appl Therm Eng* 2013;50:1257–73. doi:10.1016/J.APPLTHERMALENG.2012.06.041.
- [19] Mitra S, Muttakin M, Thu K, Saha BB. Study on the influence of adsorbent particle size and heat exchanger aspect ratio on dynamic adsorption characteristics. *Appl Therm Eng* 2018;133:764–73. doi:10.1016/J.APPLTHERMALENG.2018.01.015.
- [20] Ismail A Bin, Li A, Thu K, Ng KC, Chun W. Pressurized adsorption cooling cycles driven by solar/waste heat. *Appl Therm Eng* 2014;67:106–13. doi:10.1016/j.applthermaleng.2014.02.063.
- [21] Thu K, Kim Y-D, Shahzad MW, Saththasivam J, Ng KC. Performance investigation of an advanced multi-effect adsorption desalination cycle. *Soc. Air-conditioning Refrig. Eng. Korea, SAREK*, vol. 159, Elsevier; 2014, p. 469–77. doi:10.1016/j.apenergy.2015.09.035.
- [22] Thu K, Kim Y-D, Amy G, Chun WG, Ng KC. A hybrid multi-effect distillation and adsorption cycle. *Appl Energy* 2013;104:810–21. doi:10.1016/j.apenergy.2012.12.007.
- [23] Mitra S, Thu K, Saha BB, Srinivasan K, Dutta P. Modeling study of two-stage, multi-bed air cooled silica gel + water adsorption cooling cum desalination system. *Appl Therm Eng* 2017;114. doi:10.1016/j.applthermaleng.2016.12.011.
- [24] Thu K, Mitra S, Saha BB, Murthy SS. Thermodynamic feasibility evaluation of hybrid dehumidification – mechanical vapour compression systems. *Appl Energy* 2018;213:31–44. doi:https://doi.org/10.1016/j.apenergy.2018.01.024.
- [25] Qin M, Deshmukh A, Epsztein R, Patel SK, Owoseni OM, Walker WS, et al. Comparison of energy consumption in desalination by capacitive deionization and reverse osmosis. *Desalination* 2019;455:100–14. doi:10.1016/J.DESAL.2019.01.003.
- [26] Werber JR, Deshmukh A, Elimelech M. Can batch or semi-batch processes save energy in reverse-osmosis desalination? *Desalination* 2017;402:109–22. doi:10.1016/J.DESAL.2016.09.028.
- [27] Elimelech M, Phillip WA. The Future of Seawater Desalination: Energy, Technology, and the Environment. *Science* (80-) 2011;333:712–7. doi:10.1126/science.1200488.
- [28] Li T, Wang Q, Zhu J, Hu K, Fu W. Thermodynamic optimization of organic Rankine cycle using two-stage evaporation. *Renew Energy* 2015;75:654–64. doi:10.1016/J.RENENE.2014.10.058.

- [29] Fu H, He Q, Song J, Shi X, Hao Y, Du D, et al. Thermodynamic of a novel advanced adiabatic compressed air energy storage system with variable pressure ratio coupled organic rankine cycle. *Energy* 2021;227:120411. doi:10.1016/J.ENERGY.2021.120411.
- [30] Liu B-T, Chien K-H, Wang C-C. Effect of working fluids on organic Rankine cycle for waste heat recovery. *Energy* 2004;29:1207–17. doi:10.1016/J.ENERGY.2004.01.004.
- [31] Lee W-Y, Kim M, Sohn Y-J, Kim S-G. Power optimization of a combined power system consisting of a high-temperature polymer electrolyte fuel cell and an organic Rankine cycle system. *Energy* 2016;113:1062–70. doi:10.1016/J.ENERGY.2016.07.093.
- [32] Ho T, Mao SS, Greif R. Increased power production through enhancements to the Organic Flash Cycle (OFC). *Energy* 2012;45:686–95. doi:10.1016/J.ENERGY.2012.07.023.
- [33] Mondal S, Alam S, De S. Performance assessment of a low grade waste heat driven organic flash cycle (OFC) with ejector. *Energy* 2018;163:849–62. doi:10.1016/J.ENERGY.2018.08.160.
- [34] Smith IK, da Silva RPM. Development of the Trilateral Flash Cycle System Part 2: Increasing Power Output with Working Fluid Mixtures. *Proc Inst Mech Eng Part A J Power Energy* 1994;208:135–44. doi:10.1243/PIME_PROC_1994_208_022_02.
- [35] Smith IK, Stošić N, Aldis CA. Development of the Trilateral Flash Cycle System: Part 3: The Design of High-Efficiency Two-Phase Screw Expanders. *Proc Inst Mech Eng Part A J Power Energy* 1996;210:75–93. doi:10.1243/PIME_PROC_1996_210_010_02.
- [36] Smith IK. Development of the Trilateral Flash Cycle System: Part 1: Fundamental Considerations. *Proc Inst Mech Eng Part A J Power Energy* 1993;207:179–94. doi:10.1243/PIME_PROC_1993_207_032_02.
- [37] Bahrampoury R, Behbahaninia A. Thermodynamic investigation of dual-separator Kalina cycle system: Comparative study. *Proc Inst Mech Eng Part A J Power Energy* 2018;232:282–92. doi:10.1177/0957650917720288.
- [38] Jurgen RK. The promise of the Kalina cycle. *IEEE Spectrum*; (United States) n.d.
- [39] Moran MJ, Shapiro HN, Boettner DD, Bailey MB. *Fundamentals of Engineering Thermodynamics*. Wiley; 2010.
- [40] Bejan A, Tsatsaronis G, Moran MJ. *Thermal Design and Optimization*. Wiley; 1996.
- [41] Agnew B, Anderson A, Potts I, Frost TH, Alabdoadaim MA. Simulation of combined Brayton and inverse Brayton cycles. *Appl Therm Eng* 2003;23:953–63. doi:10.1016/S1359-4311(03)00019-X.
- [42] Wilson DG, Duntelman NR. *The Inverted Brayton Cycle for Waste-Heat Utilization* 1973. doi:10.1115/73-GT-90.
- [43] Galanis N, Cayer E, Roy P, Denis ES, Désilets M. Electricity generation from low temperature sources. *J Appl Fluid Mech* 2009;2:55–67.
- [44] Iglesias Garcia S, Ferreiro Garcia R, Carbia Carril J, Iglesias Garcia D. A review of thermodynamic cycles used in low temperature recovery systems over the last two years. *Renew Sustain Energy*

Rev 2018;81:760–7. doi:10.1016/J.RSER.2017.08.049.

- [45] Chagnon-Lessard N, Copeland C, Mathieu-Potvin F, Gosselin L. Maximizing specific work output extracted from engine exhaust with novel inverted Brayton cycles over a large range of operating conditions. *Energy* 2020;191:116350. doi:10.1016/J.ENERGY.2019.116350.
- [46] Bianchi M, Negri di Montenegro G, Peretto A, Spina PR. A Feasibility Study of Inverted Brayton Cycle for Gas Turbine Repowering. *J Eng Gas Turbines Power* 2005;127:599–605. doi:10.1115/1.1765121.
- [47] Kennedy I, Chen Z, Ceen B, Jones S, Copeland CD. Experimental Investigation of an Inverted Brayton Cycle for Exhaust Gas Energy Recovery. *J Eng Gas Turbines Power* 2018;141. doi:10.1115/1.4041109.
- [48] Copeland CD, Chen Z. The Benefits of an Inverted Brayton Bottoming Cycle as an Alternative to Turbo-Compounding 2015. doi:10.1115/GT2015-42623.
- [49] Bianchi M, De Pascale A. Bottoming cycles for electric energy generation: Parametric investigation of available and innovative solutions for the exploitation of low and medium temperature heat sources. *Appl Energy* 2011;88:1500–9. doi:10.1016/J.APENERGY.2010.11.013.
- [50] Kennedy I, Chen Z, Ceen B, Jones S, Copeland CD. Inverted Brayton Cycle With Exhaust Gas Condensation. *J Eng Gas Turbines Power* 2018;140. doi:10.1115/1.4039811.
- [51] Di Battista D, Fatigati F, Carapellucci R, Cipollone R. Inverted Brayton Cycle for waste heat recovery in reciprocating internal combustion engines. *Appl Energy* 2019;253:113565. doi:10.1016/J.APENERGY.2019.113565.
- [52] Kakaras E, Doukelis A, Karellas S. Compressor intake-air cooling in gas turbine plants. *Energy* 2004;29:2347–58. doi:10.1016/J.ENERGY.2004.03.043.
- [53] Fujii S, Kaneko K, Otani K, Tsujikawa Y. Mirror Gas Turbines: A Newly Proposed Method of Exhaust Heat Recovery. *J Eng Gas Turbines Power* 2000;123:481–6. doi:10.1115/1.1366324.
- [54] Hingst R. Process for Producing Energy from Gases and Gas Steam Mixtures of Low Pressure, e. B. Exhaust gases from internal combustion engines. Deutsches Patent No. 852015, 1944.
- [55] Liu C, Zheng Q, Wang Q, Lin A, Jiang Y, Luo M. Sensitivity Analysis of Multistage Compressor Characteristics Under the Spray Atomization Effect Using a CFD Model. *Energies* 2019;12. doi:10.3390/en12020301.
- [56] Duan Z, Zhan C, Zhang X, Mustafa M, Zhao X, Alimohammadisagvand B, et al. Indirect evaporative cooling: Past, present and future potentials. *Renew Sustain Energy Rev* 2012;16:6823–50. doi:10.1016/J.RSER.2012.07.007.
- [57] Zhu F, Chen L, Wang W. Thermodynamic Analysis and Optimization of an Irreversible Maisotsenko-Diesel Cycle. *J Therm Sci* 2019 284 2019;28:659–68. doi:10.1007/S11630-019-1153-1.
- [58] Zhu G, Chow TT, Fong KF, Lee CK. Comparative study on humidified gas turbine cycles with

- different air saturator designs. Appl Energy 2019;254:113592.
doi:10.1016/J.APENERGY.2019.113592.
- [59] Chen L, Shen J, Ge Y, Wu Z, Wang W, Zhu F, et al. Power and efficiency optimization of open Maisotsenko-Brayton cycle and performance comparison with traditional open regenerated Brayton cycle. Energy Convers Manag 2020;217:113001.
doi:10.1016/J.ENCONMAN.2020.113001.
- [60] Zhu F, Chen L, Wang W. Thermodynamic Analysis of an Irreversible Maisotsenko Reciprocating Brayton Cycle. Entropy (Basel) 2018;20. doi:10.3390/E20030167.
- [61] Shen J, Chen L, Ge Y, Zhu F, Wu Z. Optimum ecological performance of irreversible reciprocating Maisotsenko-Brayton cycle. Eur Phys J Plus 2019 1346 2019;134:1–14.
doi:10.1140/EPJP/I2019-12648-4.
- [62] Matsui K, Thu K, Miyazaki T. A hybrid power cycle using an inverted Brayton cycle with an indirect evaporative device for waste-heat recovery. Appl Therm Eng 2020;170:115029.
doi:10.1016/J.APPLTHERMALENG.2020.115029.
- [63] Lin J, Thu K, Bui TD, Wang RZ, Ng KC, Chua KJ. Study on dew point evaporative cooling system with counter-flow configuration. Energy Convers Manag 2016;109:153–65.
doi:10.1016/j.enconman.2015.11.059.
- [64] Incropera FP, DeWitt DP, Bergman TL, Lavine AS. Fundamentals of Heat and Mass Transfer. vol. 6th. John Wiley & Sons; 2007. doi:10.1016/j.applthermaleng.2011.03.022.
- [65] Lin J, Bui DT, Wang R, Chua KJ. On the fundamental heat and mass transfer analysis of the counter-flow dew point evaporative cooler. Appl Energy 2018;217:126–42.
doi:10.1016/J.APENERGY.2018.02.120.
- [66] Engineers TJS of M. Mechanical Engineering Handbook. 1985.
- [67] Welty J, Rorrer GL, Foster DG. Fundamentals of Momentum, Heat, and Mass Transfer. Wiley; 2014.
- [68] Mills A. Heat and Mass Transfer. Taylor & Francis; 2018.
- [69] Runge C. Ueber die numerische Auflösung von Differentialgleichungen. Math Ann 1895;46:167–78. doi:10.1007/BF01446807.
- [70] Powell MJD. An efficient method for finding the minimum of a function of several variables without calculating derivatives. Comput J 1964;7:155–62. doi:10.1093/comjnl/7.2.155.
- [71] Bell IH, Wronski J, Quoilin S, Lemort V. Pure and Pseudo-pure Fluid Thermophysical Property Evaluation and the Open-Source Thermophysical Property Library CoolProp. Ind Eng Chem Res 2014;53:2498–508. doi:10.1021/ie4033999.
- [72] Riangvilaikul B, Kumar S. An experimental study of a novel dew point evaporative cooling system. Energy Build 2010;42:637–44. doi:10.1016/J.ENBUILD.2009.10.034.



九州大学

KYUSHU UNIVERSITY

Faculty of Engineering Sciences
Advanced Environmental Science and Engineering

6-1 Kasuga-koen Kasuga-city Fukuoka 816-8580, Japan
Tel +81 92-583-7831
Fax +81 92-583-7833

10 Mar 2022

To

Professor Henrik Lund

Editor-in-Chief

Energy

Department of Planning, Aalborg University,

Fibigerstræde 13, DK-9220 Aalborg, Denmark

&

Prof. Lingai LUO,

Subject Editor

Energy

**Subject: Submission of the revised manuscript (R4) for the possible publication in Energy
Journal**

Dear Prof. Henrik Lund and Prof. Lingai LUO,

Thank you very much for handling and processing our manuscript. The authors are grateful to the Editorial team and the reviewers for their valuable comments which help improve the manuscript. We are very pleased to submit the revised manuscript entitled, “**On the Performance Improvement of an Inverted Brayton Cycle using a Regenerative Heat and Mass Exchanger**” authored by Mr Kohei Matsui, Dr Lin Jie, Prof. Takahiko Miyazaki and me for the possible publication in Energy Journal under the “Full length Article” category.



九州大学

KYUSHU UNIVERSITY

Faculty of Engineering Sciences
Advanced Environmental Science and Engineering

6-1 Kasuga-koen Kasuga-city Fukuoka 816-8580, Japan
Tel +81 92-583-7831
Fax +81 92-583-7833

The reviewer requested to elaborate more on “the applicability of using $Nu=7.54$ in the manuscript.” This value for the rectangular channels (as in the M-cycle) can be found in Table 8.1, pp. 553 of Incropera et al. (Fundamentals of heat and mass transfer, 7th edition). We opine that this is a common knowledge. We have elaborated it in the manuscript as well as responded to the comments in details.

I declare that the current revised manuscript is unpublished. I also further declare that the work done in the manuscript has not been submitted or published elsewhere.

I am looking forward to hearing from you at your earliest convenience.

Sincerely yours,

A handwritten signature in blue ink, consisting of a stylized, cursive script.

Kyaw Thu, PhD

Associate Professor

Department of Advanced Environmental Science and Engineering

Faculty of Engineering Sciences, Kyushu University,

Kasuga-koen 6-1, Kasuga-shi, Fukuoka 816-8580, Japan

Tel: +81-92-583-7831

Fax: +81-92-583-7833

Email: kyaw.thu.813@m-kyushu-u.ac.jp

On the Performance Improvement of an Inverted Brayton Cycle using a Regenerative Heat and Mass Exchanger

Kohei Matsui¹, Jie Lin², Kyaw Thu^{1,3,*}, Takahiko Miyazaki^{1,3,*}

¹ Department of Advanced Environmental Science and Engineering, Faculty of Engineering
Sciences, Kyushu University

Kasuga-koen 6-1, Kasuga-city, Fukuoka 816-8580, Japan

² Department of Engineering Science, University of Oxford
Parks Road, Oxford OX1 3PJ, United Kingdom

³ Thermal Science and Engineering Division, International Institute of Carbon-Neutral
Energy Research (I2CNER), Kyushu University
744 Motoooka, Nishi-ku, Fukuoka 819-0395, Japan

Corresponding authors' email: kyaw.thu.813@m.kyushu-u.ac.jp (K. Thu)
miyazaki.takahiko.735@m.kyushu-u.ac.jp (T. Miyazaki)

Abstract

Recovery of the low-temperature waste heat for electricity generation has been gaining a significant interest. An Inverted Brayton Cycle (IBC) is often employed to convert the low-temperature waste-heat to electricity while the thermal efficiency and specific work output are poor. In this paper, a new energy recovery scheme is introduced incorporating the IBC with a Regenerative Heat and Mass Exchanger (RHME). The RHME is a heat and mass exchanger that consolidates a recuperator (for thermal efficiency improvement) and an Indirect Evaporative Cooler (for enhanced specific work). Numerical models for RHME and the IBC were judiciously developed where possible condensation in the product air channel was accounted for. The model was validated with the experimental data and the cycle was investigated for various waste-heat sources (50 – 150 °C). When compared to a conventional air-cooling IBC system, incorporating the current energy recovery scheme increases the thermal efficiency from 8.13% to 14.36% and specific work output from 10.38 to 12.46 kJ/kg

equivalent to 76.63% and 20.1% improvements, respectively. The unprecedented performance improvement is realised from the exploitation of the regenerative and air-saturation (cooling) mechanisms for both energy recovery and cooling of the working fluid.

Keywords: Inverted Brayton cycle; Indirect evaporative cooler; Waste heat utilisation; Power generation

Nomenclature

c_p	specific heat capacity	kJ/kg/K
d	channel height	m
D	mass diffusivity	m ² /s
D_h	hydraulic diameter	m
Gz	Graetz number	–
h	convective heat transfer coefficient, specific enthalpy	W/m ² /K, kJ/kg
h_m	convective mass transfer coefficient	m/s
k	thermal conductivity	W/m/K
l	length	m
Nu	Nusselt number	–
P	pressure	Pa
Pr	Prandtl number	–
q	specific thermal energy	kJ/kg
RH	relative humidity	%
Re	Reynolds number	–
Sc	Schmidt number	–
Sh	Sherwood number	–
St	Stanton number	–
St_m	mass transfer Stanton number	–
T	temperature	K
t	thickness	m
v	velocity	m/s
w	specific work	kJ/kg
x	humidity ratio	g/kg [DA]
z	distance	m

Greek symbols

1	ε	convergence criteria	—
2			
3	η	efficiency	—
4			
5	κ	specific heat ratio	—
6			
7	λ	friction coefficient	—
8			
9	μ	viscosity	Pa s
10			
11	π	pressure ratio	—
12			
13	ρ	density	kg/m ³
14	ϕ	thermal resistance ratio	—
15			
16			
17			
18	<i>Subscripts</i>		
19			
20	d	dry channel	
21			
22	en	entry region	
23			
24	H	heater	
25	IEC	indirect evaporative cooler	
26			
27	net	net	
28			
29	opt	optimum	
30			
31	p	product channel	
32			
33	rec	recuperator	
34			
35	s	surface	
36			
37	th	thermal	
38			
39	tot	total	
40			
41	w	wet channel	
42			
43	wd	w adjacent to d	
44			
45	wp	w adjacent to p	

1 Introduction

Electricity, considered as the most flexible and convenient form of energy, plays an important role in multi-energy system (MES) and integrated energy systems [1,2]. Hence, demand and generation of electricity are increasing with the latest demand in the electrification of transport sector [3–6] while, transitions to renewable power generation have been actively pursued [7,8]. On the other hand, recovery and utilisation of waste heat from multiple processes can be effective means for securing power since waste heat accounts for 23 – 53% of the world's energy input [9]. Tchanche [10] and Ammar et al. [11] reported the temperature range and capacities of waste heat from various sources, such as transportation and industrial sectors.

Waste heat is often converted into cooling/heating [12–14] (absorption [15–17] and adsorption [18–20] heat pumps) and/or potable water [21–23]. However, these commodities are not exchangeable to other forms or

among them without the additional energy input. On the other hand, electricity can be utilised to obtain any of the aforesaid commodities using systems such as mechanical vapour compression [24], capacitive deionization [25] and reversed osmosis [26,27] at reasonable efficiencies. Thus, the direct conversion of waste heat to electricity has been gaining significant attention. Electricity generating cycles using low-temperature waste heat include Organic Rankine Cycle (ORC) [28–30], Organic Flash Cycles (OFC) [31–33], Trilateral Flash Cycle (TFC) [34–36], Kalina cycle [37,38] and Brayton-type cycles (conventional and inverted type) [39–42]. Detailed reviews on the thermodynamic cycles for electricity generation from low-temperature heat sources can be found in the works of Galanis et al. [43] and Garcia et al. [44].

An Inverted Brayton Cycle (IBC) which is the interest of the present article, operates at atmosphere to sub-atmospheric pressures. The advantages of an IBC over other cycles (e.g. ORC and Kalina cycle) lie in its simplicity and availability of the required turbomachinery components [42,45]. A typical IBC exerts a back pressure below the atmospheric pressure on the working air, and the cycle does not raise the pressure significantly above the atmosphere which is ideal for co-generative applications [46–48]. An influential study by Bianchi and De Pascale [49] compared three bottoming cycles (ORC, Stirling and IBC) for various heat source temperatures. The specific energy output of the IBC was reported to be in the range of 10 – 70 kJ/kg depending on the temperature and amount of condensable water at the inter-cooler outlet. The authors concluded that IBC systems were innovative and promising solutions yet with lower performance than the ORC technology, especially, for low temperatures (200 – 400 °C).

Interest in IBC has been growing. IBCs were adopted in many applications over the last few years. For example, Chen et al. proposed an IBC system for heat recovery from the exhaust gas of a gasoline turbocharged engine and reported 3.15% reduction in the fuel consumption at the optimal turbine pressure ratio [45]. Experimental and numerical works on IBC systems for waste-heat recovery from the internal combustion (IC) engine with the exhaust gas condensation were reported by Kennedy et al. [47,50]. The authors concluded that the turbine inlet temperature, turbine expansion ratio, heat exchanger pressure drop and coolant temperature were the most significant parameters that influenced the performance. Recently, Battista et al. reported that utilisation of an IBC for the waste-heat recovery of a reciprocating IC engine lead to an average power recovery of approximately 2% of the engine brake power [51].

The temperature of the compressor suction air significantly influences the performance of the IBC. According to Kakaras et al., the high-temperature intake of the compressor resulted in up to 20% power loss [52]. Fujii et al. utilized a multi-stage cooling and multi-stage compression cycle configuration and identified the inlet coolant temperature as one of the most significant parameters for the performance [53]. Various cooling schemes have been attempted for the performance improvement of the IBC [54,55]. These works considered the direct vaporisation technique where the wet-bulb temperature of the air was often the limit. On the other hand, an indirect evaporative cooler (IEC) can cool the air to temperatures close to the dew point [56,57]. Another significant benefit of using an IEC in the gas turbine cycle is the increased moisture content of the working fluid. For instance, Zhu et al. highlighted a higher system efficiency when using the humidified gas turbine cycle [58]. Thus, Brayton Cycles were often hybridized with IECs for improved performance [59–

61]. Our previous work [62] investigated the performance of the IEC-IBC system and compared with a conventional air cooling cycle and a recuperative cycle. The improved specific work output was realised by the IEC-IBC system. However, the thermal efficiency of the IEC-IBC could be higher than that of a recuperative cycle only for intake air with low humidity (20 – 40 %). This is because heat recuperation improves the thermal efficiency of a power cycle. In IEC-IBC systems, most of the thermal energy from the turbine outlet air is utilized by the IEC for moisture saturation and cooling of the air, resulting in lower thermal efficiency when compared to a recuperative cycle. Most of the sensible heat recovered in an IEC-IBC system is used up for the vaporisation of water, which subsequently increases the amount of heat input to the system.

To further advance the IBC system for effective waste-heat recovery, it is necessary to develop recovery scheme for both improved thermal efficiency and specific work output; yet, very few or no previous research work is reported in this regard. Filling the knowledge gap, thus the objective of the present work is to introduce an innovative concept, i.e., a regenerative heat and mass exchanger (RHME) which significantly improves both thermal efficiency and specific work output. The proposed RHME apportions the recovered energy for the sensible heat recuperation and evaporative cooling. The RHME consolidates the recuperative and IEC components in one unit. The performance of the RHME-IBC cycle was evaluated for various turbine inlet temperatures, mass flow rates and relative humidity values of the outdoor air. One crucial parameter that significantly influences the performance of the RHME-IBC system is the apportionment of the energy for the heat recuperation and vaporisation, i.e., the ratio of the length of the intercooler (IEC part) to the total length i.e., L_{IEC} / L_{tot} . The system was studied for various L_{IEC} / L_{tot} values. The performance of the proposed RHME-IBC system was compared with those of the recuperative and conventional IEC-IBC systems.

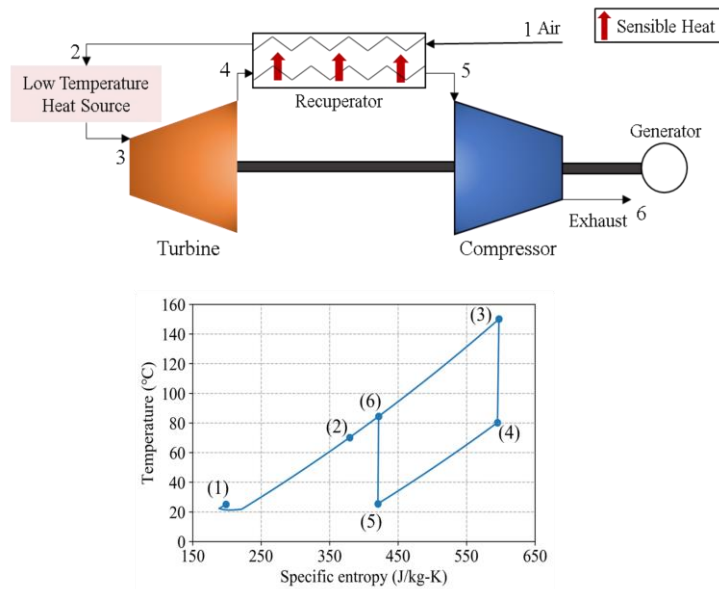
2 Description of the cycles

The objective of the present work is to develop an energy recovery scheme for an IBC for improved thermal efficiency and specific work output with the effective conversion of the waste heat to electricity. In an IBC, the heated air first flows through the turbine while rejecting the heat before being exhausted by the compressor. The power produced by the turbine exceeds that to the compressor, and thus the cycle produces a net power output. However, the thermal efficiency of a typical IBC is known to be low when operated using low-temperature heat source. For the performance improvement of the IBC in terms of thermal efficiency and the specific work output, an innovative cycle is introduced by hybridising the IBC with a regenerative heat and mass exchanger (RHME).

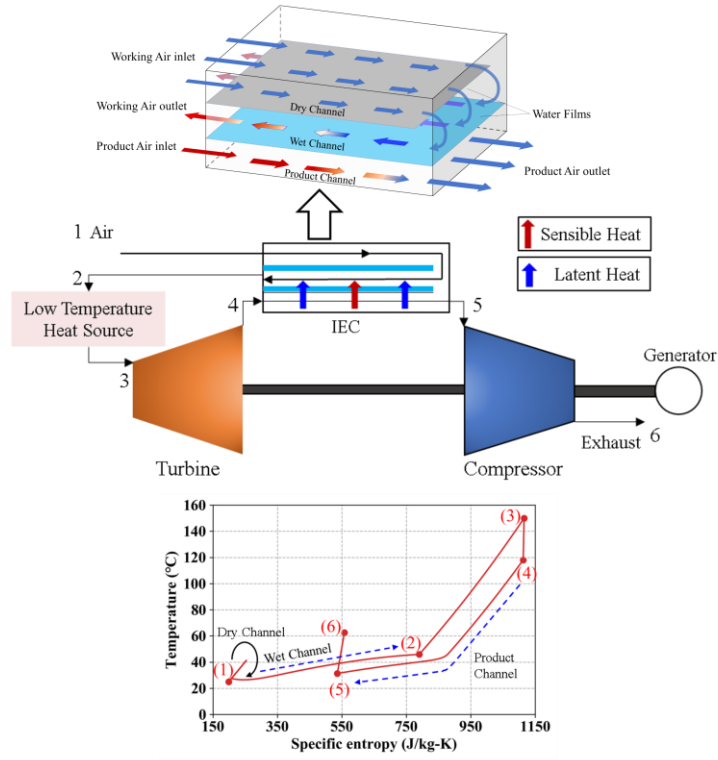
Figure 1 shows three configurations of IBC systems with different heat recovery or cooling schemes and their thermodynamic states on the temperature-entropy diagrams. Figure 1(a) shows the cycle with the sensible heat recovery only using a recuperator for the intermediate cooling. In this configuration, the outdoor air is utilised to cool down the turbine outlet temperature using a recuperator for the sensible heat exchange. Thus, the temperature and entropy of the outdoor air increase (state points 1 – 2 on the T-s diagram) and the reverse is true for the turbine outlet air (4 – 1 on the T-s diagram of Fig. 1(a)). Heat addition occurs in the process 2 to

3.

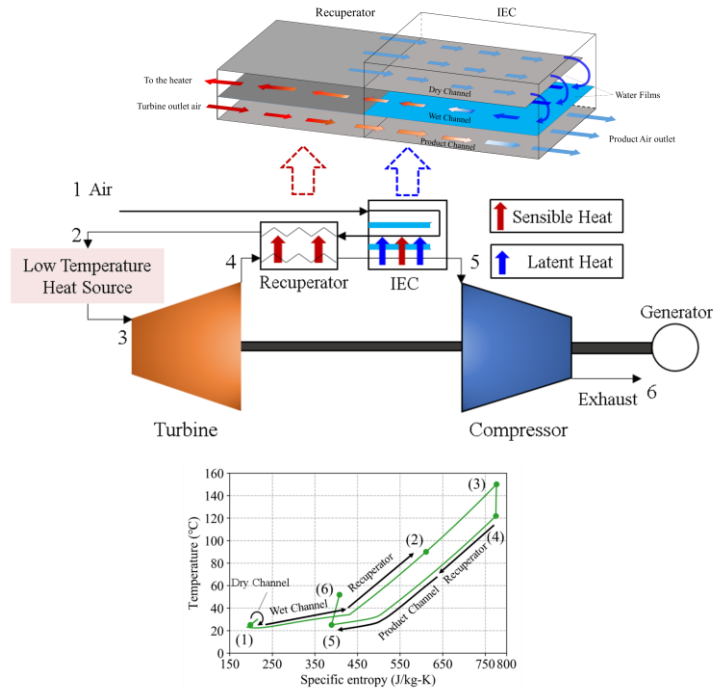
Figure 1(b) shows the hybrid IBC-IEC system that applies an indirect evaporative cooler to introduce the air cooling and saturation of the working fluid (see our previous work [62] for more details.). In this configuration, 100% of the thermal energy from the turbine outlet air is utilized in the indirect evaporative cooler (IEC) for cooling while the air temperature at state point 2 is lower when compared to that of the air at the same point in the configuration shown in Fig. 1(a). Thus, the energy input to the system in this configuration increases. Figure 1(c) shows the IBC system that incorporates the proposed regenerative heat and mass exchanger (RHME) for the recuperation, cooling and saturation of the working fluid. The RHME is a heat and mass exchanger device consolidating a recuperator (for sensible heat recovery) and an IEC (for air saturation and cooling). The objective here is to recover the sensible heat from the turbine outlet air for humidification of the intake air while cooling it down. Besides, the IEC is an essential component for reducing the compressor power. In the RHME device, the turbine outlet air is first utilized to heat up the air coming out from the wet channel of the IEC before being further cooled by the IEC. Thus, air saturation (humidification) of the outdoor air is achieved in the wet channel of the IEC which is part of the RHME while the sensible heat recovery in the recuperator. The process is illustrated on the T-s diagram in Fig. 1(c) where two slopes can be observed for the process 1 to 2 due to the air saturation in the IEC and sensible heating in the recuperator. It is expected that incorporating the RHME device will provide a significant performance improvement both in terms of thermal efficiency and the specific work output. This is because the increase in the inlet air temperature (sensible heat recovery) reduces the required heat input to the cycle. On the other hand, higher moisture content in the intake air is desirable as the specific heat of the working air increases at high humidity.



(a)



(b)



(c)

Fig. 1: Schematic diagrams and T-s plots of the inverted Brayton cycles with (a) Recuperator, (b) Indirect Evaporative Cooler, and (c) Regenerative Heat and Mass Exchanger (the proposed system)

3 Mathematical models

3.1 Regenerative heat and mass exchanger

The mathematical model of a counterflow-type regenerative heat and mass exchanger (RHME) was established by considering the energy and material balances in each channel. A steady-state, one-dimensional model was developed accounting for the distributions of the temperature and humidity along each channel. The following assumptions were adopted in the present model:

- (1) Adiabatic boundary between the system and the surrounding i.e., no heat loss from the RHME, the recuperator and the IBC.
- (2) The wet channel is covered with a very thin saturated water film, which is stationary [63].
- (3) The advection term is dominant, with a negligible diffusion term.
- (4) Fluid properties are assumed to be constant with uniform properties within each control volume.

Figure 2 shows the schematic diagrams of the proposed regenerative heat and mass exchanger (RHME) highlighting the air channels and the differential control volumes in an Eulerian system emphasising the inlet and outlet temperatures, and the humidity ratio in the IEC section, Fig. 2(b), and the recuperator section Fig. 2(c). Applying the assumption of stationary and dominant advection terms in the IEC dry channel, the temperature distribution is written as [62],

$$\left(\rho c_p v d \frac{\partial T}{\partial z} \right)_d = h_d (T_{ds} - T_d) \quad (1)$$

Here, ρ is the density of air, v is the velocity, c_p is the specific heat and h is the heat transfer coefficient of the air in the dry channel. Applying the assumptions mentioned above, the heat and mass transfer in the wet channel are modelled as [62],

$$\left(\rho c_p v d \frac{\partial T}{\partial z} \right)_w = h_w (T_{wsd} + T_{wsp} - 2T_w) \quad (2)$$

$$\left(v d \frac{\partial x}{\partial z} \right)_w = h_{mw} (x_{wsd} + x_{wsp} - 2x_w) \quad (3)$$

where x is the humidity of the wet channel air and h_{mw} is the convective mass transfer coefficient while the subscript, w , stands for the wet channel. Similarly, within the product channel, temperature and humidity changes are expressed as,

$$\left(\rho c_p v d \frac{\partial T}{\partial z} \right)_p = h_p (T_{ps} - T_p) \quad (4)$$

$$\left(\nu d \frac{\partial x}{\partial z} \right)_p = h_m (x_{ps} - x_p) \quad (5)$$

The surface temperatures of the plate separating the dry channel and the wet channel (dry channel side; T_{ds} , wet channel side; T_{wsd}) derived from the energy balance are written as,

$$T_{ds} = (1 - \phi_d) T_d + \phi_d \left[T_w - \frac{St_m}{St_w} \frac{L_w}{c_{pw}} (x_{ws} - x_w) \right] \quad (6)$$

$$T_{wsd} = \phi_{wd} T_d + (1 - \phi_{wd}) \left[T_w - \frac{St_m}{St_w} \frac{L_w}{c_{pw}} (x_{ws} - x_w) \right] \quad (7)$$

The temperatures of the plate surface separating the wet channel and the product channel were derived in the similar fashion. Note that the condensation can occur in the product channel because of the possibility of the working air in the product channel with high humidity. In the present model, the amount of condensation is calculated from the gradient between the humidity of the working air in the product channel and the plate surface humidity. Therefore, the surface temperatures of the partition plate on the wet channel side and the product channel side T_{wsp} and T_{ps} are respectively expressed by the following equations.

$$T_{wsp} = \phi_{wp} T_p + (1 - \phi_{wp}) \left[T_w - \frac{St_{mw}}{St_w} \frac{L_w}{c_{pw}} (x_{wsp} - x_w) - \frac{St_{mp}}{St_p} \frac{L_{wp}}{c_{pp}} (x_{ps} - x_p) \right] \quad (8)$$

$$T_{ps} = (1 - \phi_p) T_p + \phi_p \left[T_w - \frac{St_{mw}}{St_w} \frac{L_w}{c_{pw}} (x_{wsp} - x_w) - \frac{St_{mp}}{St_p} \frac{L_{wp}}{c_{pp}} (x_{ps} - x_p) \right] \quad (9)$$

If the surface saturation humidity is higher than the humidity of the working air in the product channel, (i.e., condensation does not occur in the channel), the third term in the brackets of the above two equations is zero. Here, ϕ is a dimensionless number calculated from the ratio of the thermal resistance. The expressions of ϕ in the dry channel and the wet channel are described as,

$$\phi_d = \frac{1/h_d}{1/h_d + t_{pl}/k_{pl} + 1/h_w} \quad (10)$$

$$\phi_{wd} = \frac{1/h_w}{1/h_d + t_{pl}/k_{pl} + 1/h_w} \quad (11)$$

Figure 2(c) shows the control volume of the recuperator section of the RHME where the low-temperature side of the recuperator is connected to the wet channel of the IEC, and the high-temperature side (turbine outlet air-flow path) of the recuperator is connected to the product channel. Here, the subscripts w and p , as well as rec , are adopted. The energy balances of the air streams in the control volume of the recuperator part of RHME (Fig. 2(c)) are written as,

$$\left(\rho c_p v d \frac{\partial T}{\partial z} \right)_{w,rec} = h_{w,rec} (T_{ws,rec} - T_{w,rec}) \quad (12)$$

$$\left(\rho c_p v d \frac{\partial T}{\partial z} \right)_{p,rec} = h_{p,rec} (T_{ps,rec} - T_{p,rec}) \quad (13)$$

The humidity change in the high-temperature channel of the recuperator is expressed by equation (14). Again, the change in humidity is zero if the saturation humidity of air does not exceed the saturation humidity of the wall surface.

$$\left(v d \frac{\partial x}{\partial z} \right)_{p,rec} = h_{m,p,rec} (x_{ps,rec} - x_{p,rec}) \quad (14)$$

The wall temperature, $T_{ws,rec}$ and $T_{ps,rec}$, in the recuperator are expressed by the following equations. Similar to equations (8) and (9), if the saturation humidity of air does not exceed the saturation humidity of the wall surface, the second term in the brackets becomes zero.

$$T_{wsp,rec} = \phi_{wp,rec} T_{p,rec} + (1 - \phi_{wp,rec}) \left[T_{w,rec} - \frac{St_{mp,rec}}{St_{p,rec}} \frac{L_{ps,rec}}{c_{pp,rec}} (x_{ps,rec} - x_{p,rec}) \right] \quad (15)$$

$$T_{ps,rec} = (1 - \phi_{p,rec}) T_{p,rec} + \phi_{p,rec} \left[T_{w,rec} - \frac{St_{mp,rec}}{St_{p,rec}} \frac{L_{ps,rec}}{c_{pp,rec}} (x_{ps,rec} - x_{p,rec}) \right] \quad (16)$$

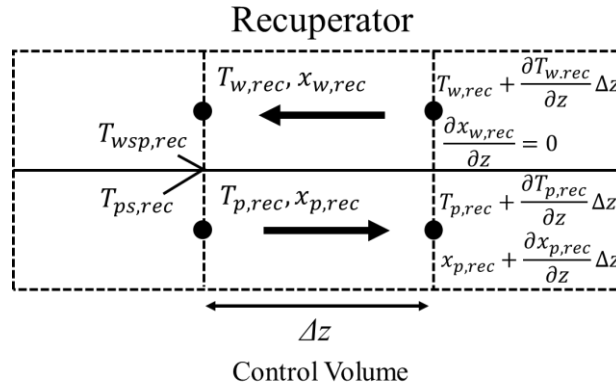
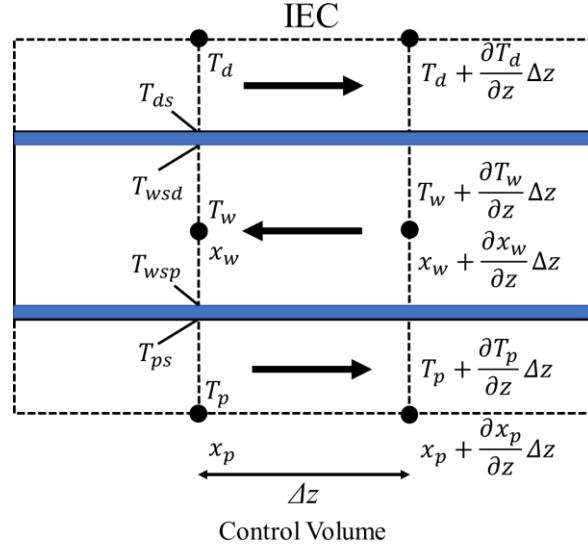
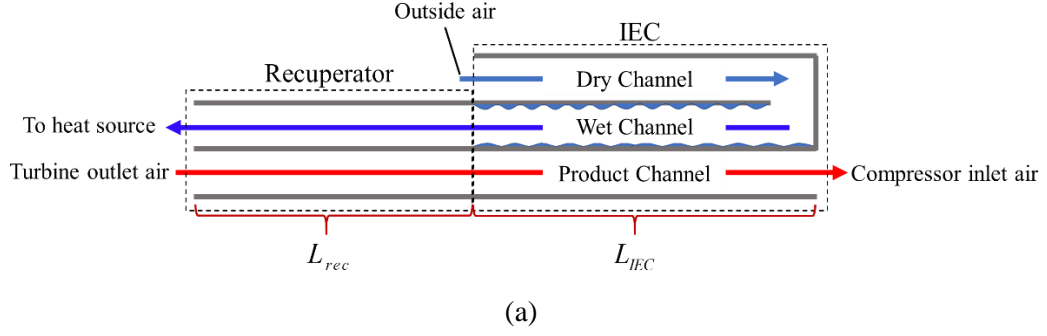


Fig. 2: Flow direction in the proposed cycle and control volumes describing the temperature and humidity for the model development, (a) flows in the channels of RHME, (b) control volume of the IEC section of the RHME and (c) control volume of the Recuperator section of RHME

The Nusselt number is used for estimating the heat transfer coefficient. As the surface temperature varies in a small range [63], the Nusselt number at constant temperature in laminar flow is employed to approximate the convective heat transfer between the channel surface and the air flow, except for the entry region [64,65]

as,

$$Nu = 7.54 \quad (17)$$

The entry length l_{en} is calculated from Reynolds number Re , Prandtl number Pr and hydraulic diameter $D_h = 4A/P$ as [64],

$$l_{en} = 0.05 Re Pr D_h \quad (18)$$

Nusselt number in the entry region is calculated using Graetz number, $Gz = D_h Re Pr / z$ and Prandtl number, Pr , by the following equation [63] as

$$Nu = \frac{\frac{7.54}{\tanh\left(2.264 Gz^{\frac{1}{3}} + 1.7 Gz^{\frac{2}{3}}\right)} + 0.0499 Gz \tanh(Gz^{-1})}{\tanh\left(2.432 Pr^{\frac{1}{6}} Gz^{\frac{1}{6}}\right)} \quad (19)$$

The mass transfer coefficient is obtained from Sherwood number $Sh = h_m D_h / D$, applying the analogy of heat transfer and mass transfer, and is expressed in terms of Schmidt number $Sc = \mu / \rho D$, and Prandtl number Pr as,

$$Sh = Nu \left(\frac{Sc}{Pr} \right)^{\frac{1}{3}} \quad (20)$$

The mass diffusivity, D , used in Sherwood number is computed as [66],

$$D = 22.0 \times 10^{-6} \left(\frac{T}{273.15} \right)^{1.75} \left(\frac{101325}{p} \right) \quad (21)$$

Stanton number, St , and mass transfer Stanton number, St_m are given as,

$$St = \frac{h}{\rho c_p v} \quad (22)$$

$$St_m = \frac{h_m}{v} \quad (23)$$

The pressure loss in the channel is accounted for and calculated using the Darcy–Weisbach equation as [67][68],

$$\Delta p = \lambda \frac{\Delta z}{D_h} \frac{\rho v^2}{2} \quad (24)$$

Here, λ is the laminar friction coefficient, $\lambda=64/Re$. The temperature and humidity distributions of the working air in the recuperator and IEC shown above were solved using the fourth-order Runge-Kutta method [69], and the surface temperature of the partition was solved using the modified Powell method [70]. Figure 3 shows the simulation flow of the system. The area to be calculated was divided into multiple control volumes, and calculations were performed sequentially based on the initial conditions. First, equations for the working fluid were solved followed by computation of the temperatures of the partition plate surface from the temperature, humidity, velocity, and pressure. These calculations were repeated until the solution converged. Thermodynamic properties of moist air and water were adopted from HAPropsSI routines of CoolProp [71].

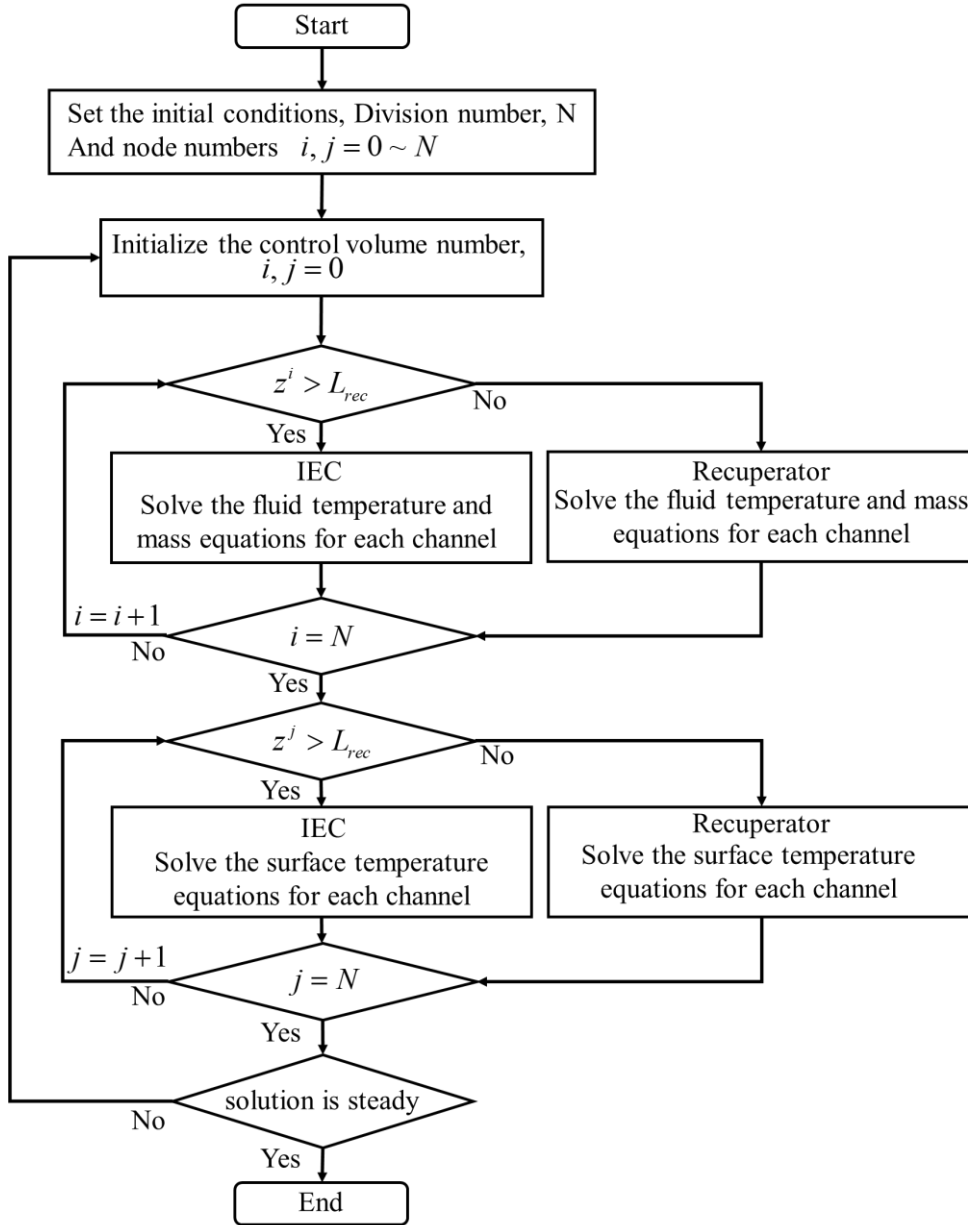


Fig. 3: The calculation flow of the indirect evaporative cooler

3.2 Validation of the numerical model

The numerical model was first validated using the experimental data of a counterflow IEC conducted by Riangvilaikul and Kumar [72]. Table 1 summarises the outlet air temperatures for various temperatures and humidity values of the inlet air comparing the experimental data. The maximum absolute average deviation (AAD) is observed to be 3.95% while the lowest AAD is 0.12% showing a good agreement between experimental data and predictions of the current model.

Table 1. The validation of the IEC model with the experimental results of Riangvilaikul and Kumar [72]

Humidity	Inlet	Air	Outlet Air Temperature (°C)	AAD (%)
----------	-------	-----	-----------------------------	---------

(g/kg [DA])	Temperature (°C)	<i>Experiment</i>	<i>Present model</i>	
6.9	25.01	15.51	15.05	2.94
	30.02	16.45	16.30	0.93
	35.03	17.32	17.30	0.12
	39.92	17.97	18.12	0.81
	45.02	18.62	18.81	1.02
11.2	24.84	19.35	18.58	3.95
	30.11	20.43	19.76	3.31
	35.03	21.09	20.64	2.10
	40.53	21.88	21.45	1.99
	45.02	22.68	21.99	3.06
20.0	30.02	26.23	25.82	1.58
	35.00	26.88	26.52	1.35
	40.04	27.68	27.10	2.10
	45.02	28.48	27.58	3.17
26.4	32.32	30.07	29.84	0.79
	35.43	30.51	30.18	1.07
	40.33	31.45	30.65	2.54
	44.99	32.10	31.03	3.35

3.3 Thermodynamic model of the inverted Brayton cycle (IBC)

Referring to the schematic diagram of the IBC (Fig. 1c), the thermodynamic model is summarised in Table 2. General assumptions invoked in the IBC models are: (1) constant specific heat and specific heat ratio across the turbine and compressor, (2) the same pressure ratios for the compressor and turbine with no pressure drop, and (3) ideal gas assumption for the working fluid. The optimum pressure ratio π_{opt} that maximises the cycle thermal efficiency can be obtained by differentiating w_{net} with respect to π and setting it to zero while the derivation can be found in [62]. The cycle calculation was carried out following the flow chart as shown in Fig. 4 until the convergence criteria was met. The thermophysical properties of the air (enthalpy, specific heat, etc.) in the turbine and compressor were computed at their inlets as functions of temperature, pressure and humidity ratio at specific points using the Humid Air Properties (HAPropsSI routines) of CoolProp.

Table 2. Summary of the mathematical equations for the cycle performance calculation of the IBC

No.	Component	Equation	Remarks
-----	-----------	----------	---------

			$h(T, p, x)$ values were adopted from HAPropsSI of CoolProp.
1	Net specific work, w_{net}	$w_{net} = (h_3 - h_4) - (h_6 - h_5)$	
2	Pressure ratio, π	$\pi = \frac{p_4}{p_3}$	
3	Turbine outlet temperature, T_4	$T_4 = T_3 \pi^{\frac{\kappa-1}{\kappa} \eta_r}$	$\kappa = 1.4$, constant $c_p(T, p, x)$ across the turbine and compressor.
4	Compressor outlet temperature, T_6	$T_6 = T_5 \pi^{\frac{\kappa-1}{\kappa} \frac{1}{\eta_c}}$	
5	Optimum pressure ratio, π_{opt}	$\pi_{opt} = \left(\frac{1}{\eta_T \eta_C} \frac{c_{p,5} T_5}{c_{p,3} T_3} \right)^{\frac{1}{\gamma \left(\eta_r + \frac{1}{\eta_c} \right)}}$	$c_p(T, p, x)$ values were adopted from HAPropsSI of CoolProp.
6	Specific heat input, q_H	$q_H = h_3 - h_2$	
7	Cycle thermal efficiency, η_{th}	$\eta_{th} = \frac{w_{net}}{q_H}$	

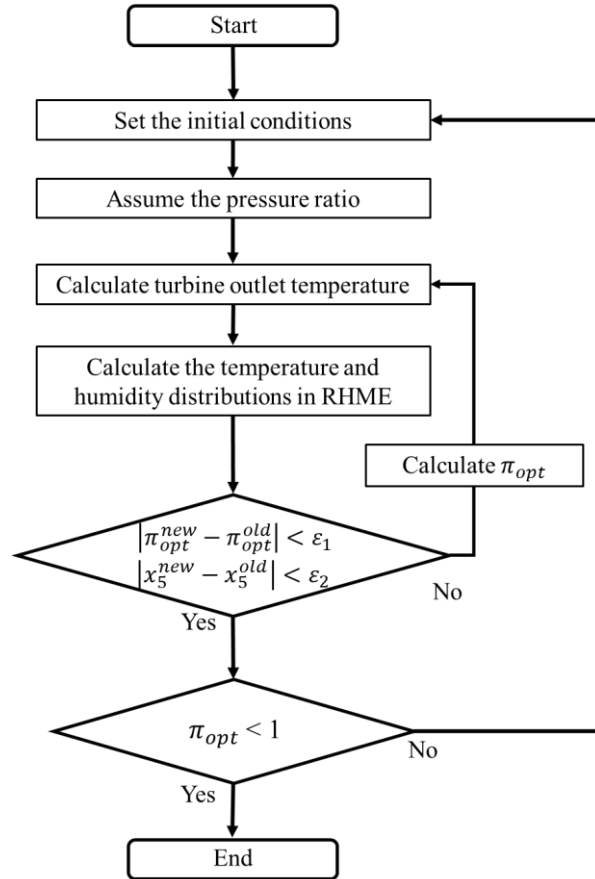


Fig. 4: Cycle calculation flow of the proposed RHME-IBC system

4 Results and Discussion

The performance of the proposed RHME-IBC system is investigated for various operating conditions and Table 3 lists the parameters used in the calculations. These conditions (compressor inlet temperatures, efficiencies of the compressor and turbine etc.) are adopted from many studies on IBC systems reported in the literature [41,45,49,58]. This section first describes the effect of the adiabatic efficiency of the compressor on the cycle performance. The temperature distribution and the humidity distribution in the recuperator and IEC in the cycle are confirmed, and detailed behaviour is scrutinised. Then, the effects of various parameters on cycle performance are evaluated and discussed. Finally, the performance of the present RHME-IBC is compared with other configurations, i.e., a conventional air-cooling system, a recuperative IBC system and an IEC-IBC system.

Table 3 List of parameters used in simulations

Parameter (Unit)	Value	Nominal values
Ambient temperature (°C)	25	25
Ambient pressure (Pa)	101325	101325
Ambient Relative humidity (%)	20 – 100	60
Turbine inlet temperature (°C)	50 – 150	150
Total length, L_{tot} (m)	2 – 10	5
Ratio of IEC length to total length, L_{IEC} / L_{tot} (–)	0.1 – 0.9	0.3
Channel height (mm)	10	10
Total inflow area (m ²)	1.0	1.0
Inlet mass flow rate (kg/s)	1.0 – 5.0	1.0
Compressor isentropic efficiency, η_C (%)	80 – 100	100
Turbine isentropic efficiency, η_T (%)	80 – 100	100
Other mechanical efficiency (%)	100	100

4.1 Cycle performance analysis with varying turbine and compressor efficiencies

The effect of turbine and compressor efficiencies on the cycle performance was first examined (Figure 5). The adiabatic efficiencies of both turbine and compressor were varied independently from 80% to 100%, while other parameters were set at their nominal values given in Table 3. In general, the thermal efficiency and specific work output improve at higher turbine and compressor efficiency. The maximum thermal efficiency

of the cycle was observed to be 10.63% at ideal turbine and compressor efficiency (i.e., 100%), corresponding to the specific work output of 13.43 kJ/kg. At the bottom left of the figure, where the turbine and compressor efficiency values approach 80%, the thermal efficiency and specific work output are gradually reduced.

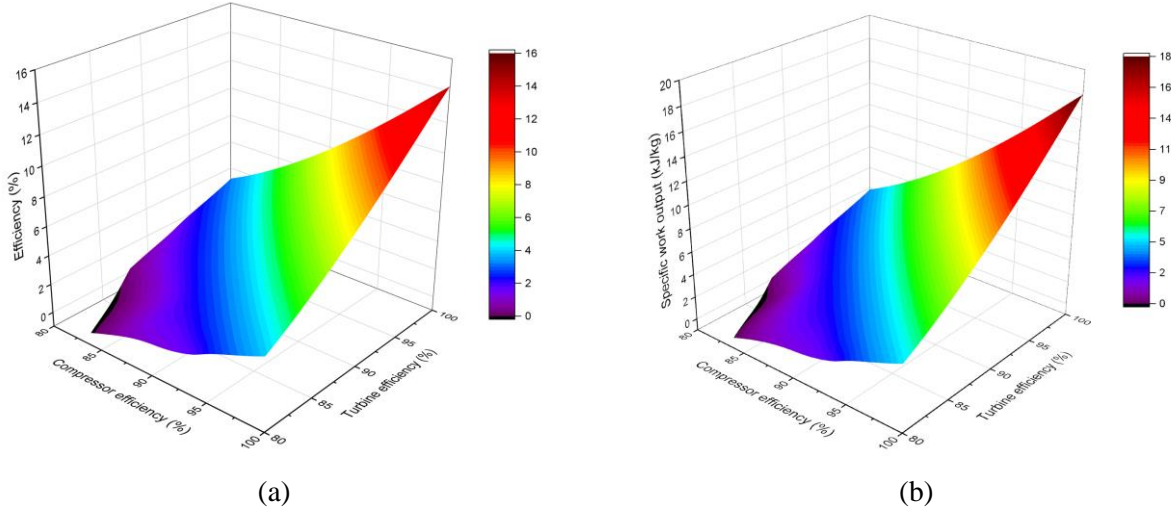
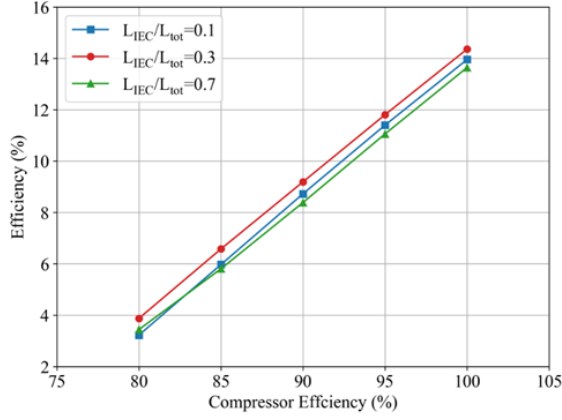
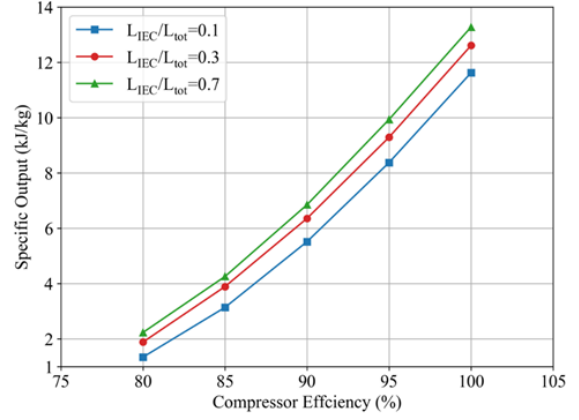


Fig.5: The performance of the cycle for various turbine and compressor efficiency (a) Thermal efficiency, and (b) Specific work output

The effects of varying apportionments of the recuperator and the IEC of the RHME, L_{IEC} / L_{tot} , were investigated. Figure 6 shows the effects of the compressor adiabatic efficiency on the cycle thermal efficiency, and the specific work output for L_{IEC} / L_{tot} values of 0.1, 0.3 and 0.7. The ratio, L_{IEC} / L_{tot} , is an important parameter in optimising the system performance. It is noted that higher values of L_{IEC} / L_{tot} prioritise the recovery for the latent heat and air saturation while the lower ratios favour the sensible heat recovery. From Fig. 6(a), it can be observed that the thermal efficiency linearly varies with the compressor efficiency as a general trend. The efficiency first increases with increasing value of L_{IEC} / L_{tot} , i.e., from 0.1 to 0.3. However, a further increase in L_{IEC} / L_{tot} value leads to a lower efficiency. This is because the amount of recuperative heat influences the heat input to the cycle and increasing L_{IEC} / L_{tot} results in the substantial heat input to the cycle. On the other hand, a higher specific work is realised when the IEC section is increased, i.e., the increased L_{IEC} / L_{tot} value (see Fig. 6(b)) irrespective of the compressor efficiency. The thermal efficiency results highlight the existence of the optimal ratio of the heat recuperation and air-saturation (cooling) by the IEC sections. Figure 7 shows the cycle thermal efficiency and the specific work output for varying L_{IEC} / L_{tot} value at constant turbine inlet temperature of 150 °C while keeping the compressor efficiency values 100% (Fig. 7(a)) and 80% (Fig. 7(b)). The maximum thermal efficiency is realised at the L_{IEC} / L_{tot} value of 0.3 for both cases. However, the rates of change in the thermal efficiency and specific work output are different. In Fig. 7(a), when L_{IEC} / L_{tot} exceeds 0.3, the decrease in the thermal efficiency is relatively steep. On the other hand, from Fig. 7(b), the efficiency decrement is rather gradual, highlighting the sensitivity of the performance to the compressor adiabatic efficiency.

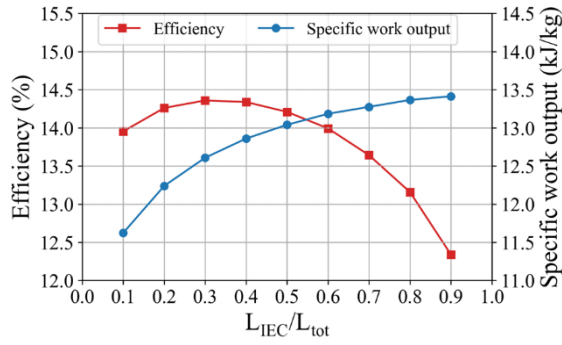


(a)

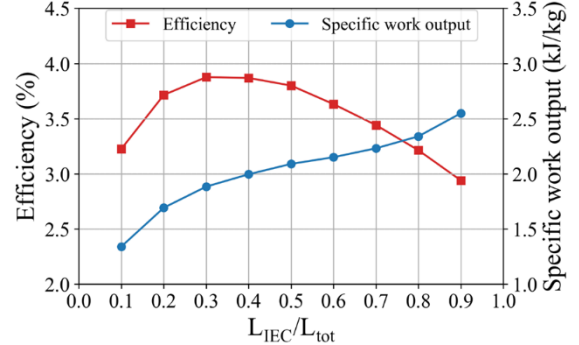


(b)

Fig.6: The effect of the compressor efficiency for three sets of L_{IEC}/L_{tot} values on (a) Efficiency, and (b) Specific output



(a)



(b)

Fig.7: Thermal efficiency and specific work output at various L_{IEC}/L_{tot} values at the constant turbine inlet temperature of 150 °C with (a) 100% compressor adiabatic efficiency, and (b) 80% compressor adiabatic efficiency

Figure 8 shows the temperature and humidity distributions in the channels of the regenerative heat and mass exchanger (RHME) highlighting the recuperator and IEC sections for the compressor efficiency of 100%. The left side of the dotted line in Fig. 8 is the recuperator section and the right side the IEC part. As shown in Fig. 1(c), the atmospheric air flows into the dry channel before flowing into the wet channel at the right end of the RHME device. The turbine outlet air enters the product channel from the left end while being cooled along the channel. From Fig. 8, it can be observed that the increase in the ratio of L_{IEC}/L_{tot} leads to the decrease in the product air temperature which correctly demonstrates the influence of the heat and mass exchanger (IEC). Note, however, that the temperature of the air at the wet channel outlet also decreases, consequently, leading to the increase in the heat input to the cycle for the isobaric heating process. The results highlight the trade-off between the heat recuperation and the intermediate cooling of the working air, which can be adjusted by

varying L_{IEC} / L_{tot} value. From the perspectives of thermal efficiency and specific work output, it is necessary to employ the optimal L_{IEC} / L_{tot} value.

As highlighted in the previous section, condensation may occur in the channels for some apportionments of the recuperator and IEC sections. Figure 9 shows the temperature and humidity distribution in the RHME when the compressor efficiency is set at 80%. It is noted that condensation occurs in the product channel for L_{IEC} / L_{tot} values greater than 0.1. Condensation in the product channel occurs due to the increase in the humidity of the working air, which can be seen from the humidity distribution plots. When the condensation occurs, the cooling of the working air in the product channel is limited by the release of latent heat. The cycle is further

analysed using the cooling efficiency, $\theta = \frac{T_{Tout} - T_{ac}}{T_{Tout} - T_{amb}}$, which is the ratio of the temperature difference of the air across the product channel to that between the RHME outlet and the ambient air. Figure 10 shows the relationship between the cooling efficiency, θ , and L_{IEC} / L_{tot} values for the compressor efficiency values of 80%, 90%, and 100%. As can be seen from Fig. 10, L_{IEC} / L_{tot} values for the maximum cooling efficiency decreases with decreasing compressor efficiency. This is because of the increase in the turbine outlet air temperature, which is attributable to the increase in the pressure ratio at low compressor efficiencies. The results further highlight that extending the IEC region of the RHME does not necessarily improve cooling efficiency.

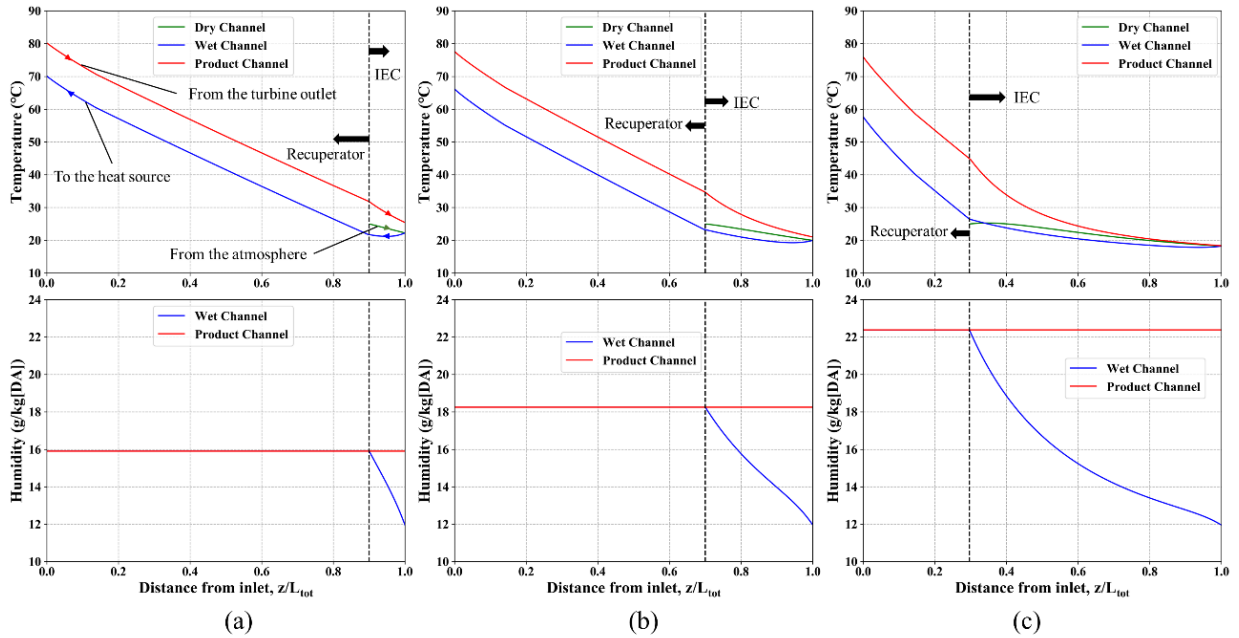


Fig.8: Temperature and humidity distribution along the channels at the compressor efficiency of 100 % with
(a) $L_{IEC} / L_{tot} = 0.1$, (b) $L_{IEC} / L_{tot} = 0.3$, and (c) $L_{IEC} / L_{tot} = 0.7$

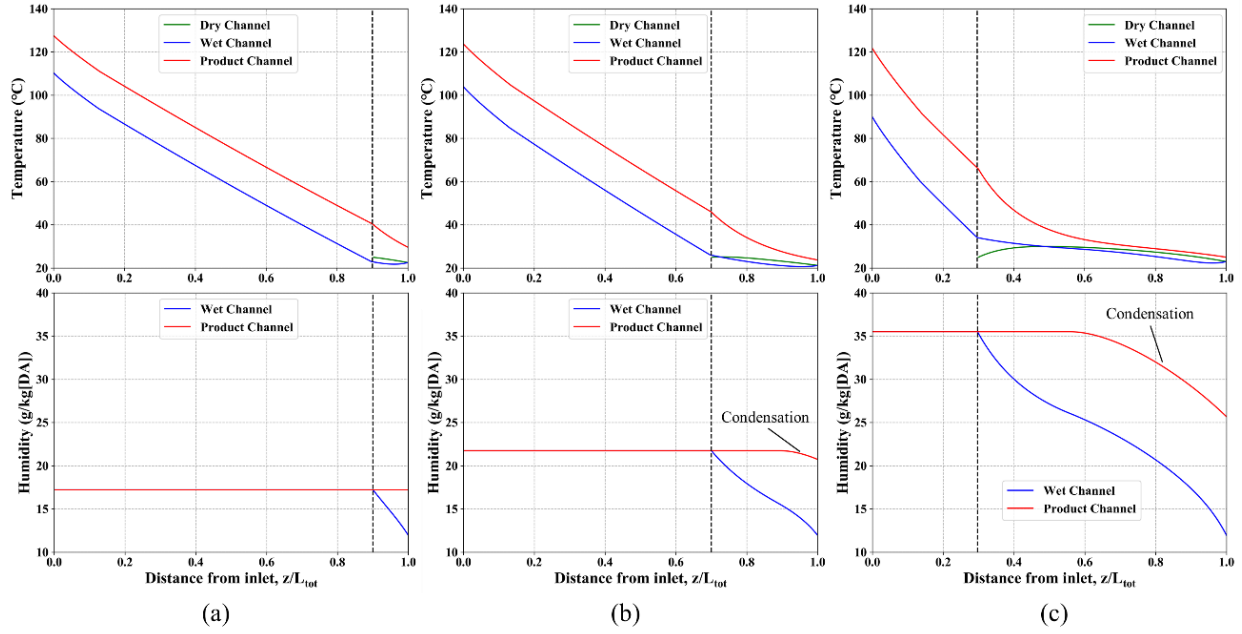


Fig.9: Temperature and humidity distribution along the channels at the compressor efficiency of 80 % with (a) $L_{IEC} / L_{tot} = 0.1$, (b) $L_{IEC} / L_{tot} = 0.3$, and (c) $L_{IEC} / L_{tot} = 0.7$ highlighting condensation

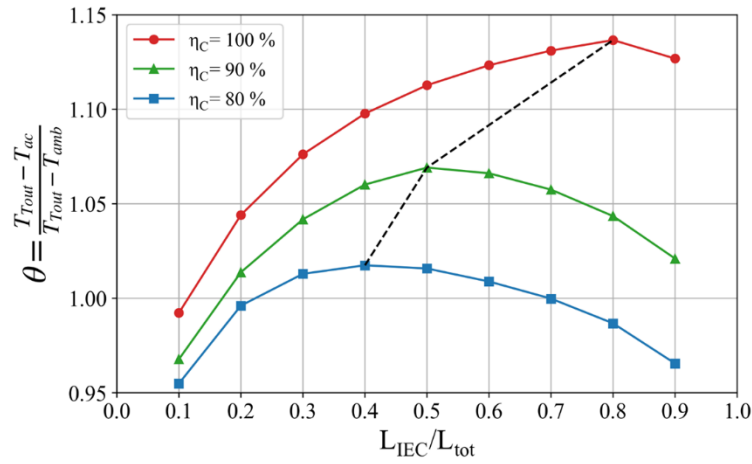


Fig. 10: The effect of varying L_{IEC} / L_{tot} value on the cooling efficiency, θ

4.2 Effect of the turbine inlet air temperature

The optimal recuperative to IEC ratio of the RHME is further confirmed by varying the turbine inlet temperature. Figure 11 shows the change in the cycle thermal efficiency and specific work output depending on the turbine inlet temperature where the highest cycle thermal efficiency is observed when L_{IEC} / L_{tot} equals 0.3 for all turbine inlet temperatures (Fig. 11(a)). It is noted that larger apportionment of the IEC in the RHME device provides higher thermal efficiency when the turbine inlet temperature is below 80 °C. However, a further increase in the turbine inlet temperature favours a smaller apportionment of the IEC. The lower the

turbine inlet temperature, the lower sensible heat regeneration by the recuperator, and the greater the specific work output. This is because the increase in the humidity of the air by the IEC contributes to a high cycle thermal efficiency. Nevertheless, the specific work output increases if the IEC portion of the RHME is increased for all turbine inlet temperatures.

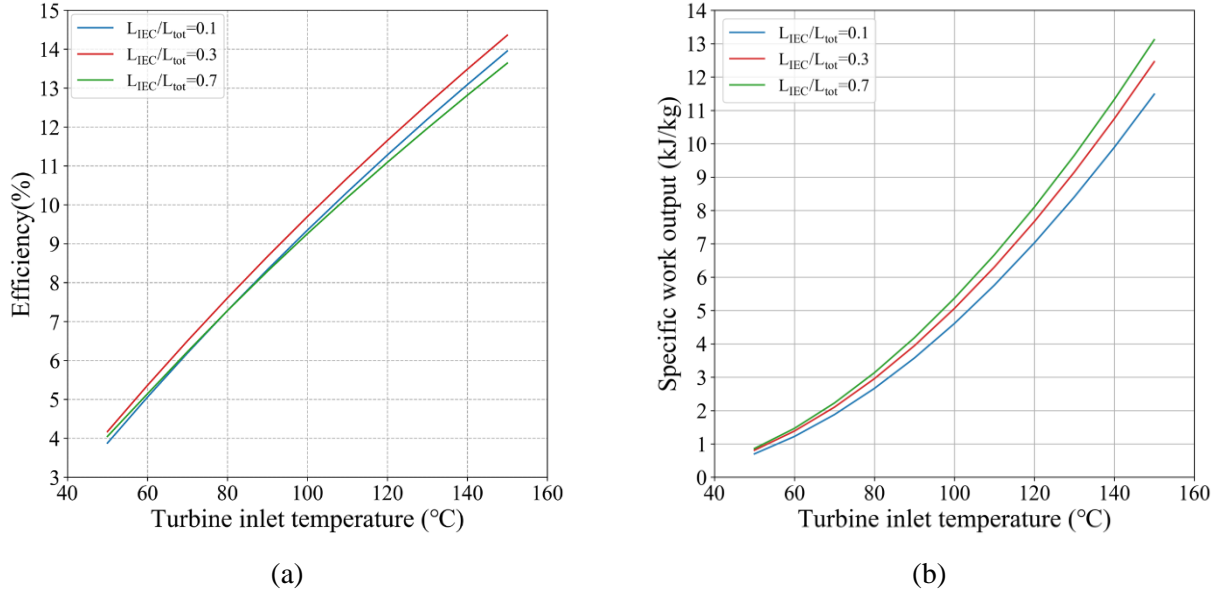


Fig. 11: The impact of the turbine inlet temperature on (a) Thermal efficiency, and (b) Specific work output for three sets of L_{IEC} / L_{tot} values

4.3 Effect of mass flow rate on the cycle performance

Changes in the intake mass flow lead to the variations in the fluid velocity inside the RHME device. As the intake mass flow increases, the fluid velocity in the cooler naturally increases while the cooling efficiency decreases due to the higher flow velocity. Figure 12 shows the cycle thermal efficiency and the specific work output with varying intake mass flow rates. It is noted that low flow rates of the intake air exhibit high efficiency and specific work output. As can be seen in Fig. 12(b), the specific work output increases with increasing L_{IEC} / L_{tot} value for all mass flow rates. However, the L_{IEC} / L_{tot} value for optimal thermal efficiency changes significantly highlighting that a shorter recuperative portion is desirable for low air velocities. For higher air flow rates, the temperature gradient along the channel decreases because of the higher velocity. The dependency of the thermal efficiency of the proposed cycle on the intake mass flow rate and L_{IEC} / L_{tot} value is depicted in Fig. 12 (c). The results further highlight that higher thermal efficiency values can be realised at low air intake flow and higher apportionment of the sensible heat recovery, i.e., low L_{IEC} / L_{tot} value.

Table 4 summarises the detailed cycle parameters for inlet mass flow rates of 1 kg/s and 5 kg/s with varying L_{IEC} / L_{tot} values. When the inlet air mass flow rate is 1 kg/s, the temperature difference of the product air, T_5 , between L_{IEC} / L_{tot} values of 0.1 and 0.9 is 6.9 °C. Therefore, the pressure ratio does not change significantly, and the effect of the recuperator on thermal efficiency becomes relatively large. On the other hand, when the

inlet mass flow rate is 5 kg/s, there is a large difference in the temperature after cooling, T_5 , i.e., 22.6 °C (51.7 °C for $L_{IEC} / L_{tot} = 0.1$ and 29.1 °C for $L_{IEC} / L_{tot} = 0.9$). The better intercooling performance due to the increase in the IEC ratio improves the pressure ratio and decreases the thermal efficiency since the rise in the inlet mass flow rate becomes insignificant.

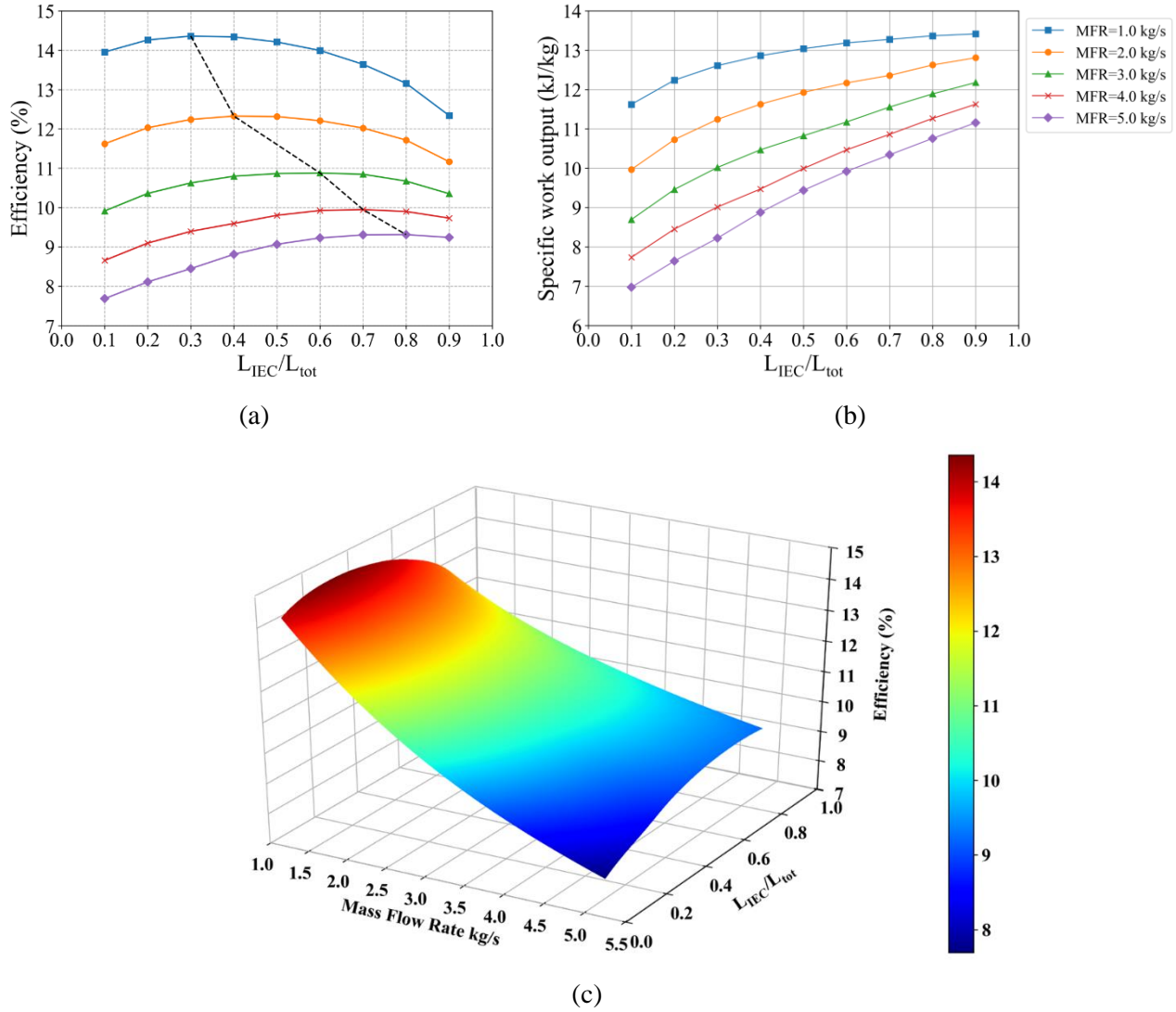


Fig. 12: The performance of the cycle for various L_{IEC} / L_{tot} values and mass flow rates (a) Thermal efficiency, (b) Specific work output and (c) Efficiency variation with mass flow rate and IEC ratio

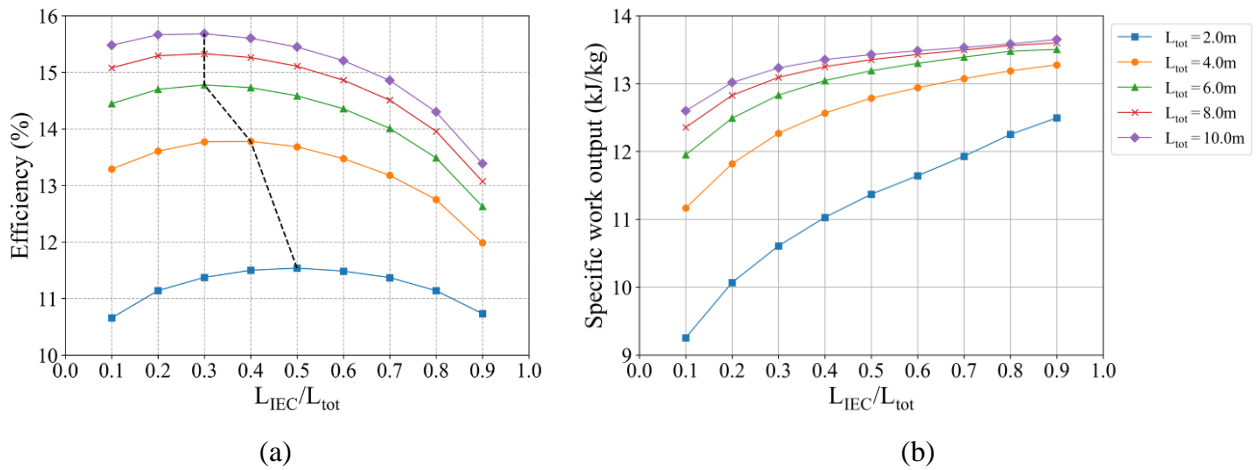
Table 4. Detailed on the cycle parameters for the inlet mass flow rates of 1 kg/s and 5 kg/s

Inlet mass flow rate (kg/s)	L_{IEC} / L_{tot}	Temperature before heating, T_2 (°C)	Input Heat, q_H (kJ/kg)	Pressure ratio, P_4/P_3	Temperature after cooling, T_5 (°C)
1.0	0.1	70.1	82.3	0.53	25.4
	0.3	66.1	86.8	0.52	21.0

		0.5	62.6	90.7	0.51	19.2
		0.7	57.7	96.2	0.51	18.3
		0.9	47.8	107.4	0.51	18.5
		0.1	62.7	89.7	0.62	51.7
		0.3	57.0	96.2	0.59	44.1
	5.0	0.5	51.2	102.9	0.57	37.4
		0.7	45.2	109.8	0.56	32.9
		0.9	37.0	119.3	0.54	29.1

4.4 Effect of the total length of RHME on the cycle performance

The performance of the RHME-IBC system is investigated for different lengths of the RHME device, as shown in Fig. 13. In general, increasing the length of the RHME device provides higher efficiency and specific work output. However, Fig. 13(b) depicts that improvement in the specific work output becomes insignificant when the length is more than 6.0 m. In Fig. 13(a), the thermal efficiency tends to decrease as the IEC ratio (L_{IEC} / L_{tot}) increases, so the total length and IEC ratio are always important factors to be considered. From these results (the effects of inlet mass flow rate and the total length), the ratio of IEC should be increased if the conditions are not favourable for the heat recuperation. Fig. 13(c) demonstrates the influence of the total length and L_{IEC} / L_{tot} value on the efficiency of the cycle depicting the improved thermal efficiency of the RHME-IBC system for low L_{IEC} / L_{tot} value and extended total length of the RHME unit. It is noted that air situation, i.e., the high L_{IEC} / L_{tot} value is beneficial for the RHME with shorter length in terms of thermal efficiency.



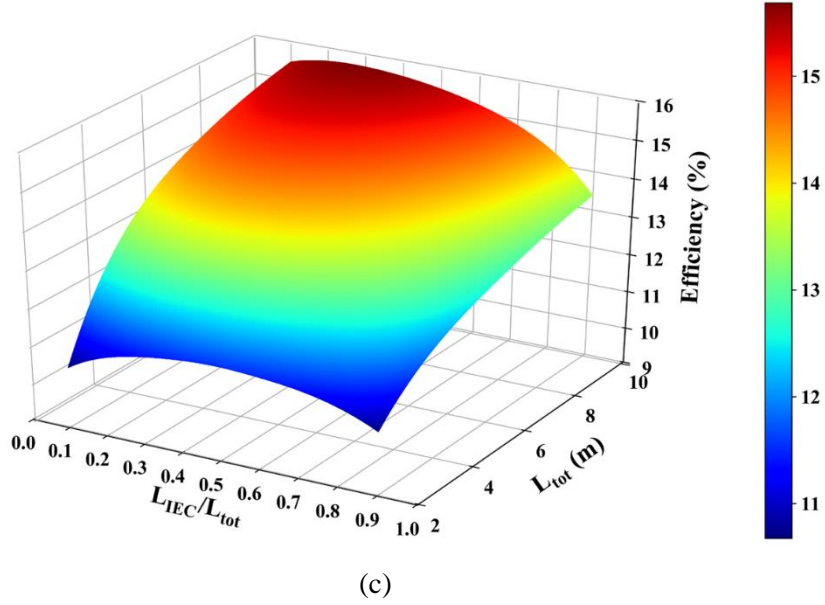
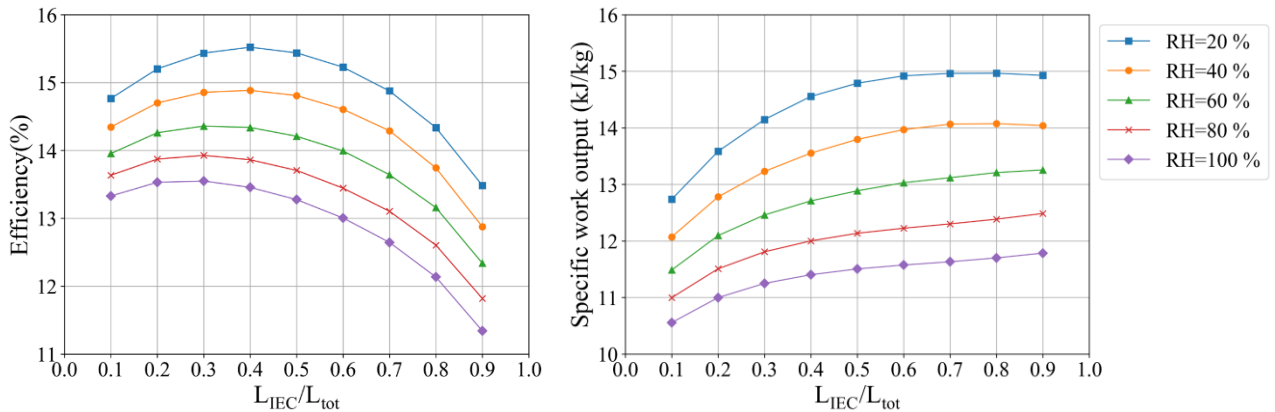


Fig. 13: The performance of the cycle for various L_{IEC} / L_{tot} values and the total length of RHME (a) Thermal efficiency, (b) Specific work output and (c) Efficiency variation with the total length and IEC ratio

4.5 Impact of relative humidity

The relative humidity of the working air is an important parameter for the performance of an IEC device. In general, the lower the atmospheric air humidity, the better the IEC cooling performance. Figure 14 shows the cycle performance with varying relative humidity of the surrounding air from 20% to 100%. From Fig. 14(a) and 14(b), it can be observed that the cycle performance improves for low relative humidity of the intake air. Thermal efficiency increases almost linearly with decreasing relative humidity. Figure 14(a) shows that the optimum L_{IEC} / L_{tot} value changes depending on the relative humidity of the intake air. Operating the system using the intake air with low relative humidity requires higher air situation ratio (higher L_{IEC} / L_{tot} value) to attain the optimal performance. This is because an extended section of the IEC is required for sufficient air situation in the wet channel. Fig. 14(c) shows the thermal efficiency with varying relative humidity and L_{IEC} / L_{tot} value highlighting the thermal efficiency at low RH and optimal L_{IEC} / L_{tot} value.



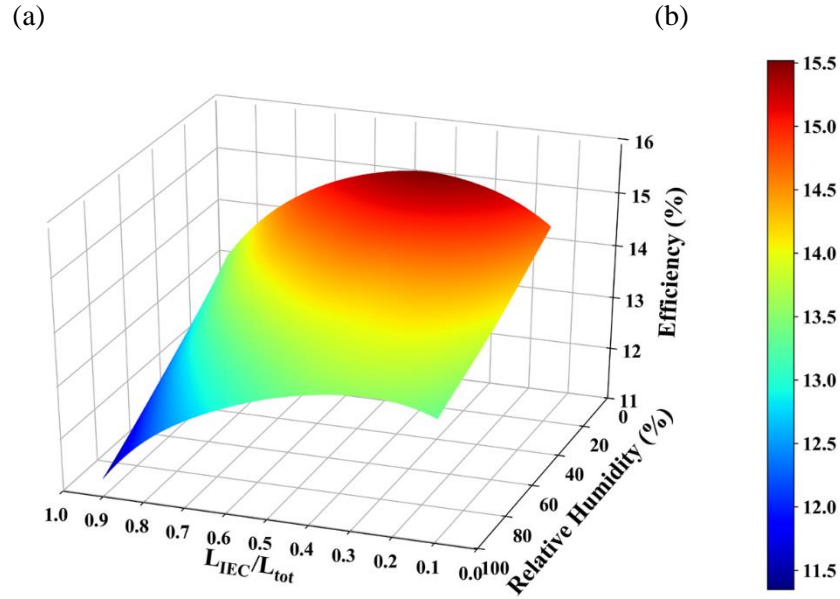


Fig. 14: The performance of the cycle for various L_{IEC} / L_{tot} values and the relative humidity of the intake air
 (a) Thermal efficiency, (b) Specific work output, (c) Efficiency variation with the humidity of the intake air and IEC ratio

4.6 Performance comparison with various IBC cycles

The performance improvement by the proposed RHME-IBC cycle is assessed against a conventional air-cooling system, a recuperative IBC system and an IEC-IBC system. Figure 15 shows the thermal efficiency and the specific work output of various IBC-based cycles for different turbine inlet temperatures. The proposed RHME-IBC cycle exhibits a significant improvement in thermal efficiency, for all L_{IEC} / L_{tot} values (0.1, 0.3 and 0.7). As reported in our previous work, the thermal efficiency of an IEC-IBC system is rather low since almost all sensible heat is used for the vaporisation of water. When comparing the present system having $L_{IEC} / L_{tot} = 0.3$ with the Recuperator IBC system, the thermal efficiency is improved to 4.12% from 3.0% at the turbine inlet temperature of 50 °C. The improvement in the thermal efficiency is more significant at higher turbine inlet temperatures. In terms of specific work output, the results highlight that higher L_{IEC} / L_{tot} ratios lead to the enhanced specific work at the expense of the thermal efficiency. Nevertheless, the proposed RHME-IBC cycle offers a comparable specific work output to that of an IEC-IBC system. It is observed that the apportionment of the recuperator and the IEC device in RHME (L_{IEC} / L_{tot}) at 0.3 provides the highest thermal efficiency with comparable specific work output with IEC-IBC system.

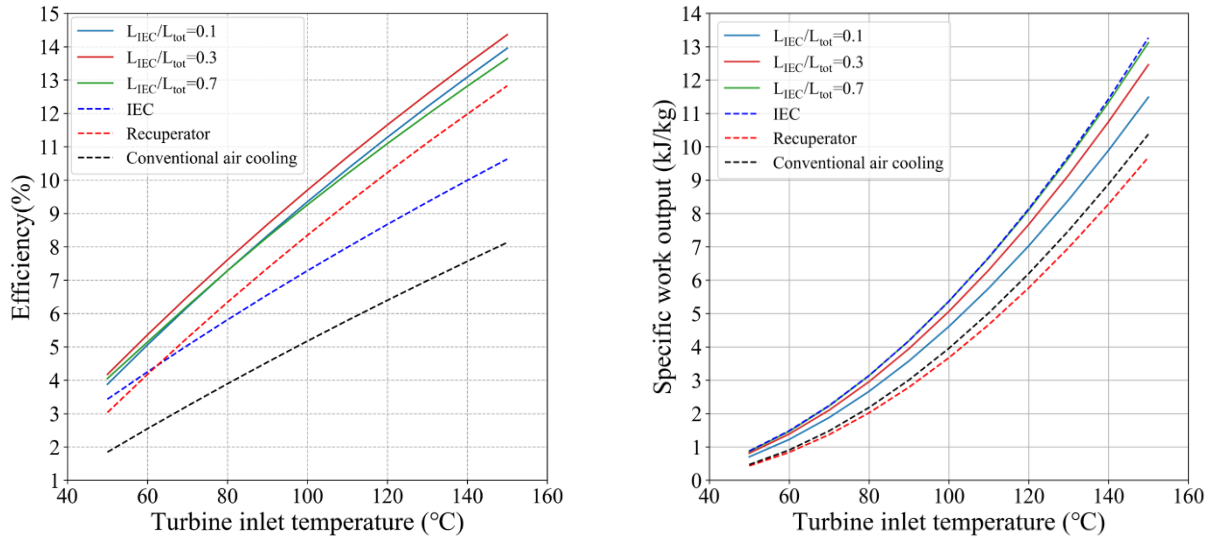


Fig. 15: Performance comparison of the RHME-IBC system with a conventional air-cooling cycle, a recuperative cycle and the hybrid IEC-IBC cycles (a) Thermal efficiency and (b) Specific work output

Table 5. The percentage improvement by the RHME-IBC system in terms of thermal efficiency and the specific work output

Parameter	Baseline	% improvement as compared to the baseline cycle (%)		
	Air-cooling	Recuperator	IEC-IBC	RHME-IBC ($L_{IEC} / L_{tot} = 0.3$)
η_{th} (%)	8.13	57.79	30.77	76.63
w_{net} (kJ/kg)	10.38	-6.66	27.86	20.08

Table 5 summarises the percentage improvement in the performance by the proposed regenerative heat and mass exchanger system incorporated with the IBC system keeping a conventional air-cooling cycle as a baseline. It is noted that the current cycle offers up to 76.63% improvement in thermal efficiency while exhibiting 20.08% increase in the specific work output. Such an unprecedentedly high performance (both thermal efficiency and specific work output) is realised due to exploitation of the regenerative and air-saturation (cooling) mechanisms for the energy recovery and cooling of the working fluid.

5 Conclusions

In this paper, an innovative energy recovery scheme for Inverted Brayton Cycles (IBCs) was introduced for improved thermal efficiency and specific work output realising the effective conversion of the waste heat to electricity. The proposed recovery scheme utilises a Regenerative Heat and Mass Exchanger (RHME) that consolidates the recuperator for the sensible heat recovery and an Indirect Evaporative Cooler (IEC) for the air situation. A numerical model for both RHME and the IBC has been judiciously developed accounting for the

possible condensation in the product air channel. The experimentally-verified IEC model was incorporated into the performance calculation of the cycle. The cycle was investigated for various low-temperature waste-heat (50 to 150 °C) sources. A comprehensive investigation was conducted to evaluate the influences of the adiabatic efficiencies of the compressor and the turbines, the air situation ratio (L_{IEC} / L_{tot} ratio), turbine inlet temperatures, intake air conditions (flow rates and relative humidity) and length of the recovery device comparing against the conventional IBC system. The key contributions and important observations of the present work are as follows:

- The proposed hybrid cycle achieves high cooling efficiency, thus high specific work output by using the latent heat of the water through an evaporative cooling technique.
- Different optimal values of situation ratio (L_{IEC} / L_{tot}) were observed; $L_{IEC} / L_{tot} = 0.3$ for the optimal thermal efficiency and $L_{IEC} / L_{tot} = 0.7$ for the specific work output.
- Both thermal efficiency and specific work output increase with lowering intake air flow rates while higher apportionment of sensible heat recovery (recuperator) in the RHME device is necessary for low air intake flows for optimal thermal efficiency ($L_{IEC} / L_{tot} = 0.3$ for air intake of 1.0 kg/s).
- For the RHME with a shorter total length, the increased air situation, i.e., the high L_{IEC} / L_{tot} value is beneficial for the thermal efficiency.
- The current cycle increases the thermal efficiency from 8.13% to 14.36% (76.63% improvement), while exhibiting 20.08% increase in the specific work output when comparing to a conventional air-cooling IBC cycle.

References

- [1] Kong X, Sun F, Huo X, Li X, Shen Y. Hierarchical optimal scheduling method of heat-electricity integrated energy system based on Power Internet of Things. *Energy* 2020;210:118590. doi:10.1016/J.ENERGY.2020.118590.
- [2] Dancker J, Klabunde C, Wolter M. Sensitivity factors in electricity-heating integrated energy systems. *Energy* 2021;229:120600. doi:10.1016/J.ENERGY.2021.120600.
- [3] Chen Y, Zhang L, Xu P, Di Gangi A. Electricity demand response schemes in China: Pilot study and future outlook. *Energy* 2021;224:120042. doi:10.1016/J.ENERGY.2021.120042.
- [4] Kan X, Reichenberg L, Hedenus F. The impacts of the electricity demand pattern on electricity system cost and the electricity supply mix: A comprehensive modeling analysis for Europe. *Energy* 2021;235:121329. doi:10.1016/J.ENERGY.2021.121329.
- [5] Eshraghi H, Rodrigo de Queiroz A, Sankarasubramanian A, DeCarolus JF. Quantification of climate-induced interannual variability in residential U.S. electricity demand. *Energy* 2021;236:121273. doi:10.1016/J.ENERGY.2021.121273.
- [6] Energy Information Administration U. International Energy Outlook 2019. 2019.
- [7] Nagatomo Y, Ozawa A, Kudoh Y, Hondo H. Impacts of employment in power generation on renewable-based energy systems in Japan— Analysis using an energy system model. *Energy* 2021;226:120350. doi:10.1016/J.ENERGY.2021.120350.
- [8] Lohrmann A, Child M, Breyer C. Assessment of the water footprint for the European power sector during the transition towards a 100% renewable energy system. *Energy* 2021;233:121098. doi:10.1016/J.ENERGY.2021.121098.
- [9] Firth A, Zhang B, Yang A. Quantification of global waste heat and its environmental effects. *Appl Energy* 2019;235:1314–34. doi:10.1016/J.APENERGY.2018.10.102.
- [10] F. Tchanche B, Pétrissans M, Papadakis G. Heat resources and organic Rankine cycle machines. *Renew Sustain Energy Rev* 2014;39:1185–99. doi:10.1016/J.RSER.2014.07.139.
- [11] Ammar Y, Joyce S, Norman R, Wang Y, Roskilly AP. Low grade thermal energy sources and uses from the process industry in the UK. *Appl Energy* 2012;89:3–20. doi:10.1016/J.APENERGY.2011.06.003.
- [12] Hiltunen P, Syri S. Low-temperature waste heat enabling abandoning coal in Espoo district heating system. *Energy* 2021;231:120916. doi:10.1016/J.ENERGY.2021.120916.
- [13] Wang S, Zhang L, Liu C, Liu Z, Lan S, Li Q, et al. Techno-economic-environmental evaluation of a combined cooling heating and power system for gas turbine waste heat recovery. *Energy* 2021;231:120956. doi:10.1016/J.ENERGY.2021.120956.
- [14] Xu J, Luo E, Hochgreb S. A thermoacoustic combined cooling, heating, and power (CCHP) system for waste heat and LNG cold energy recovery. *Energy* 2021;227:120341. doi:10.1016/J.ENERGY.2021.120341.

- [15] Aly WIA, Abdo M, Bedair G, Hassaneen AE. Thermal performance of a diffusion absorption refrigeration system driven by waste heat from diesel engine exhaust gases. *Appl Therm Eng* 2017;114:621–30. doi:10.1016/J.APPLTHERMALENG.2016.12.019.
- [16] Sun F, Li J, Fu L, Li Y, Wang R, Zhang S. New configurations of district heating and cooling system based on absorption and compression chillers driven by waste heat of flue gas from coke ovens. *Energy* 2020;193:116707. doi:10.1016/J.ENERGY.2019.116707.
- [17] Hu T, Shen Y, Kwan TH, Pei G. Absorption chiller waste heat utilization to the desiccant dehumidifier system for enhanced cooling – Energy and exergy analysis. *Energy* 2022;239:121847. doi:10.1016/J.ENERGY.2021.121847.
- [18] Chan CW, Ling-Chin J, Roskilly AP. A review of chemical heat pumps, thermodynamic cycles and thermal energy storage technologies for low grade heat utilisation. *Appl Therm Eng* 2013;50:1257–73. doi:10.1016/J.APPLTHERMALENG.2012.06.041.
- [19] Mitra S, Muttakin M, Thu K, Saha BB. Study on the influence of adsorbent particle size and heat exchanger aspect ratio on dynamic adsorption characteristics. *Appl Therm Eng* 2018;133:764–73. doi:10.1016/J.APPLTHERMALENG.2018.01.015.
- [20] Ismail A Bin, Li A, Thu K, Ng KC, Chun W. Pressurized adsorption cooling cycles driven by solar/waste heat. *Appl Therm Eng* 2014;67:106–13. doi:10.1016/j.applthermaleng.2014.02.063.
- [21] Thu K, Kim Y-D, Shahzad MW, Saththasivam J, Ng KC. Performance investigation of an advanced multi-effect adsorption desalination cycle. *Soc. Air-conditioning Refrig. Eng. Korea, SAREK*, vol. 159, Elsevier; 2014, p. 469–77. doi:10.1016/j.apenergy.2015.09.035.
- [22] Thu K, Kim Y-D, Amy G, Chun WG, Ng KC. A hybrid multi-effect distillation and adsorption cycle. *Appl Energy* 2013;104:810–21. doi:10.1016/j.apenergy.2012.12.007.
- [23] Mitra S, Thu K, Saha BB, Srinivasan K, Dutta P. Modeling study of two-stage, multi-bed air cooled silica gel + water adsorption cooling cum desalination system. *Appl Therm Eng* 2017;114. doi:10.1016/j.applthermaleng.2016.12.011.
- [24] Thu K, Mitra S, Saha BB, Murthy SS. Thermodynamic feasibility evaluation of hybrid dehumidification – mechanical vapour compression systems. *Appl Energy* 2018;213:31–44. doi:https://doi.org/10.1016/j.apenergy.2018.01.024.
- [25] Qin M, Deshmukh A, Epsztein R, Patel SK, Owoseni OM, Walker WS, et al. Comparison of energy consumption in desalination by capacitive deionization and reverse osmosis. *Desalination* 2019;455:100–14. doi:10.1016/J.DESAL.2019.01.003.
- [26] Werber JR, Deshmukh A, Elimelech M. Can batch or semi-batch processes save energy in reverse-osmosis desalination? *Desalination* 2017;402:109–22. doi:10.1016/J.DESAL.2016.09.028.
- [27] Elimelech M, Phillip WA. The Future of Seawater Desalination: Energy, Technology, and the Environment. *Science* (80-) 2011;333:712–7. doi:10.1126/science.1200488.
- [28] Li T, Wang Q, Zhu J, Hu K, Fu W. Thermodynamic optimization of organic Rankine cycle using two-stage evaporation. *Renew Energy* 2015;75:654–64. doi:10.1016/J.RENENE.2014.10.058.

- [29] Fu H, He Q, Song J, Shi X, Hao Y, Du D, et al. Thermodynamic of a novel advanced adiabatic compressed air energy storage system with variable pressure ratio coupled organic rankine cycle. *Energy* 2021;227:120411. doi:10.1016/J.ENERGY.2021.120411.
- [30] Liu B-T, Chien K-H, Wang C-C. Effect of working fluids on organic Rankine cycle for waste heat recovery. *Energy* 2004;29:1207–17. doi:10.1016/J.ENERGY.2004.01.004.
- [31] Lee W-Y, Kim M, Sohn Y-J, Kim S-G. Power optimization of a combined power system consisting of a high-temperature polymer electrolyte fuel cell and an organic Rankine cycle system. *Energy* 2016;113:1062–70. doi:10.1016/J.ENERGY.2016.07.093.
- [32] Ho T, Mao SS, Greif R. Increased power production through enhancements to the Organic Flash Cycle (OFC). *Energy* 2012;45:686–95. doi:10.1016/J.ENERGY.2012.07.023.
- [33] Mondal S, Alam S, De S. Performance assessment of a low grade waste heat driven organic flash cycle (OFC) with ejector. *Energy* 2018;163:849–62. doi:10.1016/J.ENERGY.2018.08.160.
- [34] Smith IK, da Silva RPM. Development of the Trilateral Flash Cycle System Part 2: Increasing Power Output with Working Fluid Mixtures. *Proc Inst Mech Eng Part A J Power Energy* 1994;208:135–44. doi:10.1243/PIME_PROC_1994_208_022_02.
- [35] Smith IK, Stošić N, Aldis CA. Development of the Trilateral Flash Cycle System: Part 3: The Design of High-Efficiency Two-Phase Screw Expanders. *Proc Inst Mech Eng Part A J Power Energy* 1996;210:75–93. doi:10.1243/PIME_PROC_1996_210_010_02.
- [36] Smith IK. Development of the Trilateral Flash Cycle System: Part 1: Fundamental Considerations. *Proc Inst Mech Eng Part A J Power Energy* 1993;207:179–94. doi:10.1243/PIME_PROC_1993_207_032_02.
- [37] Bahrampoury R, Behbahaninia A. Thermodynamic investigation of dual-separator Kalina cycle system: Comparative study. *Proc Inst Mech Eng Part A J Power Energy* 2018;232:282–92. doi:10.1177/0957650917720288.
- [38] Jurgen RK. The promise of the Kalina cycle. *IEEE Spectrum*; (United States) n.d.
- [39] Moran MJ, Shapiro HN, Boettner DD, Bailey MB. *Fundamentals of Engineering Thermodynamics*. Wiley; 2010.
- [40] Bejan A, Tsatsaronis G, Moran MJ. *Thermal Design and Optimization*. Wiley; 1996.
- [41] Agnew B, Anderson A, Potts I, Frost TH, Alabdoadaim MA. Simulation of combined Brayton and inverse Brayton cycles. *Appl Therm Eng* 2003;23:953–63. doi:10.1016/S1359-4311(03)00019-X.
- [42] Wilson DG, Duntelman NR. *The Inverted Brayton Cycle for Waste-Heat Utilization* 1973. doi:10.1115/73-GT-90.
- [43] Galanis N, Cayer E, Roy P, Denis ES, Désilets M. Electricity generation from low temperature sources. *J Appl Fluid Mech* 2009;2:55–67.
- [44] Iglesias Garcia S, Ferreiro Garcia R, Carbia Carril J, Iglesias Garcia D. A review of thermodynamic cycles used in low temperature recovery systems over the last two years. *Renew Sustain Energy*

Rev 2018;81:760–7. doi:10.1016/J.RSER.2017.08.049.

- [45] Chagnon-Lessard N, Copeland C, Mathieu-Potvin F, Gosselin L. Maximizing specific work output extracted from engine exhaust with novel inverted Brayton cycles over a large range of operating conditions. *Energy* 2020;191:116350. doi:10.1016/J.ENERGY.2019.116350.
- [46] Bianchi M, Negri di Montenegro G, Peretto A, Spina PR. A Feasibility Study of Inverted Brayton Cycle for Gas Turbine Repowering. *J Eng Gas Turbines Power* 2005;127:599–605. doi:10.1115/1.1765121.
- [47] Kennedy I, Chen Z, Ceen B, Jones S, Copeland CD. Experimental Investigation of an Inverted Brayton Cycle for Exhaust Gas Energy Recovery. *J Eng Gas Turbines Power* 2018;141. doi:10.1115/1.4041109.
- [48] Copeland CD, Chen Z. The Benefits of an Inverted Brayton Bottoming Cycle as an Alternative to Turbo-Compounding 2015. doi:10.1115/GT2015-42623.
- [49] Bianchi M, De Pascale A. Bottoming cycles for electric energy generation: Parametric investigation of available and innovative solutions for the exploitation of low and medium temperature heat sources. *Appl Energy* 2011;88:1500–9. doi:10.1016/J.APENERGY.2010.11.013.
- [50] Kennedy I, Chen Z, Ceen B, Jones S, Copeland CD. Inverted Brayton Cycle With Exhaust Gas Condensation. *J Eng Gas Turbines Power* 2018;140. doi:10.1115/1.4039811.
- [51] Di Battista D, Fatigati F, Carapellucci R, Cipollone R. Inverted Brayton Cycle for waste heat recovery in reciprocating internal combustion engines. *Appl Energy* 2019;253:113565. doi:10.1016/J.APENERGY.2019.113565.
- [52] Kakaras E, Doukelis A, Karellas S. Compressor intake-air cooling in gas turbine plants. *Energy* 2004;29:2347–58. doi:10.1016/J.ENERGY.2004.03.043.
- [53] Fujii S, Kaneko K, Otani K, Tsujikawa Y. Mirror Gas Turbines: A Newly Proposed Method of Exhaust Heat Recovery. *J Eng Gas Turbines Power* 2000;123:481–6. doi:10.1115/1.1366324.
- [54] Hingst R. Process for Producing Energy from Gases and Gas Steam Mixtures of Low Pressure, e. B. Exhaust gases from internal combustion engines. *Deutsches Patent No.* 852015, 1944.
- [55] Liu C, Zheng Q, Wang Q, Lin A, Jiang Y, Luo M. Sensitivity Analysis of Multistage Compressor Characteristics Under the Spray Atomization Effect Using a CFD Model. *Energies* 2019;12. doi:10.3390/en12020301.
- [56] Duan Z, Zhan C, Zhang X, Mustafa M, Zhao X, Alimohammadisagvand B, et al. Indirect evaporative cooling: Past, present and future potentials. *Renew Sustain Energy Rev* 2012;16:6823–50. doi:10.1016/J.RSER.2012.07.007.
- [57] Zhu F, Chen L, Wang W. Thermodynamic Analysis and Optimization of an Irreversible Maisotsenko-Diesel Cycle. *J Therm Sci* 2019 284 2019;28:659–68. doi:10.1007/S11630-019-1153-1.
- [58] Zhu G, Chow TT, Fong KF, Lee CK. Comparative study on humidified gas turbine cycles with

- different air saturator designs. *Appl Energy* 2019;254:113592. doi:10.1016/J.APENERGY.2019.113592.
- [59] Chen L, Shen J, Ge Y, Wu Z, Wang W, Zhu F, et al. Power and efficiency optimization of open Maisotsenko-Brayton cycle and performance comparison with traditional open regenerated Brayton cycle. *Energy Convers Manag* 2020;217:113001. doi:10.1016/J.ENCONMAN.2020.113001.
- [60] Zhu F, Chen L, Wang W. Thermodynamic Analysis of an Irreversible Maisotsenko Reciprocating Brayton Cycle. *Entropy (Basel)* 2018;20. doi:10.3390/E20030167.
- [61] Shen J, Chen L, Ge Y, Zhu F, Wu Z. Optimum ecological performance of irreversible reciprocating Maisotsenko-Brayton cycle. *Eur Phys J Plus* 2019 1346 2019;134:1–14. doi:10.1140/EPJP/I2019-12648-4.
- [62] Matsui K, Thu K, Miyazaki T. A hybrid power cycle using an inverted Brayton cycle with an indirect evaporative device for waste-heat recovery. *Appl Therm Eng* 2020;170:115029. doi:10.1016/J.APPLTHERMALENG.2020.115029.
- [63] Lin J, Thu K, Bui TD, Wang RZ, Ng KC, Chua KJ. Study on dew point evaporative cooling system with counter-flow configuration. *Energy Convers Manag* 2016;109:153–65. doi:10.1016/j.enconman.2015.11.059.
- [64] Incropera FP, DeWitt DP, Bergman TL, Lavine AS. Fundamentals of Heat and Mass Transfer. vol. 6th. John Wiley & Sons; 2007. doi:10.1016/j.applthermaleng.2011.03.022.
- [65] Lin J, Bui DT, Wang R, Chua KJ. On the fundamental heat and mass transfer analysis of the counter-flow dew point evaporative cooler. *Appl Energy* 2018;217:126–42. doi:10.1016/J.APENERGY.2018.02.120.
- [66] Engineers TJS of M. Mechanical Engineering Handbook. 1985.
- [67] Welty J, Rorrer GL, Foster DG. Fundamentals of Momentum, Heat, and Mass Transfer. Wiley; 2014.
- [68] Mills A. Heat and Mass Transfer. Taylor & Francis; 2018.
- [69] Runge C. Ueber die numerische Auflösung von Differentialgleichungen. *Math Ann* 1895;46:167–78. doi:10.1007/BF01446807.
- [70] Powell MJD. An efficient method for finding the minimum of a function of several variables without calculating derivatives. *Comput J* 1964;7:155–62. doi:10.1093/comjnl/7.2.155.
- [71] Bell IH, Wronski J, Quoilin S, Lemort V. Pure and Pseudo-pure Fluid Thermophysical Property Evaluation and the Open-Source Thermophysical Property Library CoolProp. *Ind Eng Chem Res* 2014;53:2498–508. doi:10.1021/ie4033999.
- [72] Rianguilaikul B, Kumar S. An experimental study of a novel dew point evaporative cooling system. *Energy Build* 2010;42:637–44. doi:10.1016/J.ENBUILD.2009.10.034.

Reviewers' comments:

Reviewer #4: The authors have addressed the comments properly. There is only a minor question the authors should further elaborate. In Eq(17), the well-recognized equation for calculating the heat transfer coefficient of fully developed laminar flow in parallel plates should be $Nu=8.235$.

Please elaborate the applicability of using $Nu=7.54$ in the manuscript.

Authors' response

We are grateful for the comments. This is a good question, although it has already been discussed in our earlier work [63]. Both 8.235 and 7.54 are analytical solutions of Nusselt number in fully developed laminar flow, but at different thermal boundary conditions [64]. The former is for constant heat flux, while the latter is for constant surface temperature. Both types of the Nusselt number have been employed to approximate the heat transfer coefficient in the literature [1,2,3,4]. However, in the regenerative heat and mass exchanger, the channel surface is neither at constant heat flux or temperature, so both values are indeed approximation of the true Nusselt number value [5]. Nonetheless, if we take a close look on the surface heat flux and surface temperature, we can find that the variation of surface temperature is confined in a small range which is similar to the difference between inlet and outlet air temperatures. In contrast, the surface heat flux can vary in several order of magnitude [63]. Hence, we believe the Nusselt number under constant surface temperature ($Nu=7.54$) is a more reasonable estimation. The above information has been added before Eq. (17).

References

- [1] Duan Z. Investigation of a novel dew point indirect evaporative air conditioning system for buildings. PhD thesis. University of Nottingham; 2011.
- [2] Rianguilaikul B, Kumar S. Numerical study of a novel dew point evaporative cooling system. *Energ Build* 2010;42:2241–50.
- [3] Jradi M, Riffat S. Experimental and numerical investigation of a dew-point cooling system for thermal comfort in buildings. *Appl Energ* 2014;132:524–35.
- [4] Hasan A. Indirect evaporative cooling of air to a sub-wet bulb temperature. *Appl Therm Eng* 2010;30:2460–8.
- [5] Lin J, Bui DT, Wang R, Chua KJ. On the fundamental heat and mass transfer analysis of the counter-flow dew point evaporative cooler. *Appl Energ* 2018;217:126–42.